EVALUATION OF THE DISPLACEMENT DISCONTINUITY METHOD WITH TESSELLATIONS TO SIMULATE THE INDIRECT TENSION STRENGTH TEST

By

CHOTE SORANAKOM

A THESIS PRESENTED TO THE GRADUATE SCHOOL
OF THE UNIVERSITY OF FLORIDA IN PARTIAL FULFILLMENT
OF THE REQUIREMENTS FOR THE DEGREE OF ENGINEER

UNIVERSITY OF FLORIDA

2003

Copyright 2003

by

Chote Soranakom

ACKNOWLEDGMENTS

Many wishes were sent with a very special acknowledgment to my advisor, Dr. Bjorn Birgisson, Assistant Professor of Civil and Coastal Engineering, who supervised the project. His enthusiasm and research creativity in the field of pavement made the project possible and successful.

I would also like to thank Dr. Reynaldo Roque for his assistance in providing test data and useful recommendation for my research. Special thanks go to Dr. John A.L. Napier, who let us use his boundary element code and provided technical assistance throughout the research. I also would like to thank Dr. Bhavani V. Sankar for his kindness, teaching and participation as a member of my committee.

I would like to take this opportunity to acknowledge the Florida Department of Transportation for providing us financial support. Also, I would like to thank many of my friends, Boonchai Sangpetngam, Daniel Darku, Oscar Tazoe, Chirstos Drakos, whose advice, assistance, support and friendship helped me throughout the project.

Finally, a very special acknowledgement is sent to my parents, Chewpore and Wongsa Soranakom, for their love, encouragement and constant advice throughout my academic life away from home. I would also like to thank my brothers and sister in law Charn, Chuan and Bongkoch for their love and emotional support throughout the good and difficult times of doing research.

TABLE OF CONTENTS

page

LIST OF TABLES

LIST OF FIGURES

Abstract of Thesis Presented to the Graduate School
of the University of Florida in Partial Fulfillment of the
Requirements for the Degree of Engineer

EVALUATION OF
THE DISPLACEMENT DISCONTINUITY METHOD WITH TESSELLATIONS
TO SIMULATE THE INDIRECT TENSION STRENGTH TEST

By

Chote Soranakom

May, 2003

Chair: Bjorn Birgisson
Cochair: Reynaldo Roque
Major Department: Civil and Coastal Engineering

The research focused on the use of the displacement discontinuity method to simulate cracking behavior of the indirect tension strength test of asphalt mixtures. From numerical experiments, it was found that the granular structure of asphalt mixtures could be best represented by Voronoi tessellations with internal fracture paths. Two distinct crack growth rules, SEQUENTIAL and PARALLEL, were evaluated and no difference was found in terms of the predicted crack patterns and stress strain responses. However, the PARALLEL crack growth rule that activates all crack sites when the stress exceeds failure limit is more efficient than the SEQUENTIAL crack growth rule that activates the most overstressed crack site one at a time. The study of the aggregate size effects revealed a small size effect. An increase in average aggregate diameter from 4.5 mm to 12.0 mm increased the ultimate tensile strength of the specimen by 11%. It was also found that the optimal particle size was around 40 to 60% passing of gradation.

The sensitivity analysis of material parameters revealed that the mastic properties were a key factor controlling the cracking behavior of mixtures.

Finally the method was used to simulate crack propagation of three mixtures and evaluate their tensile strength and fracture energy density. The numerical results showed reasonable predictions of crack patterns and stress strain responses. The predicted tensile strength and fracture energy density were acceptable.

CHAPTER 1
INTRODUCTION

1.1 Background

It has long been accepted that cracking of hot-mix asphalt (HMA) pavements is a major mode of premature failure. A solid understanding of the mechanisms of crack initiation and crack growth is essential to predict pavement performance in the context of thickness design, as well as in the design and optimization of mixtures. Any hope of developing more crack resistant mixes relies on improved understanding of the mechanics of crack initiation and crack growth in HMA mixtures. Unfortunately, the complexity of modeling crack initiation and crack growth has been an obstacle to the incorporation of fracture mechanics-based approaches in the bituminous pavement area.

With an increasing of computer power, numerical analysis of cracking becomes possible. Bazant (1986) provided a good review for cracking models that have been used for granular material such as concrete and rocks. Cracking in material is normally analyzed by either a fracture mechanics approach or smeared crack approach. The former assumes a single line of crack initiates from a pre-existing flaw and propagates through material according to a certain crack growth criterion such as maximum energy release rate. In contrast, the latter assumes cracks are smeary distributed over a finite region such that an average tensile strain can adequately represent crack. Even though fracture mechanics and smeared crack approaches can predict cracking behavior, they do not really capture the characteristic of cracks in

granular material in which cracks randomly initiate at critical locations and coalesce, forming major crack bands.

Explicit fracture modeling using random assemblies of displacement discontinuity boundary elements provides a more realistic approach for analyzing discrete cracks in granular material (Napier, 1990; Napier and Hildyard, 1992; Napier and Pierce, 1995(a-b); Malan and Napier, 1995; Kuijpers and Napier, 1996; Napier et al., 1997; Napier and Malan, 1997, Steen et al., 2001, Birgisson et al., 2002(a-b) and Soranakom et al., 2003). The method takes advantage of the known solutions of displacement discontinuity in an infinite medium to formulate system of equation; thus, the method is efficient and yields good results for crack-type problems.

The change of geometry due to crack propagation in material can easily be handled by placing displacement discontinuity elements along the anticipated crack paths, which are normally assumed at the boundaries of the grain particles and perhaps internal to the grains as well. Another advantage of using the boundary element approach is that the dimension of the problem decreases by one. That means a two-dimensional problem needs one-dimensional element with a simple failure law; therefore, the computational cost is greatly reduced. For the advantages mentioned above, this method provides an elegant way to simulate and analyze cracks in asphalt mixtures.

1.2 Problem Statement

The displacement discontinuity boundary element method has successfully been used in the field of rock mechanics and mining engineering to model the cracking behavior in rock mass and/or excavations underground. Based on this work, it was determined that the method had the potential to be used in the field of pavements to study the effects of cracking on asphalt mixtures. Since no previous work has been performed

on the use and implementation of this method to simulate and evaluate the cracking behavior of asphalt mixtures, several questions regarding the appropriate set of numerical components arise, which are summarized below:

- What is the best tessellation schemes to simulate the cracking behavior of asphalt mixtures? This includes the type of tessellation scheme (Delaunay triangles, Voronoi polygons or Vornonoi with internal fracture paths) and the optimal particle size used in tessellations to represent aggregate structure of IDT specimen.

- Identification of appropriate crack growth rules for using in simulation of cracking behavior of mixtures. This includes an evaluation of appropriate numerical schemes for predicting the crack growth. Currently, two basic schemes have been evaluated, namely the SEQUENTIAL and PARALLEL crack growth rules. In the PARALLEL crack growth rule, all elements that reach failure in any given loading step are allowed to crack. In the SEQUENTIAL crack growth law, only the most overstressed element is allowed to crack, and the resulting redistribution of stresses is performed and the process is repeated until all overstressed elements at any given load step have been allowed to crack.

- Evaluation of the current failure law implemented in the boundary element code DIGS. In the displacement discontinuity boundary element method, all nonlinear behavior is lumped into the displacement discontinuity. The rest of the material is considered linear elastic. This allows for the formulation of various local "failure laws" to simulate the fracture behavior of materials. For example, a typical assumption would be that the local failure in a sliding mode at a given displacement discontinuity is governed by a Mohr-Coulomb failure law, such that once the stress state reaches the failure envelope, sliding is initiated. Similarly, in tension, a typical failure law would be that the material would open in tension once a given local tensile strength criteria is reached. The nature of these failure laws can be very flexible, allowing for peak- and residual strength criteria, with degradation laws describing the transition from the peak strength to the residual strength.

- It is also important to determine consistent means of obtaining key material parameters for mixtures. This includes the identification of parameters that can be obtained directly from existing laboratory testing procedures, as well as from calibration. In particular, any parameters that need to be obtained from calibration need to be scrutinized in terms of the consistency of the calibration approach used from one mixture to another.

- The potential of the method needs to be evaluated in terms of how well it captures key mixture characteristics and trends observed under carefully controlled laboratory testing conditions. In particular, to what extent this method can predict cracking behavior of asphalt mixtures in the laboratory is of interest. This includes determining how well the method can simulate

- The pre- and post-peak stress-strain behavior under tensile loading conditions
- The initiation of fracture
- The fracture energy and tensile strength at the point of fracture

1.3 Research Hypothesis

The displacement discontinuity boundary element method with an appropriate tessellation scheme can be used to simulate the observed cracking behavior of asphalt mixtures in the laboratory under controlled loading and environmental conditions. Therefore, it is possible to identify an appropriate set of model conditions to describe the fracture behavior of HMA from a micromechanical point of view.

1.4 Objectives

The objectives of this research are summarized below:

- Identify the appropriate tessellation schemes and optimal particle size to simulate aggregate structure of asphalt mixtures.
- Identify the appropriate crack growth rule for simulating indirect tension strength test under monotonic loading conditions.
- Evaluate the performance of the current Mohr-Coulomb type of failure to model cracking behavior of mixture.
- Establish numerical calibration procedure to obtain material parameters from a given mixture.
- Evaluate the potential of using displacement discontinuity method with tessellation to determine tensile strength and fracture energy density of mixtures

1.5 Scope

This study focuses on the implementation of the displacement discontinuity method to the field of pavements. The project will start with a study to identify the appropriate tessellation schemes and crack growth rules. Then, the study will focus on the evaluating the sensitivity of stress-strain predictions to the various input parameters used. These include material parameters for the mastic, material parameters for fracture path inside

aggregate, and the determination of the optimal average size of aggregates.

The sensitivity of these parameters will be used to establish a standard numerical procedure to simulate indirection strength test. Finally, the numerical model will be used to simulate and evaluate how well the method can predict mixture properties such as tensile strength and fracture energy density.

1.6 Research Approach

The research was conducted in five phases:

- Learning how to use the boundary element code entitled "Discontinuity Interaction and Growth Simulation" (DIGS).
- Writing pre-and post processors to help input data and interpret results from DIGS
- Conducting the following numerical studies:
    - Compare tessellations schemes (Delaunay, Voronoi and Voronoi with internal fracture paths).
    - Compare crack growth laws (SEQUENTIAL and PARALLEL).
    - Evaluate the current failure law, which is a Mohr Coulomb type of failure law by means of evaluating the sensitivity of material parameters used on the resulting predictions of the stress-strain behavior of mixtures.
    - Evaluate any potential aggregate size effects.
- Establishing a numerical procedure to calibrate material properties from a given mix for use in a numerical model to simulate indirect tension strength test.
- Using numerical models to evaluate tensile strength and fracture energy of three mixtures: Nova Scotia, NW39_1C and I95SJN_BW.

CHAPTER 2
LITERATURE REVIEW

2.1 Overview

The purpose of this chapter was to conduct a literature review of commonly used approaches in the analysis of cracking and damage in asphalt mixtures. Another popular analytical tool, displacement discontinuity method, which has been used to analyze cracking in field of rock mechanics, was also reviewed. The four approaches that the literature review focuses on are:

- Classical fatigue approach
- Continuum damage approach
- Fracture mechanics approach
- Displacement discontinuity approach with tessellation schemes

2.2 Classical Fatigue Approach

Fatigue cracking due to repeated traffic loading is one of the major distresses in asphalt concrete pavements. The mechanism of fatigue cracking is caused by the tensile stress at either the top or the bottom of asphalt layer induced by wheel load. With several number of load passes, microcracks will develop and later coalesce to form major crack bands, weakening the pavement structure and finally leading to pavement failure.

In order to characterize the fatigue resistance of a mixture for pavement design, it was necessary to describe the behavior of AC mixtures under repeated stress or strain cyclic loading. In early developments, many researchers have proposed fatigue models to predict the number of load passes to failure based on the tensile strain at the bottom of the

asphalt layer alone. Later on, the models have been improved by including other related variables such as mixture stiffness and volume of bitumen in the mix.

The Illinois Department of Transportation presented a strain-based equation for pavement thickness design based on the studies of Thompson and Cation (1986), Gomez and Thompson (1984), and Thompson (1987). The equation had accounted for mixture composition factors, field calibration and split strength characteristics. The following equation was developed for a particular dense-graded mixture used at Illinois DOT

$$N_f = 5\times10^{-6}\left(\frac{1}{\varepsilon}\right)^{3.0} \tag{2-1}$$

where N_f is the number of repetitions to failure and ε is the maximum tensile strain.

Based on extensive laboratory test data covering a wide range of mixtures, bitumen's, and testing conditions, The Royal Dutch Shell Oil Company (Bonnaure et al., 1980) developed separate fatigue models for constant stress and constant strain beam fatigue tests. For constant stress tests, number of repetitions to failure can be defined as

$$N_f = \left[0.0252PI - 0.00126PI(V_b) + 0.00673V_b - 0.0167\right]^5 \varepsilon_t^{-5} S_m^{-1.4} \tag{2-2}$$

where PI is the penetration index, V_b is the percentage of bitumen volume in the mix, S_m is the stiffness modulus of the mix in N/m^2 and ε_t is the tensile strain, which was defined by

$$\varepsilon_t = \left[36.43PI - 1.82PI(V_b) + 9.71V_b - 24.04\right]\times10^{-6}\left(\frac{S_m}{5\times10^9}\right)^{-0.28}\left(\frac{N_f}{10^6}\right)^{-0.2} \tag{2-3}$$

In a very similar format, the number of repetitions to failure for constant strain can be defined as

$$N_f = \left[0.17PI - 0.0085PI(V_b) + 0.0454V_b - 0.112\right]^5 \varepsilon_t^{-5} S_m^{-1.8} \tag{2-4}$$

and the tensile strain ε_t was defined by

$$\varepsilon_t = \left[36.43PI - 1.82PI(V_b) + 9.71V_b - 24.04\right] \times 10^{-6} \left(\frac{S_m}{5\times10^{10}}\right)^{-0.36} \left(\frac{N_f}{10^6}\right)^{-0.2} \quad (2\text{-}5)$$

The Asphalt Institute (1982) also developed a fatigue equation, which accounted for the asphalt volume and the percent air voids in the mixture. The equation was based on the constant stress criterion, which can be expressed as

$$N_f = 0.00432C\varepsilon_t^{-3.291}\left|E^*\right|^{-0.854} \quad (2\text{-}6)$$

where C is the correction factor defined by

$$C = 10^M$$

and $$M = 4.84\left(\frac{V_b}{V_a + V_b} - 0.69\right)$$

By assuming a standard mix with an asphalt volume V_b of 11% and air void volume V_a of 5%, which makes M = 0 and C = 1. Also multiplying the equation with a factor of 18.4 to account for the difference between laboratory and field condition, the final fatigue criterion then becomes

$$N_f = 0.0796\varepsilon_t^{-3.291}\left|E^*\right|^{-0.854} \quad (2\text{-}7)$$

where E* is the dynamic modulus.

Even though several fatigue equations have been proposed so far, none of them include all the variables that may affect the fatigue failure on asphalt mixtures. The discrepancy between the number passes to failure predicted from laboratory testing and those observed in the field can be very large due to several environmental variables such as varying temperature and resting period. The studies conducted by Francken (1979) found that the fatigue life of asphalt mixtures increased with longer rest periods.

Despite the imperfections of the proposed models mentioned so far, the method still provide practical solutions to approximate the failure life of pavements while waiting for a more rational mechanistic design.

2.3 Continuum Damage Approach

The continuum damage approach approximates the progression of fatigue cracking in asphalt concrete as a reduction of stiffness due to damage incurred by repeated loading. Lee and Kim (1998a) proposed a viscoelastic constitutive model for asphalt concrete under cyclic loading, which was based on three mechanisms:

- Damage due to micro and macrocracks
- Relaxation of stress in viscoelastic material
- Healing effect of asphalt concrete

Lee and Kim employed the extended elastic-viscoelastic correspondence principle (Schapery, 1984) to convert viscoelastic stress-strain relationships to stress (σ) pseudo strain (ε_R) relationships such that undesirable relaxation effects in the mixture were removed. According to the theory, small tensile loading that does not cause damage in material yields a linear relationship of stress pseudo strain

$$\sigma = E_R \varepsilon^R \tag{2-8}$$

where E_R is the reference modulus, which is an arbitrary constant.

Higher tensile loading that causes damage in material will change the stress pseudo strain from a linear relationship to a nonlinear response with a hysteresis loop. The pseudo stiffness S_R, which defined as the ratio of a stress value to a pseudo strain value at the peak pseudo strain of each cycle, decreases as repeated loading continues. The material is considered to fail when the stiffness is reduced to 50% its original value.

Lee and Kim proposed a viscoelastic constitutive model for asphalt concrete under cyclic load, which was applicable for both stress and strain control

$$\sigma = I\left(\hat{\varepsilon}^R\right)\left[\left(1+\frac{\varepsilon_S^R}{\hat{\varepsilon}_L^R}\right)F(S_n)+G\left(\varepsilon_0^R,\frac{\varepsilon^R}{\varepsilon_L^R}\right)\right] \tag{2-9}$$

where I is the initial pseudo stiffness, $\hat{\varepsilon}^R = \varepsilon^R - \varepsilon_S^R$, which ε^R is the pseudo strain and ε_S^R is the shift of pseudo strain (for stress control mode), $\hat{\varepsilon}_L^R = \varepsilon_L^R - \varepsilon_S^R$, which ε_L^R is the largest ε^R during the ε^R history up to the current time, $F(S_n)$ is the function representing the change in normalized pseudo stiffness, $S_n = S_p/S_f$, which S_p is the damage parameter and S_f is the parameter corresponding to the 50% of the initial pseudo stiffness, The $G\left(\varepsilon_0^R,\frac{\varepsilon^R}{\varepsilon_L^R}\right)$ is the function accounting for the hysteretic behavior of stress - pseudo strain relationship, which is the function of the amplitude of pseudo strain (ε_0^R), ε^R and ε_L^R.

Lee and Kim (1998b) extended their model by including the healing effect that prolonged fatigue life. The healing function was added to the existing model, which was briefly presented in a simple form

$$\sigma = I[F+G+H]\varepsilon_e^R \tag{2-10}$$

where I is the initial pseudo stiffness, F is the function for change in pseudo stiffness, G is a function account for the hysteretic behavior of stress-pseudo strain relationship and the H is the function account for healing effect, $\varepsilon_e^R = \varepsilon^R - \varepsilon_S^R$, which ε^R is the pseudo strain and ε_S^R is the shift of pseudo strain (for stress control mode).

The application of continuum damage approach was first used to evaluate modified and unmodified mixtures for Inchon airport pavements in Korea, Lee, Daniel and Kim (2000). In their work, they used uniaxial tensile test results with cyclic loading to construct the relationship between the number of cycles to failure and strain amplitude. By using elastic layered analysis of the pavement structure, the tensile strain at the bottom pavement can be calculated and used to rank the fatigue life of each mixture. The best mixture was then recommend for the airport project.

The continuum damage approach provides another way to assess the fatigue resistance of mixtures. The method was rational and applicable for both stress and strain control modes. The model was suitable for testing and evaluating mixtures for each project. However, by looking at cracks as continuum damage, the method lacks characteristics associated with the presence of a physical crack such as stress concentration ahead of crack tip and stress redistribution due to crack growth. Therefore the approach may only be suitable for design purposes, but not for analysis of fracture.

2.4 Fracture Mechanics Approach

The science of fracture mechanics was first introduced by Griffith (1920), explaining a quantitative connection between fracture stress and flaw size. Griffith invoked the first law of thermodynamics to formulate a fracture theory based on a simple energy balance. According to his theory, the crack will increase in size if sufficient potential energy is greater than the surface energy of the material. Since then, several researchers embraced fracture mechanics concepts to quantify fracture toughness of asphalt mixtures and develop fracture mechanics-based models to predict crack growth in materials. The fracture mechanics approach used in the field of pavements will be

reviewed under two subtopics: conventional fracture mechanics and the application of fracture mechanics.

2.3.1 Conventional Fracture Mechanics

Asphalt concrete is known as viscoelastic-plastic and temperature dependent material. Under certain conditions such as at low temperature and high strain rate, the material behavior can be approximated with elastic analysis; therefore, early work in the field of pavement fracture mechanics assumed that Linear Elastic Fracture Mechanics (LEFM) is applicable. Material characterization with the fracture mechanics approach normally is conducted in two ways: monotonic loading and cyclic loading. Monotonic loading is used to determine critical stress intensity (K_{Ic}), which refers to fracture toughness of the tested mixtures. The cyclic loading is also performed to obtain fatigue test data for fitting material parameters to specific fatigue cracking models.

There are several test setups that are possible for obtaining the critical stress intensity factor (K_{Ic}) for asphalt concrete. Winnie and Wundt (1958) proposed the following equation for determining K_{Ic} ($Pa\sqrt{m}$) under three point bending test

$$K_{Ic} = 0.521\sigma_c^2 B \tag{2-11}$$

where σ_c is an applied critical remote bending stress (Pa), B = (d-a) (mm), d is a depth of the beam (mm), and a is a crack (notch) depth (mm).

Ewalds and Wanhill (1986) used a collocation method to derive the formula for determining fracture toughness K_{Ic} under three points bending test

$$K_{Ic} = \frac{Pl}{bd^{3/2}} f(\frac{a}{d}) \tag{2-12}$$

where P is a maximum load on the load deflection curve (N), l is a span of the beam (mm), b is a width of the beam (mm), d is a depth of the beam (mm), f(a/d) is a function of crack geometry = A/B, with

$$A = 3\left(\frac{a}{d}\right)^{1/2}\left[1.99 - \left(\frac{a}{d}\right)\left(1 - \frac{a}{d}\right)\left(2.15 - 3.93\left(\frac{a}{d}\right) + 2.7\left(\frac{a}{d}\right)^{2}\right)\right] \quad \text{and}$$

$$B = 2\left(1 + 2\left(\frac{a}{d}\right)\right)\left(1 - \frac{a}{d}\right)^{3/2}$$

Under normal circumstances, traffic and thermal loading create a stress intensity factor (K_I) less than the critical stress intensity (K_{Ic}); therefore, no sudden failure occurs. However, a pavement does crack due to repeated loading. Paris and Erdogan (1963) first discovered the power law relationship for fatigue crack growth in material, which is commonly known as Paris law

$$\frac{da}{dN} = A(\Delta K)^{n} \tag{2-13}$$

where da/dN is the crack growth rate (mm/cycle), ΔK is the range of stress intensity factor (Mpa-$mm^{0.5}$) during repeated loading condition, and A and n are material parameters determined from fitting fatigue test data.

Since the introduction of Paris's law, there have been several proposed models embedded into the da/dN – ΔK relationship. Weertman (1966) developed an alternative semi-empirical equation

$$\frac{da}{dN} = \frac{C\Delta K^{4}}{K_{Ic}^{2} - K_{\max}^{2}} \tag{2-14}$$

where K_{max} is the maximum service stress intensify factor.

Forman (1967) proposed the following equation

$$\frac{da}{dN} = \frac{C\Delta K^{m-1}}{\frac{K_{Ic}}{K_{\max}} - 1} \tag{2-15}$$

where C and m are the material constants

Elber (1970) proposed a modified Paris law

$$\frac{da}{dN} = C\Delta K_{eff}{}^{m} \tag{2-16}$$

where ΔK_{eff} is the effective stress intensity range, defined as $K_{max} - K_{op}$; in which K_{op} is the stress intensity factor at which the crack open.

Klesnil and Lukas (1972) also proposed a modified Paris law to account for a threshold

$$\frac{da}{dN} = C\left(\Delta K^{m} - \Delta K_{th}^{m}\right) \tag{2-17}$$

where the threshold (ΔK_{th}) is a fitting parameter to be determined from a fatigue test.

It is important to note that all Eq.2-13 through Eq.2-17 were not developed from basic mechanics considerations. They are empirical relationships containing two or more constants, which can be determined from experimental test data.

A more mechanics-based model was developed by Ramsamooj (1980). He used the nonlinear differential equation governing subcritical growth of a crack embedded in an elastic-plastic matrix up to the point of gross instability, derived by Wnuk (1971), to formulate a fatigue crack growth model for a beam on elastic foundation

$$\frac{da}{dN} = \frac{\pi}{24K_{Ic}^{2}\sigma_{t}^{2}}\left(\Delta K_{I}^{4} - K_{0}^{4}\right) \tag{2-18}$$

where σ_t is the yield stress in flexural tension, K_I is stress intensity at service load and K_o is the value of stress intensity at endurance limit.

Ramsamooj (1991) then again used the same nonlinear differential equation with an estimated value of plastic zone for asphalt concrete $\Delta = 0.125(K_I/\sigma_t)^2$ to formulate a general expression for fatigue behavior of asphalt concrete under any configuration of loading and boundary conditions

$$\frac{da}{dN} = \frac{K_{Ic}^2}{12\sigma_t^2}\left[\ln\left(1-\frac{K_0^2}{K_{Ic}^2}\right) - \ln\left(1-\frac{K_I^2}{K_{Ic}^2}\right) - \frac{K_I^2}{K_{Ic}^2} + \frac{K_0^2}{K_{Ic}^2}\right] \tag{2-19}$$

Zhang (2000 and 2001) used fracture mechanics principles with linear viscoelasticity to develop a fatigue crack growth model for crack propagation in IDT with center hole specimen under repeated loading. The approach utilized the concept of a plastic zone ahead of crack tip to accumulate damage for each cycle of loading. For the haversine 0.1 seconds load pulse, with a 0.9 second rest period; the damage due to dissipated creep strain energy (DE) per cycle is determined as follows

$$\frac{DE}{cycle} = \int_0^{0.1} \sigma_{avg} \sin(10\pi t)\dot{\varepsilon}_p \sin(10\pi t)dt \tag{2-20}$$

where σ_{avg} is an average stress in the zone of interest, $\dot{\varepsilon}_p$ is a maximum creep strain rate determined from 100 second creep test. According to the energy threshold concept introduced by Zhang (2000), the process zone ahead of the crack tip will accumulate damage, described by dissipated creep strain energy, for each cycle of loading until a dissipated creep strain energy threshold is reached. If the damage level exceeds the energy limit, macrocracks will propagate for the length of the process zone. On the other hand, if the damage level stays below the threshold, only microcracks develop and they are healable after a resting period. With this energy threshold concept, the model

predicted the progression of cracks in a stepwise manner similar to the crack propagation observed in laboratory.

2.3.2 Application of Fracture Mechanics

Since the fracture mechanics approach has been well accepted for analyzing crack growth in material, many researchers have adopted the concepts and applied them to the field of pavements.

Jacobs (1995 and 1996) used fracture mechanics principles to characterize fracture toughness and construct master curves for various tested mixtures. He conducted uniaxial static testing of double edge notch specimen (50x50x150mm) to obtain maximum tensile strength (σ_m) and fracture energy (Γ). He also conducted the fatigue tests of the double edge notch specimen to determine material parameters *A* and *n*. According to his research, he concluded that theoretical derivations for A and n for viscoelastic materials by Schapery (1973, 1975, 1978) appeared to be valid

$$A = \frac{\pi}{6\sigma_m^2 I_1^2}\left(\frac{\left(1-\nu^2\right)D_2}{2\Gamma}\right)^{1/m}\left(\int_0^{\Delta t} w(t)^n\, dt\right), \qquad \text{and} \tag{2-21}$$

$$n = 2\left(1+\frac{1}{m}\right) \qquad \text{for force controlled tests; and}$$

$$n = \frac{2}{m} \qquad \text{for displacement controlled tests}$$

where I_1 is a result of the integration of stress near the crack tip over a small region ahead of the crack tip known as the failure zone, ν is a Poisson ratio, $D(t) = D_o + D_2 t^m$ with, D_o is an initial creep compliance, D_2 is the t = 1 sec. intercept of a line drawn tangent to the double-log creep compliance $\{D(t)-D_o\}$ vs. time plot, t is a current time, m is a slope of

double-log creep compliance vs. time plot, Δt is the period of loading to complete one cycle of loading, w(t) is the wave shape of the stress intensity factor.

Ramsamooj (1993) modified an analytical solution for a thin plate resting on elastic foundation by including 3 cracking conditions: crack through in transverse direction; crack through in longitudinal direction and semi elliptical crack at the bottom of the plate. The formulas can be used to evaluate stress intensity ahead of crack tip for those three types of cracking in pavement.

Collop and Cebon (1995) investigated the causes of cracking on the top and bottom layer of an asphalt concrete pavement. According to their findings, the transverse contact traction may cause a short crack (10 mm) on the pavement surface and the repeated bending tensile stress caused crack at the bottom. They then formulated an analytical solution for determining stress intensity factor for a surface crack in a semi-infinite plate subjected to a general remote stress. They also derived a formula based on parametric studies to quantify the stress intensity factor due to traffic and thermal loading for various pavement structures at progressive crack growth in pavement.

Myers et al. (2000 and 2001) also investigated the mechanism of surface initiated cracking along the wheel path but they used measured tire contact stresses instead of the traditionally assumed circular load. According to their findings, the surface cracking was caused by transverse shear stress of a radial tire and perhaps combined with thermal stress due to rapid cooling. Then they used a fracture mechanics approach with the finite element software ABAQUS to study the propagation of top down cracking. By assuming cracks propagate perpendicular to the major principal (tensile) stress, they found the cracks grew down vertically in the pavement and then bent 30 degrees toward the wheel

load. The predicted crack path was found similar to what has been observed in the field. They also performed parametric studies to quantify the stress intensity factor ahead of the crack tip for various load positions, stiffness ratios and thickness ratios for progressive crack growth in a flexible pavement.

Sangpetngam (2003) has adopted a crack growth model developed by Zhang (2000 and 2001) into a displacement discontinuity boundary element-based pavement fracture simulator. He used crack tip elements to improve accuracy of stress distribution ahead of crack tip and replaced the process zone with yield element. The implementation of crack growth model in the numerical scheme increases the application of fracture mechanics for predicting crack growth in asphalt mixture for various geometries, loading and boundary conditions.

The use of fracture mechanics approach to analyze cracking in material is suitable for problems that experience either a single line or a few distinct lines of fracture. The mechanics of stress concentration and stress redistribution ahead of crack tip that play an important role to the failure in material are very well established. However, the accurate modeling of actual distributed crack bands found in granular materials is still missing in conventional fracture mechanics.

2.5 Displacement Discontinuity Method with Tessellation Schemes

The displacement discontinuity method developed by Crouch (1983) has been extensively used in the fields of rock mechanics and geological engineering. The method has the potential to be an analytical tool for assessing cracking in granular materials such as asphalt concrete. The clear advantage of using this method to analyze crack type problem is that cracks can be explicitly modeled in the medium and the accuracy of stress ahead of crack tip is very good.

The method can be modified to simulate cracking in granular material by creating a numerical model with two types of elements: exterior boundary elements and potential crack elements. The exterior boundary elements are placed along the boundary of a problem to simulate the edge of specimen and potential crack elements are randomly placed inside specimen to simulate predefined crack paths, which normally is assumed to be along the grain boundary or perhaps through grain as well.

The displacement discontinuity boundary element method can be used coupled with various tessellation schemes. The use of tessellations to represent granular structure in simulation of fracture process zone is very well accepted. It improves the realism of predicted failure mechanisms at the particle level. Two basic tessellation schemes Delaunay and Voronoi have been used in various fields. Both tessellations can be used to simulate polycrystalline of ductile material such as Ostoja-Starzewski (1987), Ostoja-Starzewski and Wang (1989), Van der Burg and Van der Giessen (1993), Helms, Allen and Hurtado (1999). The tessellation schemes are also applicable to simulate granular structure of brittle rocks such as Napier and Peirce (1995), Napier et al. (1997), Sellers and Napier (1997) and Steen, Vervoort and Napier (2000). The suitable choice of tessellations to represent granular structure depends on the realistic looks of failure pattern and observed responses.

Napier and Peirce (1995) invented a new boundary element solution technique, termed the “multipole method” for solving multiple interacting crack problem that involved several thousands boundary elements. They used the new technique to study the different failure mechanisms of a rectangular rock sample under displacement control using two tessellations schemes (Delaunay and Voronoi) for three levels of grain

densities. It appeared that Voronoi assemblies are less prone to shed load than the Delauney triangulations. With increasing the density of Voronoi polygons, it seemed to not change this conclusion.

Steen, Vervoort and Napier (2001) took a similar approach but with 3 tessellation patterns, Delaunay, Voronoi and Voronoi with internal fracture path to simulate a confined compression test of a rock sample. It found that the use of Voronoi tessellations with internal fracture paths best simulated the formation of shear band in the specimen. The Delaunay tessellation scheme was the second best while the Voronoi tessellation was not able to predict observed shear banding. The experiments also tested the use of two failure criteria; Rankine criterion (Chen and Han 1988) and Coulomb failure criterion to identify the appropriate failure law that allowed the formation of shear bands. The result of the simulation revealed that only Coulomb failure criterion enabled localization of shear band.

Birgisson et al. (2002a) first introduced the displacement discontinuity boundary element method to simulate crack growth in Superpave IDT specimens. They used exterior boundary elements to create a 2D plain stress specimen and randomly laid down potential crack elements forming Voronoi tessellation inside the specimen. With an appropriate set of material parameters for local failure at potential crack elements, the numerical prediction can capture stress strain responses and crack pattern. Birgisson et al. (2002b) continued studying the tessellation schemes and crack growth rules for simulating crack growth in asphalt mixture. They found that the Voronoi tessellation with internal fracture path provided realistic simulation of crack growth in asphalt mixture because aggregate is allowed to break down at high load level, which results better fit of

stress strain responses. The results of using different two crack growth rules, sequential and parallel, are not significant, but the parallel crack growth rule that activates several cracks at a time is more efficient than the sequential crack growth rule that activates crack one at a time.

Soranakom et al. (2003) used the same numerical schemes as Birgisson et al. (2002b) to evaluate mixture properties. They found that the method was capable of evaluating mixture properties with acceptable accuracy. The predicted results matched vertical compressive stress strain curve, horizontal tensile stress strain curve, crack pattern, tensile strength and fracture energy of the mixes.

The displacement discontinuity method with tessellation scheme as predefined crack paths has demonstrated its ability to simulate crack propagation in granular material such as asphalt concrete. The use of appropriate tessellation to represent grain structure improved the realism of distributed crack in granular material that macrocracks were accompanied by several microcracks.

2.6 Summary

From the literature review presented above, it was concluded that the most appropriate approach for studying the cracking behavior of asphalt mixtures was the displacement discontinuity method with tessellation schemes. The approach provides an elegant way to model aggregate and mastic separately such that the detail of aggregate structure and strength of mastic can be investigated. The approach can be used to identify the key factors that control the cracking mechanism in asphalt mixture. The understanding of microstructure and its cracking behavior will provide the rational recommendation for improving crack resistant mixture.

CHAPTER 3
DISPLACEMENT DISCONTINUITY METHOD WITH TESSELLATION SCHEME

3.1 Overview

Displacement discontinuity method (DDM) is an indirect boundary element method developed by Crouch (e.g. Crouch and Starfield, 1983). The displacement discontinuity boundary element method is uniquely well suited for dealing with problems involving fracture and crack growth. Even though the method is inherently simple to use and very flexible for many kinds of problems in various fields of engineering, it has received little attention compared to the well-known finite element and finite different methods. These are some reasons:

- The misconception that boundary element method is derived for a particular class of problems, and it cannot be applied to other classes of problems. The method may in fact be easily modified for solving other problems.
- Theoretical papers on boundary element method are viewed by many engineers as being somewhat abstruse and sometimes difficult to understand, due to the heavy mathematical detail required. Thus, the complexity of the mathematics involved in deriving the system of equations may have been an obstacle in the proliferation of the boundary element method.

The intention of this chapter is to provide a theoretical background of the displacement discontinuity boundary element method to solve problems involving fracture of materials, particularly cracking in the indirect tension specimen.

3.2 Displacement Discontinuity Method

A physical crack in material can be viewed as a discontinuity surface. The displacement discontinuity method assumes displacements in a body are continuous everywhere except at a line of discontinuity (Figure 3-1). When the displacement crosses

the line of discontinuity, its value jumps by the amount of the displacement discontinuity D_i, in which its components in local axis coordinates y-z are

$$D_i(y_q) = u_i(y_q,0_-) - u_i(y_q,0_+) \quad i = y, z; \qquad -b < y_q < b \tag{3-1}$$

where z = 0+ is the positive side and z = 0- is the negative side of the discontinuity element.

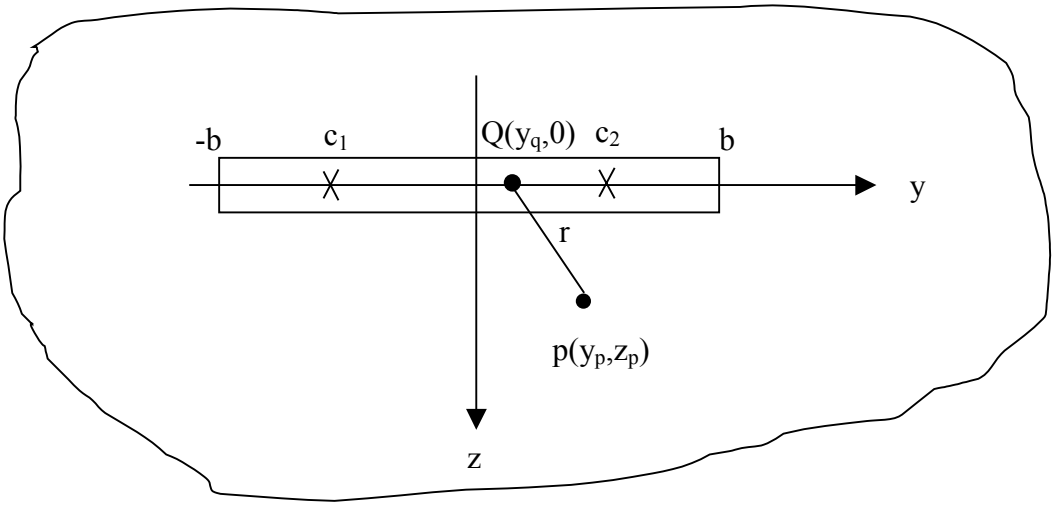

Figure 3-1. Displacement discontinuity element in local coordinate (y-z). A linear discontinuity element has a total length of 2b with two collocation points (c_1 and c_2) at y = + $(\sqrt{2}/2)$b. The distance r is measured from the field point $p(y_p,z_p)$ in the domain to the source point $Q(y_q,0)$ at boundary.

In two-dimensional plane strain problems, if the line of discontinuity has a length of 2b, centered on the y-axis of a local coordinate system y-z, and has normal vector components n_y and n_z along the surfaces, it can be shown (Peirce and Napier 1994) that the contribution of a given element to the total displacement components at point p is

$$\begin{bmatrix} u_y(p) \\ u_z(p) \end{bmatrix} = \frac{1}{8\pi(1-\nu)} \int_{-b}^{b} \begin{bmatrix} L_y & M_y & N_y \\ L_z & M_z & N_z \end{bmatrix} \begin{bmatrix} D_y(y_q)n_y \\ \frac{1}{2}(D_y(y_q)n_z + D_z(y_q)n_y) \\ D_z(y_q)n_z \end{bmatrix} dy_q \tag{3-2}$$

where u_y, u_z are the local components of the displacement vector, ν is Poisson ratio and the symbols in the matrix are given by

$$L_y = (1-\nu)\Psi_{,yyy} + (2-\nu)\Psi_{,yzz}$$

$$M_y = -\nu\Psi_{,yyz} + (1-\nu)\Psi_{,zzz}$$

$$N_y = \nu\Psi_{,yyy} - (1-\nu)\Psi_{,yzz}$$

$$L_z = -(1-\nu)\Psi_{,yyz} + \nu\Psi_{,zzz}$$

$$M_z = (1-\nu)\Psi_{,yyy} - \nu\Psi_{,yzz}$$

$$N_z = (2-\nu)\Psi_{,yyz} + (1-\nu)\Psi_{,zzz} \qquad (3\text{-}3)$$

The biharmonic function for plain strain problem is given by

$$\Psi = \frac{1}{2}(r^2 - r^2 \log r^2) \qquad \text{and} \qquad r^2 = (y_p - y_q)^2 + z_p{}^2 \qquad (3\text{-}4)$$

It can also be demonstrated (Peirce and Napier 1994) that, the contribution of the element to the total stress tensor components at point p is

$$\begin{bmatrix} \sigma_{yy}(y_p, q_p) \\ \sigma_{yz}(y_p, q_p) \\ \sigma_{zz}(y_p, q_p) \end{bmatrix} = \frac{E}{8\pi(1-\nu^2)} \int_{-b}^{b} \begin{bmatrix} -\Psi_{,zzzz} & \Psi_{,yzzz} & -\Psi_{,yyzz} \\ \Psi_{,yzzz} & -\Psi_{,yyzz} & \Psi_{,yyyz} \\ -\Psi_{,yyzz} & \Psi_{,yyyz} & -\Psi_{,yyyy} \end{bmatrix} \begin{bmatrix} D_y(y_q)n_y \\ D_y(y_q)n_z + D_z(y_q)n_y \\ D_z(y_q)n_z \end{bmatrix} dy_q$$

(3-5)

For numerical implementation, the displacement discontinuity D_i is approximated by a polynomial function, $y = a_0 + a_1x^1 + a_2x^2 + \ldots + a_nx^n$. More accurate results can be obtained by using several terms in the approximation, but it will increase computing time. It is sufficient for most practical applications to approximate the displacement discontinuity with a linear function as was done in the Discontinuity Interaction and Growth Simulation (DIGS) program, (Napier, 1990; Napier and Hildyard, 1992; Napier

and Pierce, 1995a; Malan and Napier, 1995; Kuijpers and Napier, 1996; Napier at el., 1997; Napier and Malan, 1997). The linear variation of discontinuity can be written as

$$D_i(y_q) = a_i + b_i y_q \qquad a_i \text{ and } b_i \text{ are constants} \qquad (3\text{-}6)$$

By substituting Eq.3-6 into Eq.3-5, and carrying out the mathematical manipulation, the analytical solution for normal stress on the y-axis of the local coordinate system (y-z) will have the form:

$$\sigma_{zz}(y,0) = \frac{E}{8\pi(1-\nu^2)}\left[2(\alpha_z + \beta_z y)\left(\frac{1}{y+b} - \frac{1}{y-b}\right) + \beta_z \log\left(\frac{y+b}{y-b}\right)^2\right] \qquad (3\text{-}7)$$

It is obvious from Eq.3-7 that the analytical normal stress σ_{zz} approaches infinity as y approaches the tip of the element $y = \pm b$. However, in boundary element formulations, stress in Eq.3-7 is evaluated at suitable collocation points $y = \pm c$, namely the Gauss-Chebyshev points (Crawford and Curran, 1982)

$$y_i = \cos(2i-1)\frac{\pi}{2n} \qquad i = 1, 2 \ldots, n \qquad (3\text{-}8)$$

The stresses at collocation points will have finite values and are solvable using a numerical algorithm.

3.3 Numerical Implementation

For numerical implementation, the displacement discontinuity method (DDM) employs the known solutions of the discontinuity surface to formulate a system of governing equations. For a problem with one crack in the infinite elastic body without far field stresses, the general system of governing equations can be written as:

$$\sigma_s^i = \sum_j (A_{ss}^{ij} D_s^j + A_{sn}^{ij} D_n^j)$$

$$\sigma_n^i = \sum_j (A_{ns}^{ij} D_s^j + A_{nn}^{ij} D_n^j) \qquad (3\text{-}9)$$

where σ_s^i and σ_n^i are the shear and normal stress of the element i. A_{ss}^{ij}, A_{sn}^{ij}, A_{ns}^{ij} and A_{nn}^{ij} are the influence coefficients due to element j on element i, and D_s^j and D_n^j are the displacement discontinuity components of element j, which are the unknowns of the system.

In simulations of crack interaction problems, a displacement discontinuity element will slide when driving shear stress exceeds shear strength or open up when applied tensile stress exceeds tensile strength. Even if the DDM was initially developed for an open crack, it can easily be extended to include contacting crack surfaces and sliding cracks in softening mode.

When two crack surfaces are in contact, the shear and normal stress components σ_s^i and σ_n^i depend on the stiffness (K_s and K_n) and the displacement discontinuity components (D_s^i and D_n^i). The relationships can be written in matrix forms as follows

$$\sigma_s^i = K_s D_s^i$$

$$\sigma_n^i = K_n D_n^i \tag{3-10}$$

By substituting Eq.3-10 into Eq.3-9 and rearranging the terms so that the unknowns are on the right hand side, the system of governing equations then becomes

$$0 = \sum_j (A_{ss}^{ij} D_s^j + A_{sn}^{ij} D_n^j) - K_s D_s^i$$

$$0 = \sum_j (A_{ns}^{ij} D_s^j + A_{nn}^{ij} D_n^j) - K_n D_n^i \tag{3-11}$$

When an element mobilizes, the crack surface will deform according to softening models, which will be described shortly in the next section. The residual strength of the

element i, namely σ_s^i and σ_n^i can be assumed to decrease as a function of the displacement discontinuities D_s^i and D_n^i, which can generally be expressed by

$$\sigma_s^i = f_s(D_s^i, D_n^i)$$

$$\sigma_n^i = f_n(D_s^i, D_n^i) \tag{3-12}$$

Substituting Eq.3-12 in Eq.3-9, and rearranging the unknowns to the right hand side, the system of equations becomes

$$0 = \sum_j (A_{ss}^{ij} D_s^j + A_{sn}^{ij} D_n^j) - f_s(D_s^i, D_n^i)$$

$$0 = \sum_j (A_{ns}^{ij} D_s^j + A_{nn}^{ij} D_n^j) - f_n(D_s^i, D_n^i) \tag{3-13}$$

Finally, a set of algebraic equations that consist of known driving forces, influence coefficients and the unknown displacement discontinuities can be written in a matrix form, $\{\sigma\} = [A]\{D\}$. Since the mobilization of cracks is associated with a softening model in which stresses depend on the unknown discontinuities, an iterative technique needs to be employed in solving the equations. DIGS use an efficient multi-pole method (Napier and Peirce1995a) for iterative solving. Once displacement discontinuities at all boundary elements have been determined, displacements and stresses at any designated points can be computed by using Eq.3-2 and Eq.3-5.

3.4 Example of a Crack Growth Model using DIGS

A numerical model for a Superpave indirect tension test (IDT) specimen consists of two types of elements: exterior boundary elements and potential crack elements. The exterior boundary elements are regular boundary elements that are employed to construct an edge of a specimen. Potential crack elements on the other hand allow the element to mobilize (slip or open up) when the stress exceeds a failure limit. Therefore, they are

randomly placed inside the specimen to form any desired tessellations to represent granular structure. Figure 3-2 shows examples of using three tessellations, Delaunay, Voronoi and Voronoi with internal fracture paths, to simulate the aggregate structure of an IDT specimen.

During the analysis, at each load step, stresses are computed at collocation points inside potential crack elements. The stress state at these locations is then checked against a failure limit to determine the activation of a crack. In DIGS, a nonlinear failure law, shown in Figure 3-3, is adopted for the cracking criterion. The failure law consists of a linear portion in the compression region (similar to the Mohr-Coulomb failure law) and a power law curve in the tension region, with a continuous slope at $\sigma_n = 0$. The linear portion has the following form

$$\tau = S - \tan(\phi)\sigma_n \qquad when\ \sigma_n < 0 \tag{3-14}$$

where S is the cohesion, ϕ is the friction angle and σ_n is the normal stress (tension positive) across the discontinuity. The power law curve is defined by:

$$\tau = a(\sigma_t - \sigma_n)^b \qquad when\ \sigma_n > 0 \tag{3-15}$$

where σ_t is the tensile strength and the two constant "a" and "b" are the parameters that fit the power law curve to the tension cutoff T_o at shear stress $\sigma_s = 0$ and the linear portion at normal stress $\sigma_n = 0$.

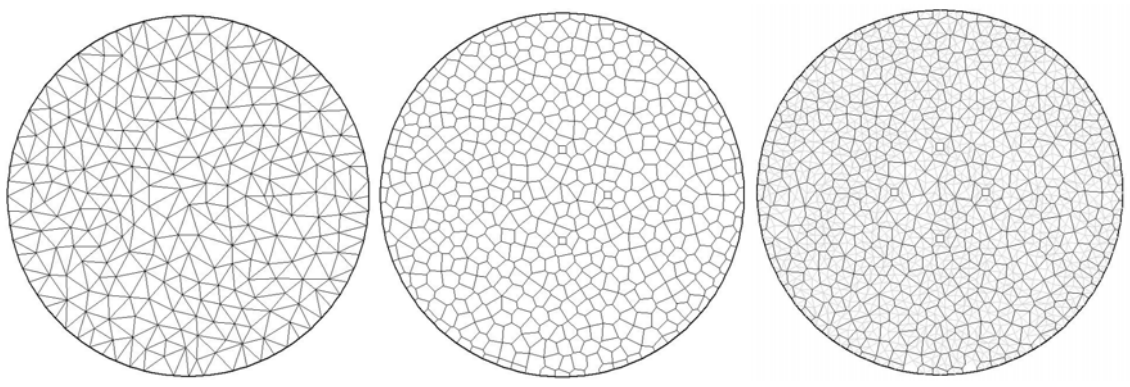

A B C

Figure 3-2. Tessellations for granular structures. Aggregate structure in indirect tension specimen can be represented by three basic tessellations: A) Delaunay, B) Voronoi and C) Voronoi with internal fracture path. Each tessellation has 503 particles, which yields an equivalent aggregate size of 6.8 mm.

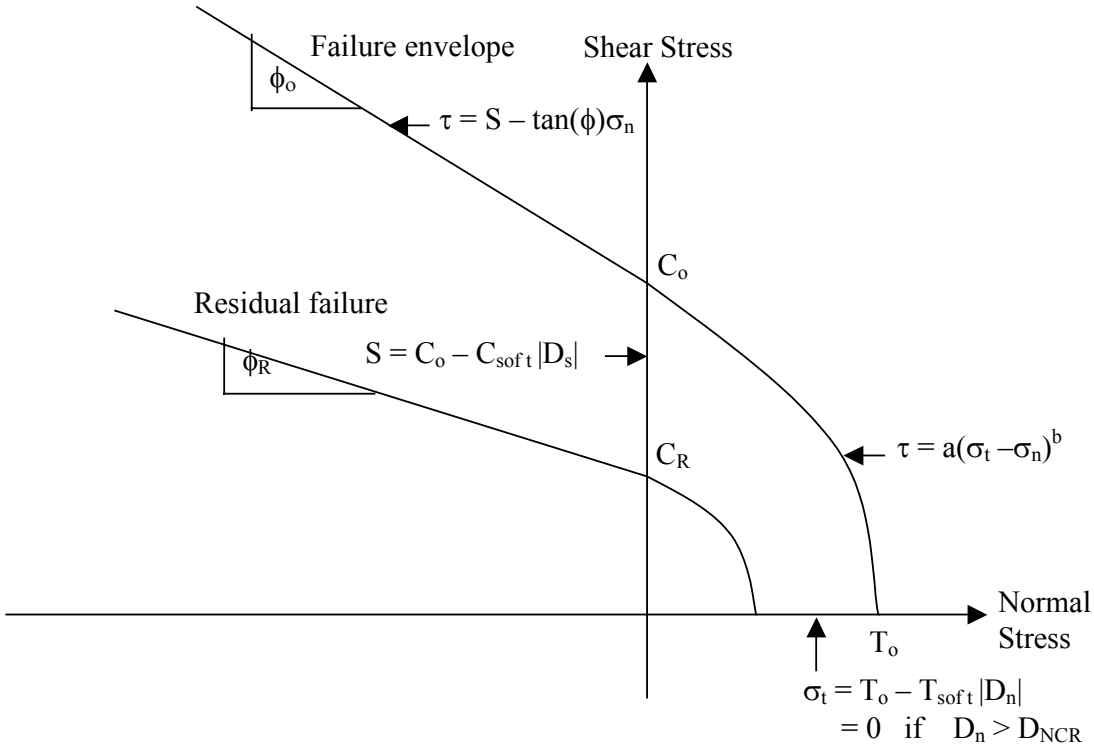

Figure 3-3. Mohr Coulomb type of failure criterion for determining crack mobilization.

For every load step, a crack search algorithm is performed to detect cracks that may occur in the specimen. There are two crack search algorithms available in DIGS, namely parallel and sequential. The parallel crack search activates all elements where the stress exceeds the failure limit. Alternatively, the sequential crack search activates only the most overstressed element found in system; thus, only the most critical crack element is activated. At the end of each search step, the detected cracks are added to the system and resolved for new stress pattern to determine new cracks in the next search step, until no more cracks found.

When potential crack element turn into a cracked state, the cohesion S is assumed to weaken as a linear function of the slip D_s

$$S = C_o - C_{soft} \mid D_s \mid \tag{3-16}$$

where C_o is the original cohesion intercept and C_{soft} is the cohesion softening slope. Similarly, the tensile strength σ_t is also assumed to weaken as a linear function of the opening displacement D_n

$$\sigma_t = T_o - T_{soft} \mid D_n \mid \tag{3-17}$$

where T_o is the tension cutoff and T_{soft} is the tension softening slope. When crack slip occurs, the tensile strength is implicitly degraded as the cohesion softens, congruently with the extent of cohesion softening. The tensile strength completely gone when the opening crack (D_n) exceeding the opening crack limit (D_{NCR})

CHAPTER 4
NUMERICAL EXPERIMENTS OF THE SUPERPAVE INDIRECT TENSION TEST USING THE DISPLACEMENT DISCONTINUITY METHOD WITH A TESSELLATION SCHEME

4.1 Overview

This chapter provides the results of a series of parametric studies that systematically evaluate the factors and parameters needed to successfully simulate the SUPERPAVE indirect tension (IDT) strength test. The appropriate set of tessellation and crack growth rules are identified, and the use of different grain sizes to represent actual gradation was also conducted to identify the optimal size that would yield the most consistent result for numerical simulations. Finally, a sensitivity study of material parameters defined for mastics and aggregate were performed to study their effects on the load-deformation and cracking behavior in the IDT strength test.

Since the displacement discontinuity method can be used to simulate different kinds of materials such as rock, concrete and asphalt concrete, a typical IDT test result of granite mixture (Nova Scotia NS619) was used to provide the target for modeling asphalt concrete. First, the input parameters (global and micro-mechanics-based parameters) for the displacement discontinuity boundary element method were calibrated so that the resulting predicted stress-strain curves matched the experimental curves. Then each component and material parameter was altered from the calibrated fit model to observe the sensitivity of the predicted results (stress-strain curves) and identify the best combination. The scopes of numerical studies were summarized below.

- Determination of appropriate tessellation schemes and crack growth rules

- Determination of uniform aggregate size to represent gradation
- Sensitivity analysis of material parameters defined for mastics
- Sensitivity analysis of material parameters defined for internal fracture path (aggregate):

After performing all analysis stated above, the appropriate set of tessellation, crack growth rules and material parameters were proposed for numerical simulation of indirect tension strength test.

4.2 Laboratory Experiment of Nova Scotia Mixture

A SuperPave^{TM} IDT strength test at 0°C was performed to obtain the experimental results used in this study. The IDT specimen was prepared according to the SuperPave^{TM} specifications. The aggregate used was granite from Nova Scotia. The gradation shown in Table 4-1 was used to design a 19-mm (0.75 in) nominal maximum aggregate size coarse-graded mix. AC-30 asphalt was used with the design content of 5.5% at N_{design} = 109 revolutions in the SuperPave^{TM} gyratory compactor. The asphalt and the aggregate were mixed at 150 °C (302°F) and subjected to short-term oven aging for two hours at 135°C (275°F). For the strength testing, specimens were compacted to produce three 4500 g (9.9 lbs), 152.4 mm (6 in) diameter gyratory compacted specimens with an air void content of 7% ($\pm$ 0.5%). All aggregate and volumetric properties of the mixture met SuperPave^{TM} requirements.

Table 4-1. Gradation of the Nova Scotia mixture

Sieve size (sieve number)	Percent passing
25 mm (1)	100
19 mm (3/4)	97
12.5 mm (1/2)	83
9.5 mm (3/8)	66
4.75 mm (#4)	38
2.36 mm (#8)	23
1.18 mm (#16)	18
600 μm (#30)	14
300 μm (#50)	10
150 μm (#100)	6.5
75 μm (#200)	3.5

The gyratory compacted specimens were sliced to obtain SuperPave^{TM} IDT test specimens, with an approximate diameter of 152.4 mm (6 in) and 50.8 mm (2 in) thickness. The IDT strength test was performed according to the SHRP Indirect Tension test procedure, presented by Roque et al (1997). A summary result of IDT strength test is shown in Table 4-2.

The applied load, horizontal and vertical deformation measured at each face of a sample can be represented by horizontal and vertical stress strain curves at the center using IDT plane stress formula as follows

$$\sigma_h = 2P/(\pi Dt)$$

$$\varepsilon_h = \Delta H/L_{gauge}$$

$$\sigma_v = 6P/(\pi Dt)$$

$$\varepsilon_v = \Delta V/L_{gauge} \qquad (4\text{-}1)$$

where, σ_h is a horizontal stress at the center of specimen, P is a total load applied, D is a diameter of a specimen, t is a thickness of a specimen, ε_h is an average horizontal strain

over a horizontal strain gauge, ΔH is a corrected horizontal deformation at a horizontal strain gauge, L_{gauge} is a gauge length, σ_v is a vertical stress at the center of specimen, ε_v is an average vertical strain over a vertical strain gauge, and ΔV is a corrected vertical deformation at a vertical strain gauge. Finally, the horizontal and vertical stress strain curves on each face of the sample were averaged and used for comparison to the numerical prediction, which will be described shortly in the next section.

Table 4-2. Material properties from IDT strength test

Parameters	Value
Tensile strength (MPa)	2.05
Fracture energy (MPa)	0.83
Poisson ratio	0.35

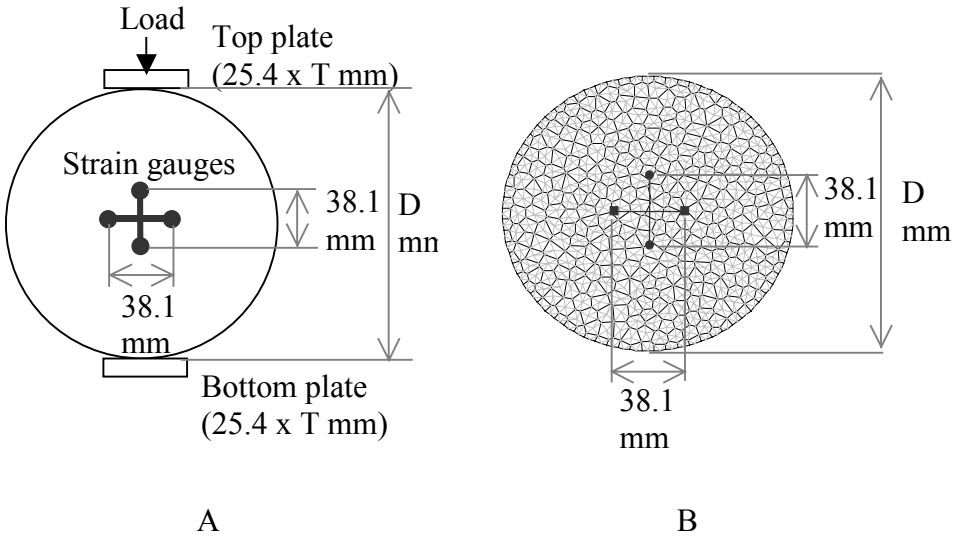

Figure 4-1. Indirect tension strength test: A) Experimental setup and B) Displacement discontinuity model.

4.3 Numerical Simulations

The experimental setup and the associated numerical model for the Superpave IDT strength test are shown in Figure 4-1. The specimen size is 152.4 mm (6") in diameter and varying in thickness (T mm). Two end plates 25.4 mm x T mm (1" x T") at the top

and the bottom are used to protect the damage to specimen due to high concentrated load. At the center of specimen, two strain gauges 38.1 mm (1.5") are placed in the vertical and horizontal directions to measure vertical and horizontal deformations in the central zone.

Figure 4-1B shows an IDT numerical sample using Voronoi with internal fracture path to represent aggregate structure. Four field points (acting like virtual strain gauges) are placed at the locations of the actual strain gauges to monitor the displacements at each load step. The perimeter of the numerical model is comprised of 152 exterior boundary elements. Of those, 8 elements are placed at the top and forced to move downward to simulate displacement control. Other 8 elements at the bottom are fixed to provide a static condition. The remaining 136 elements along the circumference are specified with zero traction to simulate traction free surface.

The displacement controlled loading was performed in 12 equal steps for a total displacement of 0.36 mm. For perfect displacement control, the predicted stress distributions at the load plates are nonuniform and they become significantly fluctuated when crack approaches the end plates. For the comparison to the actual testing results, the applied load was approximated by the average stress at the top and bottom plates multiplied with the plate area. The horizontal and vertical deformations in the center part of the specimen can be obtained by determining the relative movement of the displacements requested at the virtual strain gauges. Finally, the predicted stress strain curves for horizontal and vertical direction were computed and represented in the same way as the experiment by using Eq.4-1.

4.4 Determination of Suitable Tessellation Schemes and Crack Growth Rules

The identification of an appropriate tessellation scheme and crack growth rule was an iterative process since the effects of other relevant components such as particle size

and material parameters for the mastic and aggregate were not yet fully known. Several attempts to model IDT strength test Birgisson et at (2002 a-b) and Soranakom (2003) had previously been performed in which it was shown that it was possible to fit the stress strain curves and correctly predict the crack pattern observed in the laboratory. However, some issues still needed to be studied further, namely the establishment of a representative optimal Voronoi particle size for a given gradation, and other issues related to the "tuning" of the micromechanical material parameters. In the following, the insight gained from previous work (Birgisson, et al., 2002a-b) will be used to identify a suitable tessellation scheme and crack growth rule.

4.4.1 Numerical Experiment

Three tessellations Delaunay triangulation, Voronoi polygons and Voronoi polygons with internal fracture paths, shown in Figure 3-2, were used to model the aggregate structure of the Nova Scotia mixture. Each tessellation has 503 particles filling the circular area of 18240 mm^2, which yields an equivalent aggregate size of 6.8 mm or at D_{50} (aggregate size at 50% passing of the gradation). All three tessellation schemes were used to simulate the Superpave IDT strength test. The predicted stress-strain curves and crack patterns were then compared to the experimental results obtained for the Nova Scotia mixture. For each tessellation scheme, two crack growth rules, parallel and sequential, were compared. The modeling matrix, global and local material parameters used for the numerical experiments are provided in Table 4-3 through Table 4-5. It is note that material parameters defining mastic strength and its residual strength for Delaunay tessellation are substantially higher than those for Voronoi and Voronoi with internal fracture path in order to ovoid unstable collapsing and produce the best fit to the experimental stress strain curves.

Table 4-3. Modeling matrix for the study of suitable tessellation schemes and crack growth rules

	Tessellation schemes					
	Delaunay		Voronoi		Voronoi with internal fracture path	
Crack growth rule	Parallel	Sequential	Parallel	Sequential	Parallel	Sequential
Equivalent aggregate size (mm)	6.8	6.8	6.8	6.8	6.8	6.8
Number of potential crack element for mastic	720	720	1408	1408	1408	1408
Number of potential crack element for fracture path	-	-	-	-	2717	2717

Table 4-4. Global linear elasticity parameters for the study of suitable tessellation schemes and crack growth rules

Parameter	Value
Young modulus (MPa)	7500
Poisson ratio	0.35

Table 4-5. Local material parameters for the study of suitable tessellation schemes and crack growth rules

	Tessellation schemes			
	Delaunay	Voronoi	Voronoi with internal fracture paths	
Material parameters	Mastic	Mastic	Mastic	Internal fracture pahts
Tension cutoff, T_o (MPa)	4.00	2.30	2.30	6.50
Opening crack limit, D_{NCR} (mm)	0.15	0.11	0.11	0.07
Tension softening slop, T_{soft} (MPa/mm)	26.67	20.91	20.91	92.86
Cohesion, C_o (MPa)	4.00	2.40	2.40	6.50
Residual cohesion, C_R (MPa)	1.00	0.15	0.15	0.15
Cohesion softening slop, C_{soft} (MPa/mm)	0.50	5.00	5.00	1.00
Friction angle, ϕ_o (degree)	45	38	38	40
Residual friction angle, ϕ_R (degree)	44	30	30	32

4.4.2 Results from Numerical Simulations

The result of the numerical simulations will be discussed in the next four sections entitled: Crack growth rules, Delaunay tessellations, Voronoi tessellations, Voronoi tessellations with internal fracture path, followed by a summary of findings for the optimal crack growth rule and suitable tessellation scheme.

4.4.2.1 Crack Growth Rules

Figure 4-2 shows the amount of cracking predicted by the two crack growth rules: parallel and sequential. Both predicted approximately the same number of cracks for all load steps up to the load step at the peak of the stress-strain curves (load step 10 for the Delaunay tessellation scheme, load step 9 for Voronoi tessellation scheme and Voronoi with internal fracture path scheme (Figure 4-3 – 4-5). In the post peak region, the sequential crack growth rule predicted fewer cracks than the parallel did. Parallel and sequential crack growth rules also yielded approximately the same stress strain responses up to the peak, but started to deviate slightly in the post peak. The small differences in the post-peak stress-strain response were due to the differences in predicted post-peak crack patterns.

Figure 4-6 shows a comparison of the predicted crack patterns obtained with the three tessellations and the two crack growth rules studied. All the predicted crack patterns showed similar patterns - a major vertical opening crack in the middle region of the specimen, accompanied by several smaller size cracks, distributed over a wider band through the center of the specimen. Overall, two crack growth rules yielded approximately the same result for both predicted stress strain responses and crack patterns. However, the sequential crack growth rule that activates the most overstressed

element one by one is more computationally intensive than the parallel crack growth rule that activates all overstressed elements at the same time. Thus, in the following, the parallel crack growth rule is used in all remaining simulations.

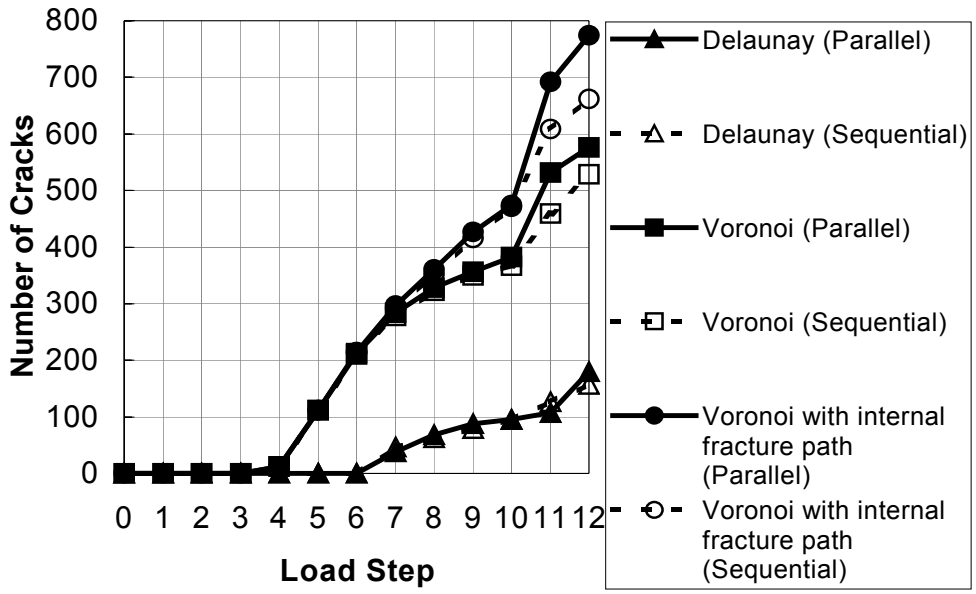

Figure 4-2. Predicted number of cracks at each load step. Three tessellations, Delaunay, Voronoi and Voronoi with internal fracture path were used with two crack growth rules, Parallel and Sequential

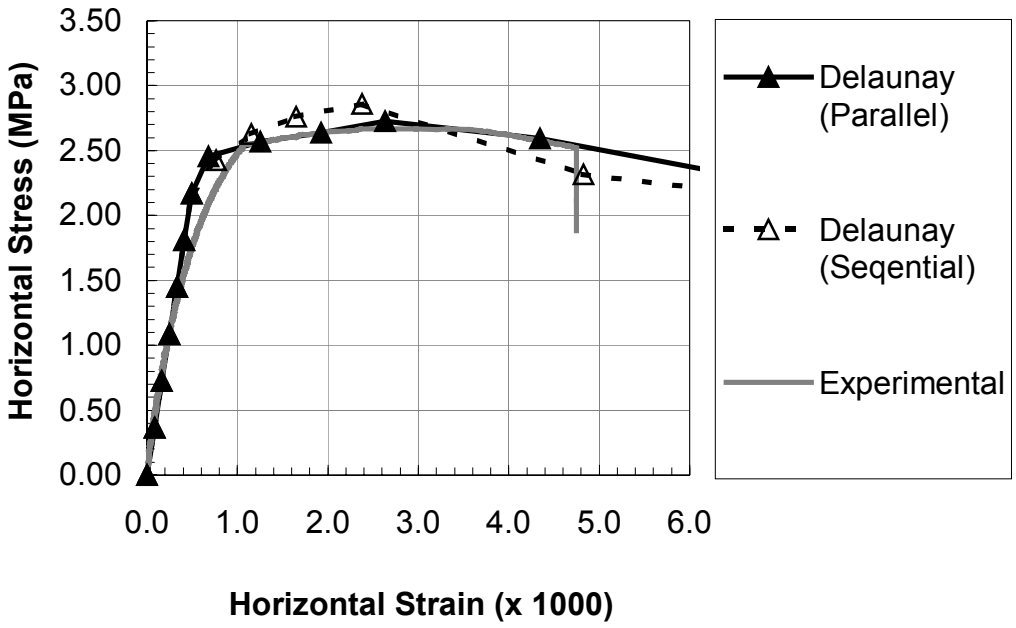

A

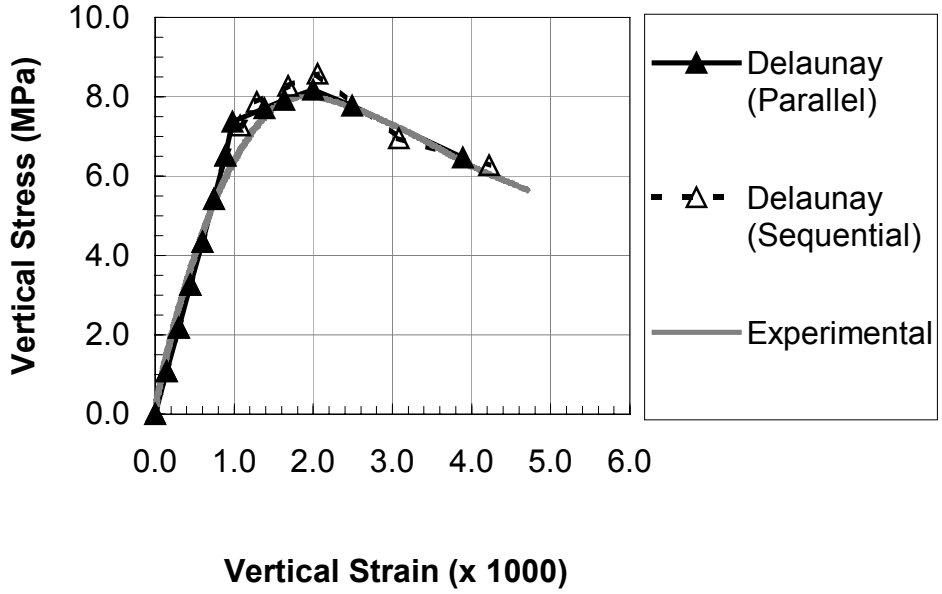

B

Figure 4-3. Comparison of predicted and measured horizontal and vertical stress-strain curves, using Delaunay tessellation: A) Horizontal stress-strain response at center of specimen and B) Vertical stress-strain response at center of specimen.

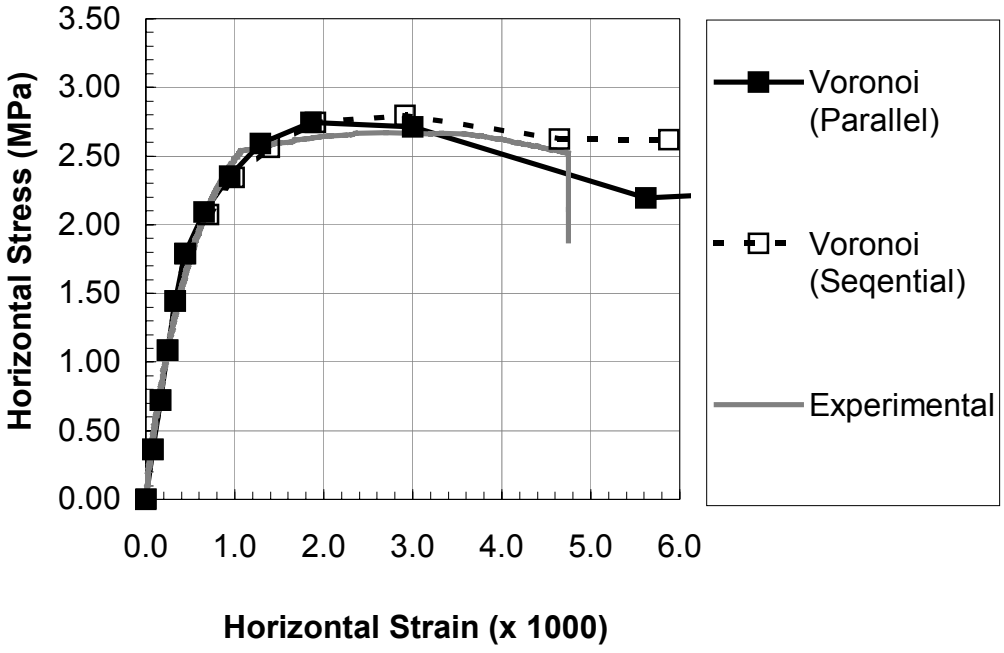

A

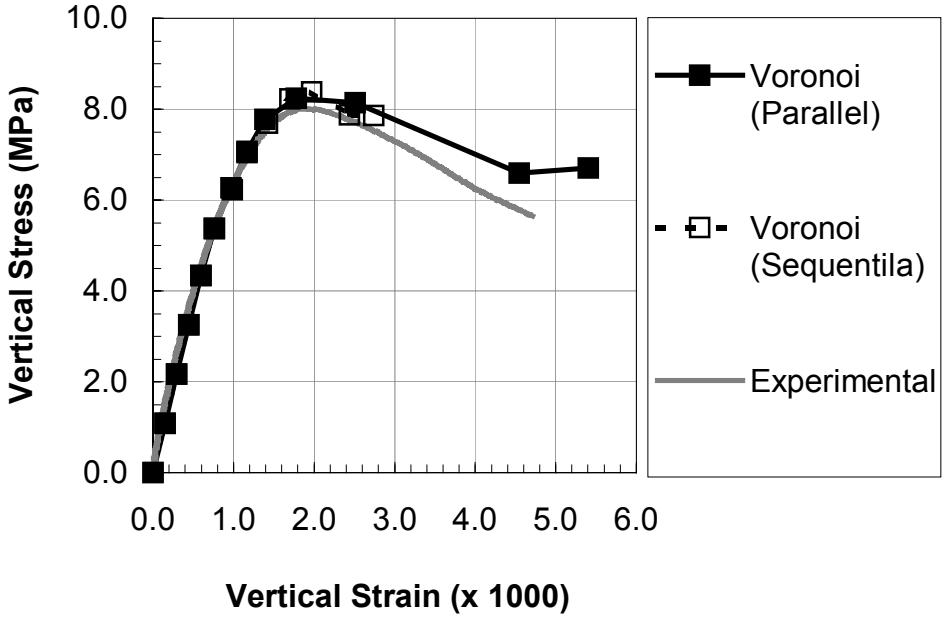

B

Figure 4-4. Comparison of predicted and measured horizontal and vertical stress-strain curves, using Voronoi tessellation: A) Horizontal stress-strain response at center of specimen and B) Vertical stress-strain response at center of specimen.

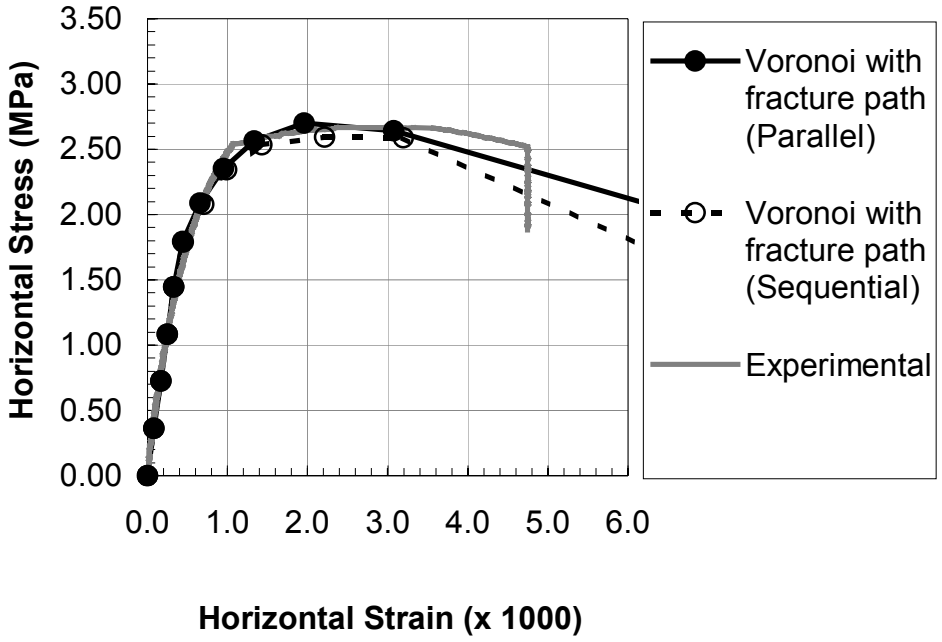

A

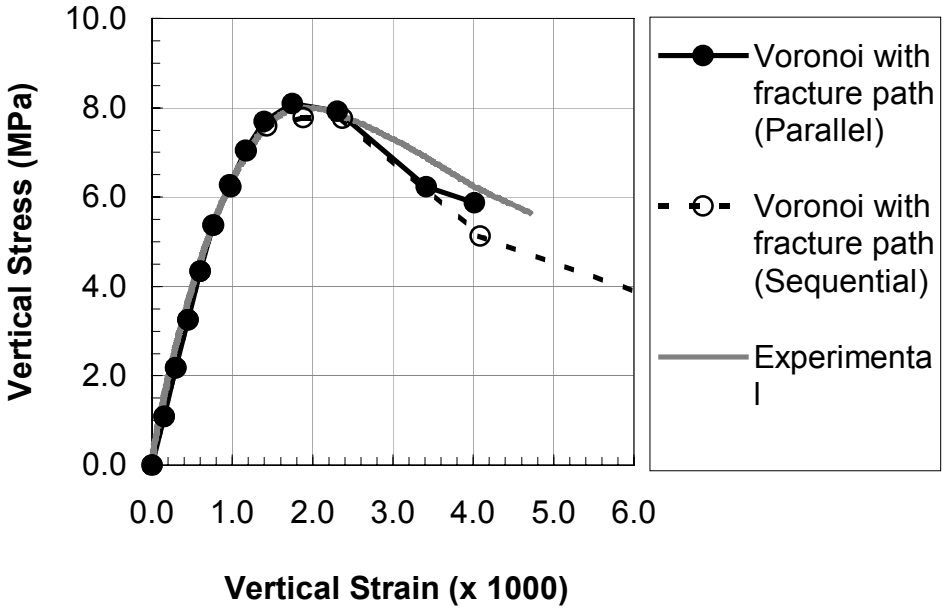

B

Figure 4-5. Comparison of predicted and measured horizontal and vertical stress-strain curves, using Voronoi with internal fracture path tessellation: A) Horizontal stress-strain response at center of specimen and B) Vertical stress-strain response at center of specimen.

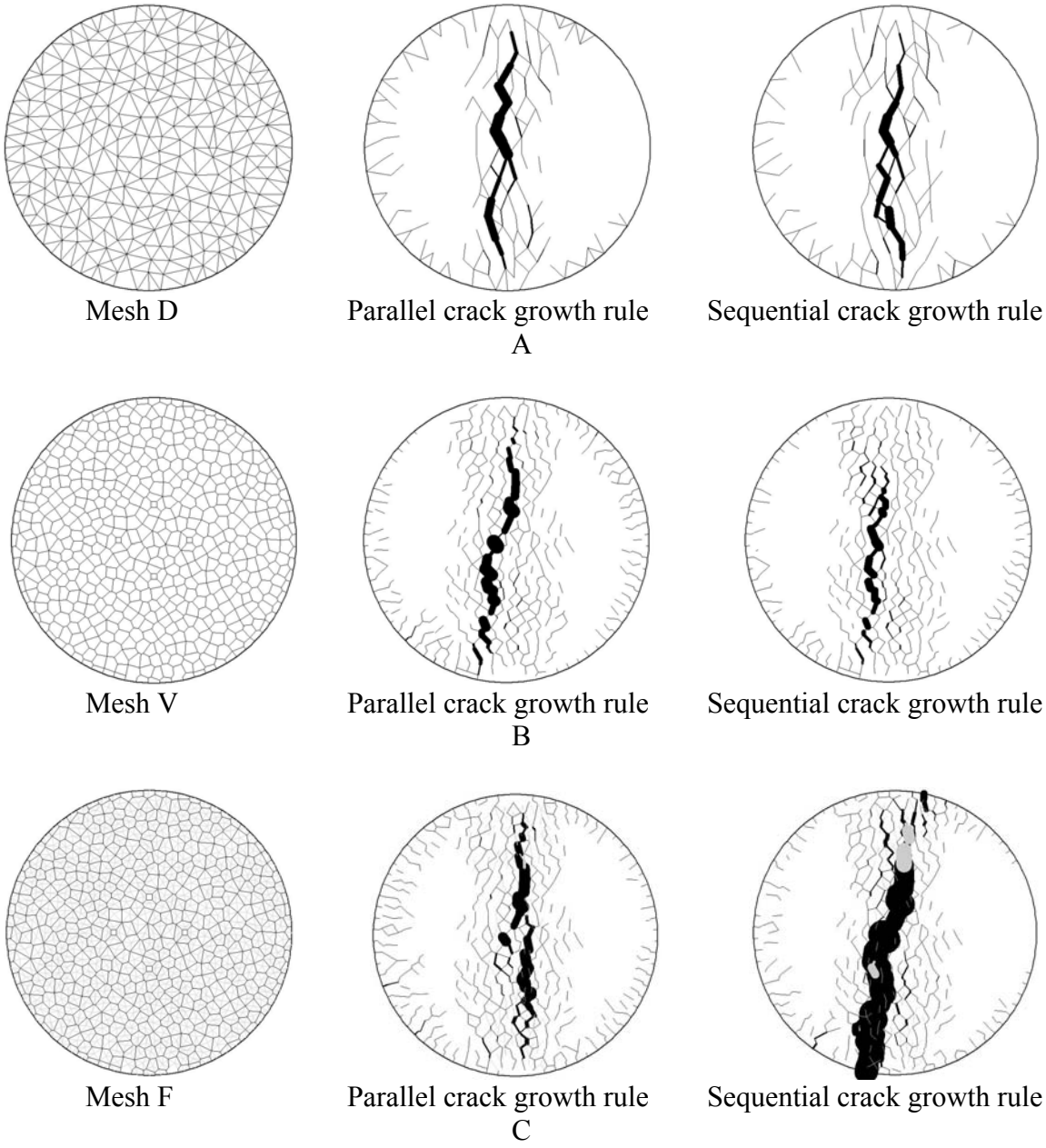

Figure 4-6. Crack patterns predicted by two crack growth rules of three tessellations: A) Delaunay, C) Voronoi and C) Voronoi with internal fracture path.

4.4.2.2 Evaluation of Delaunay Tessellation Scheme

Figure 4-6A shows a crack pattern predicted by a Delaunay tessellation scheme. The dominant large crack pattern is similar to those predicted using the Voronoi tessellation schemes (Figure 4-6B and 4-6C). The narrower band of distributed cracks, as compared to the Voronoi schemes is simply the result of using higher strength and residual strength of the mastics. In Delaunay scheme, cracks appearing on one side of a triangular particle were able to work their way to the other side easily, creating floating particles (particles completely surrounded by cracks), which weaken aggregate structure in carrying compression load. In some cases, these "floating particles" occurred in the area of the virtual strain gauge points, resulting in almost a rigid body motion. This unstable movement could be minimized by increasing the residual strength parameters of the mastic in the model.

In order to use the Delaunay tessellation structure to model the IDT strength test, substantially higher mastic strength than Voronoi tessellations and Voronoi tessellations with internal fracture path was needed. Despite using the best possible set of material parameters, the Delaunay can only obtain a rough match to the experimental stress strain responses as shown in Figure 4-3, the predicted stress-strain curves were not smooth and did not fit very well. The parameters for residual strength were unreasonable high for such a brittle material asphalt concrete. Therefore, it was concluded that the use of Delaunay tessellation scheme to model the aggregate structure for the Nova Scotia asphalt mixture studied was unsuccessful.

4.4.2.3 Evaluation of Voronoi Tessellation Scheme

Figure 4-6B shows the crack pattern at the final load step predicted using the Voronoi tessellation scheme to represent the aggregate structure of the Nova Scotia

mixture. Multiple cracks formed a wide band of cracks, within which, the material appeared to form a columnar structure defined by the overall cracking pattern. Those "broken columns" were still able to provide some strength in carrying compressive load from the top to the bottom of the specimen. This mechanism resulted in a simulated compressive softening of the ascending (near peak) portion of the predicted vertical stress strain curve (Figure 4-4B). At higher load levels, the number of distributed cracks and the size of opening crack increased, resulting in a rapidly decreased strength. Once the major opening cracks occur, the strength of specimen was diminished. By specifying appropriate values of residual strength parameters, the simulations were able to capture the post peak stress-strain response. Finally, the simulations of IDT strength test using Voronoi tessellation schemes revealed a difficulty in tuning the material properties for the mastics to adequately match experimentally observed peak and post peak load deformation responses.

4.4.2.4 Evaluation of Voronoi with Internal Fracture Paths Tessellation Scheme

Figure 4-6C shows the predicted crack pattern at the final load step predicted using a Voronoi tessellation scheme with internal fracture paths to represent aggregate structure. The predicted cracking patterns were similar to that obtained from the Voronoi tessellation scheme, except that some of the aggregates broke down at high load levels. The additional parameters for defining the aggregate can be modeled such that the predicted stress strain responses (Figure 4-5) can fit to the experimental results better. Finally, the Voronoi tessellations with internal fracture paths seemed to reasonably represent the observed load deformation behavior of the granular structure of the Nova Scotia mixture.

4.4.3 Summary of Findings on the Determination of a Suitable Crack Growth Rule and Tessellation Scheme

From the results presented, the use of Voronoi tessellations with internal fracture paths and the parallel crack growth rule resulted in reasonable simulations that corresponded with experimental stress strain curves and fracture patterns.

4.5 Determination of Average Voronoi Aggregate Size to Represent Gradation

4.5.1 Numerical Experiment

This study was conducted to identify the optimal aggregate size for the simulation of IDT strength test. A Voronoi tessellation scheme with internal fracture path (medium size 8.0 mm) was first tuned to match the experimental stress strain curves for the Nova Scotia mixture to obtain the material parameters needed to describe the mastic and the internal fracture paths of the aggregates. Once the appropriate material parameters for the asphalt concrete had been determined, a series of numerical IDT strength test simulations was performed using five uniform aggregate sizes 4.5, 6.0, 8.0, 10.0 and 12.0 mm. For more reliable test result, three samples were performed to obtain average value for each aggregate size. The averaged ultimate tensile strength and variance of residual error of the tensile stress strain curves were used to evaluate the size effects and the associated variability. All details of the numerical models and material parameters used for the study of the aggregate size are listed in Table 4-6 through Table 4-8.

Table 4-6. Modeling matrix for the study of size effect:

	Agg. 4.5 mm			Agg. 6.0 mm			Agg. 8.0 mm			Agg. 10.0 mm			Agg. 12.0 mm		
Tessellation	Voronoi with internal fracture path			Voronoi with internal fracture path			Voronoi with internal fracture path			Voronoi with internal fracture path			Voronoi with internal fracture path		
Crack growth rule	Parallel			Parallel			Parallel			Parallel			Parallel		
Equivalent aggregate size (mm)	4.5			6			8			10			12		
Exterior boundary elements	152			152			152			152			152		
Sample No.	1	2	3	1	2	3	1	2	3	1	2	3	1	2	3
Potential crack elements for mastic	3129	3123	3128	1826	1837	1829	1012	1165	1015	681	685	682	517	505	505
Potential crack elements for fracture path in aggregate	6168	6157	6163	3551	3569	3554	1923	3090	1929	1261	1269	1263	933	910	910

Table 4-7. Global linear elasticity parameters for the study of size effect

Parameter	Value
Young modulus (MPa)	7500
Poisson ratio	0.35

Table 4-8. Local material parameters for the study of size effect

Potential crack element	T_o (MPa)	D_{NCR} (mm)	T_{soft} (MPa/mm)	C_o (MPa)	C_R (MPa)	C_{soft} (Mpa/mm)	ϕ_o (degree)	ϕ_R (degree)
Mastic	2.40	0.11	21.82	2.40	0.20	1.00	38	30
Internal fracture path	6.40	0.10	64.00	6.40	0.30	1.00	38	30

4.5.2 Numerical Results

Figure 4-7 shows the averaged predicted horizontal and vertical stress strain curves for each aggregate size studied. Within the range of uniform aggregate sizes used, a small size effect is noticeable, where a larger aggregate size results in a stiffer response. This could be explained by the fact that the larger the aggregate size the fewer the resulting cracks in the specimen. Fewer cracks yield less compression softening of the vertical compressive stress strain curves and resulting in stiffer responses. Similar trend were obtained for the averaged values of the ultimate tensile strength (Figure 4-8), where the larger the aggregate size the stronger the specimen. A change of size from 4.5 mm to 12.0 mm increased the predicted strength by about 11%. The small increasing of strength could be explained by the observed cracking behavior and the differences in the formation of major crack bands. Smaller average aggregate sizes tend to yield more numerous crack planes in the specimen, such that the formation of a crack band can happen easier and sooner than for the case of the larger aggregate, where fewer crack planes are observed.

Figure 4-9 shows the variance of the residual error of the tensile stress strain curves plotted against the aggregate size. This variance is a measure of the variability among the three tested samples referenced to the experimental data. The variability of the test results is caused primarily by the initiation of distributed cracks and the formation of major crack bands. Small aggregate size yields more distributed cracks that can form more crack patterns than the large aggregate sizes that yield fewer cracks. However, the formation of a large crack has a more pronounced effect on a specimen than the formation of a smaller crack. In this experiment, it was found that the use of aggregate sizes between 5.5 to 8 mm (or at 42 to 57% of passing) yielded the least variability (below 0.011 MPa^2). Therefore, the optimal aggregate size at 40 – 60% of passing of gradation (D_{40}-D_{60}) was recommended for reliable numerical simulations of the Nova Scotia coarse mix asphalt specimen.

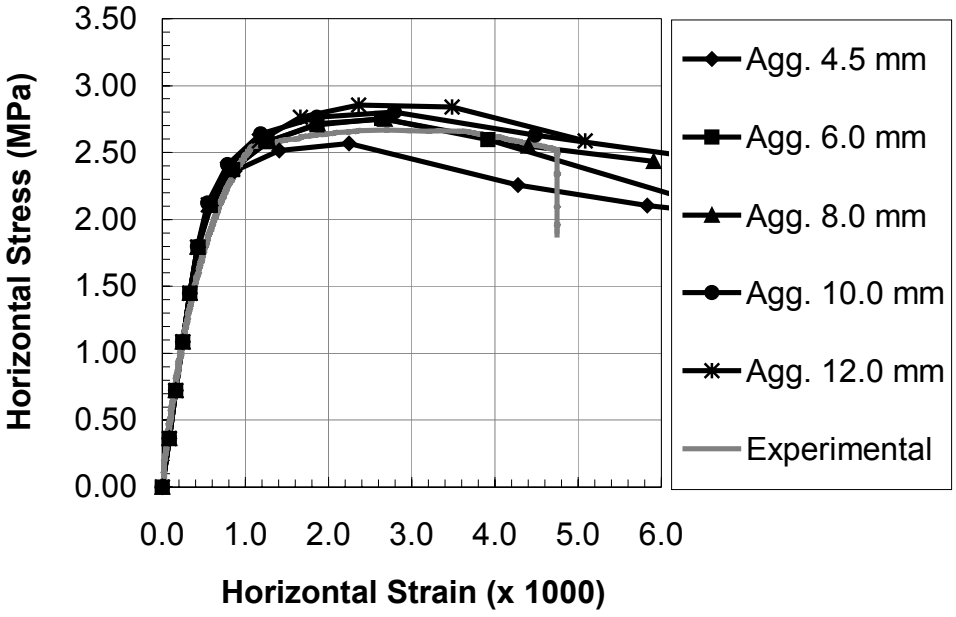

A

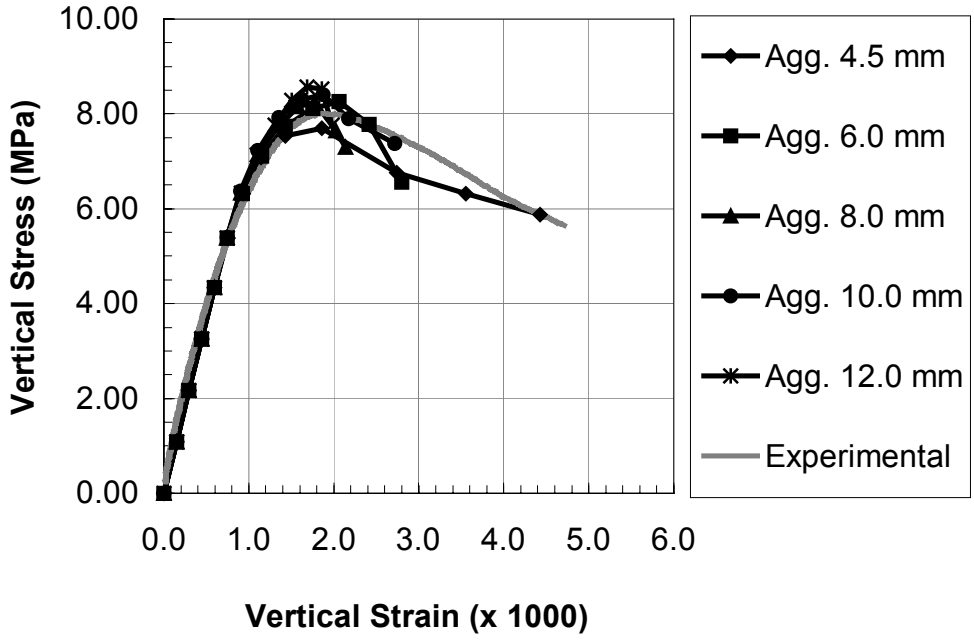

B

Figure 4-7. Comparison of predicted and measured horizontal and vertical stress-strain curves for five aggregate sizes (4.5, 6.0, 8.0, 10.0 and 12.0 mm.), using Voronoi with internal fracture path tessellation: A) Horizontal stress-strain response at center of specimen and B) Vertical stress-strain response at center of specimen.

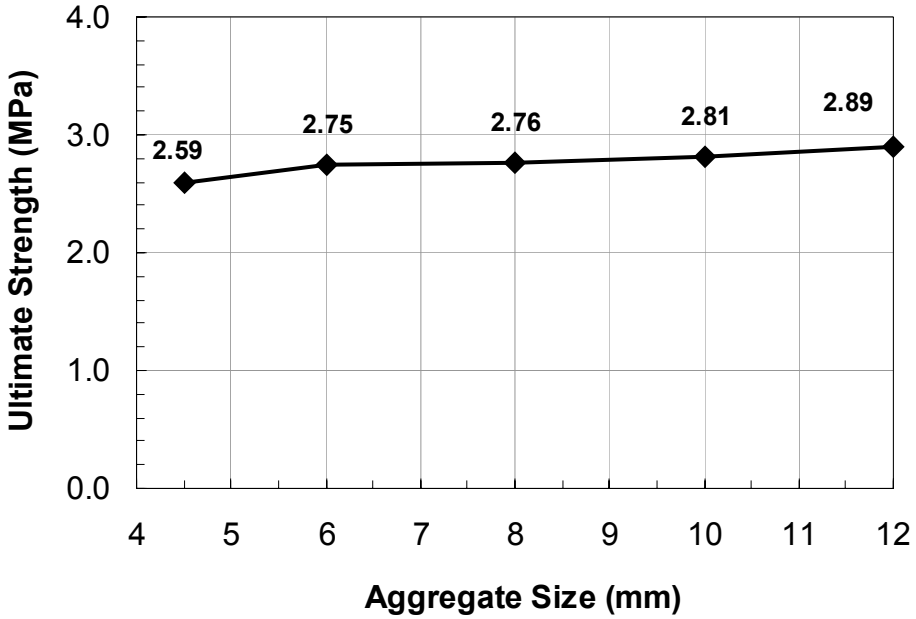

Figure 4-8. Ultimate tensile strength averaged from 3 samples for each aggregate size (4.5, 6.0, 8.0, 10.0 and 12.0 mm).

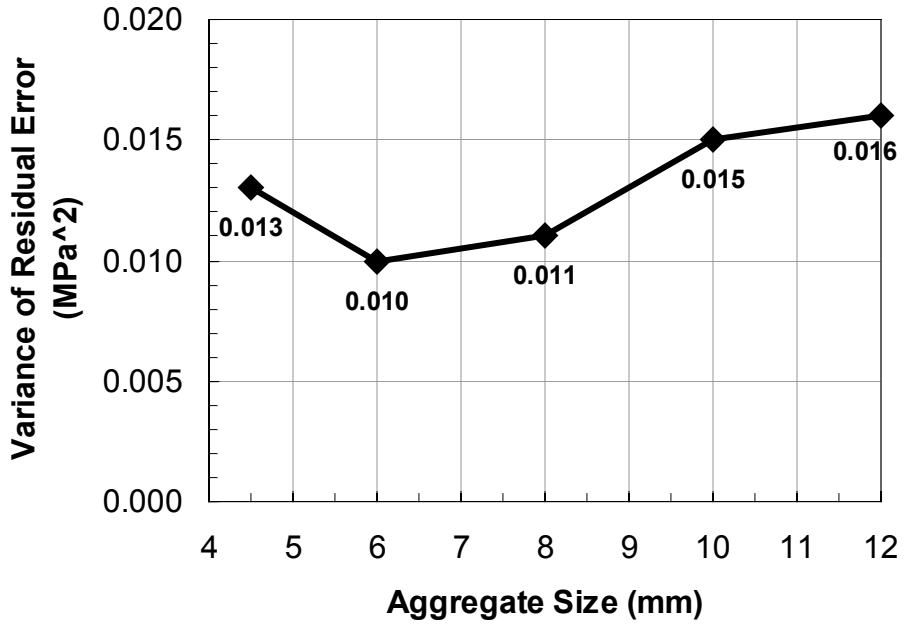

Figure 4-9. Variance of residual error of tensile stress strain curve for each aggregate size (4.5, 6.0, 8.0, 10.0 and 12.0 mm).

4.6 Sensitivity Analysis of Material Parameters Defined for Mastics

4.6.1 Numerical Experiment

This part of the study focused on the determination of the sensitivity of the parameters used to describe mastic strength. Voronoi tessellations (without internal fracture paths) that have uniform particle size of 6.8 mm were used with parallel crack growth rule in this experiment. First the numerical model was calibrated to match the stress strain curves of the Nova Scotia mixture to obtain material parameters for mastics. Then each of those calibrated parameters was altered to the higher and lower values and the resulting stress-strain response was observed. In particular, for comparison purposes, the ultimate strength was monitored and used in the comparison. The details of the numerical models and material parameters used for sensitivity analysis of the mastic are listed in Table 4-9 through Table 4-12.

Table 4-9. Modeling matrix for the parametric study of mastic

Component	Description
Tessellation	Voronoi
Crack growth rule	Parallel
Equivalent aggregate size (mm)	6.8
Exterior boundary elements	152
Potential crack elements for mastic	1408
Potential crack elements for fracture path in aggregate	0

Table 4-10. Global linear elasticity parameters for the parametric study of mastic

Parameter	Value
Young modulus (MPa)	7500
Poisson ratio	0.35

Table 4-11. Local material parameters (calibrated material parameters) for the parametric study of mastic

Potential crack element	T_o (MPa)	D_{NCR} (mm)	T_{soft} (MPa/mm)	C_o (MPa)	C_R (MPa)	C_{soft} (Mpa/mm)	ϕ_o (degree)	ϕ_R (degree)
Mastic	2.30	0.11	20.91	2.40	0.15	5.00	38	30

Table 4-12. Varying parameters from the calibrated mastic shown in Table 4-11 for the parametric study of mastic

To	D_{NCR}	Tsoft		Co	C_R	Csoft	ϕ_o	ϕ_R
(MPa)	(mm)	Linear	Nonlinear	(MPa)	(MPa)	(Mpa/mm)	(degree)	(degree)
1.90	0.03	76.67	1.00	2.00	0.000	1.00	32	24
2.10	0.07	32.86		2.20	0.075	3.00	35	27
2.30	0.11	20.91	1.00	2.40	0.150	5.00	38	30
2.50	0.15	15.33		2.60	0.225	7.00	41	33
2.70	0.19	12.11	1.00	2.80	0.300	9.00	44	36

4.6.2 Numerical Results

Figure 4-10 shows typical results of horizontal and vertical stress strain responses with variation in the cohesion (C_o). The subsequent Figures 4-11 through 4-18 show only the variation in ultimate tensile strength as the following parameters are varied: cohesion (C_o), tension cutoff (T_o), friction angle (ϕ_o), cohesion softening slope (C_{soft}), tension softening slope (T_{soft}), opening crack limit (D_{NCR}), residual cohesion (C_R) and residual friction angle (ϕ_R). It is noted that T_{soft} and D_{NCR} are redundant parameters. In DIGS, two types of tension softening slope, linear (L) and nonlinear (N), can be selected. The default linear model must set T_{soft} equal to T_o/D_{NCR}. Without doing so, the nonlinear (power law) will be chosen in which the tensile strength decreases in a nonlinear fashion from the selected tension cutoff (T_o) to zero at a specified opening crack limit (D_{NCR}). All these parameters are used to define Mohr Coulomb type of failure in Figure 3-2.

As expected, the ultimate tensile strength of specimen is strongly affected by the parameters controlling strength of failure envelope C_o, T_o and ϕ_o as shown in Figure 4-11 through 4-13). It was noticeable from Figure 4-11 and 4-12 that cohesion was slightly more sensitive than the tension cutoff. The parameters that control the rate of softening C_{soft} and T_{soft} also affected the strength of specimen as can be seen in Figure 4-14 and 4-15. The opening crack limit (Figure 4-16) has an influence to the specimen strength in the same way as the tension softening slope. The last two parameters C_R and ϕ_R (Figure 4-17 and 4-18) controlling residual strength of failure envelope were found to be less sensitive to the specimen strength.

Figure 4-19 shows the results of stress strain curves predicted by two tension-softening models, Linear and Nonlinear. There were not significantly different between these two, which may imply that the approximation of rate of tension softening were not critical for simulating the IDT strength test.

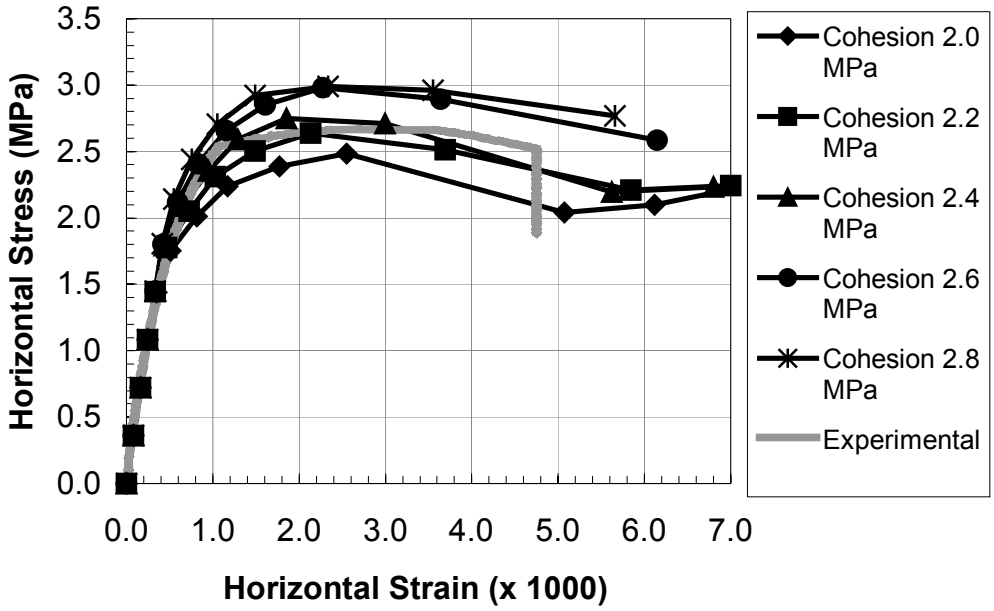

A

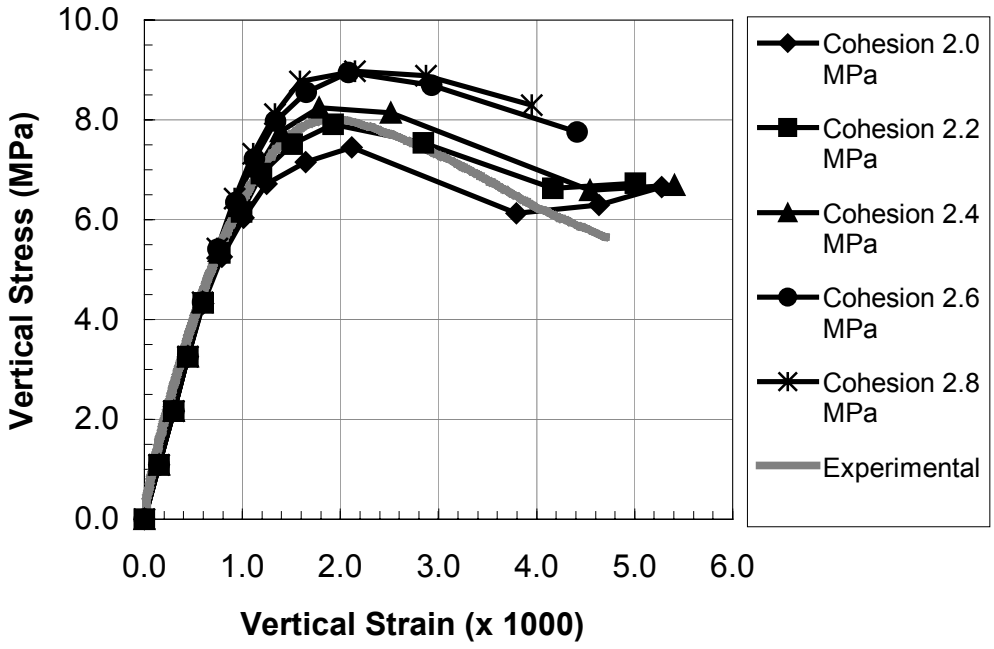

B

Figure 4-10. Change of stress-strain responses due to the varying of cohesion defined in mastic from 2.00 – 2.80 mm: A) Horizontal stress-strain response at center of specimen and B) Vertical stress-strain response at center of specimen.

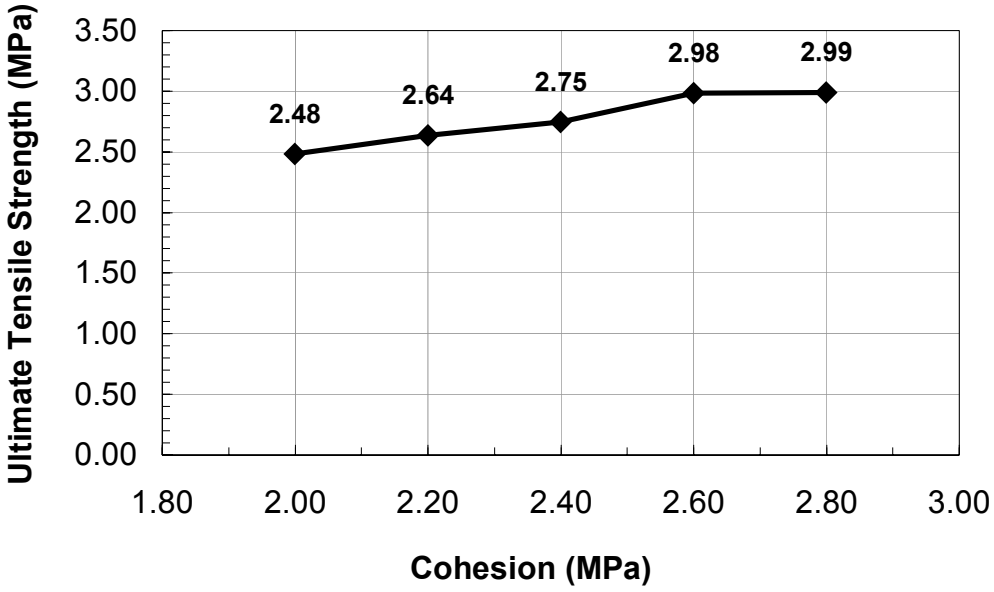

Figure 4-11. Sensitivity of the parameter cohesion defined in mastic to the ultimate tensile strength.

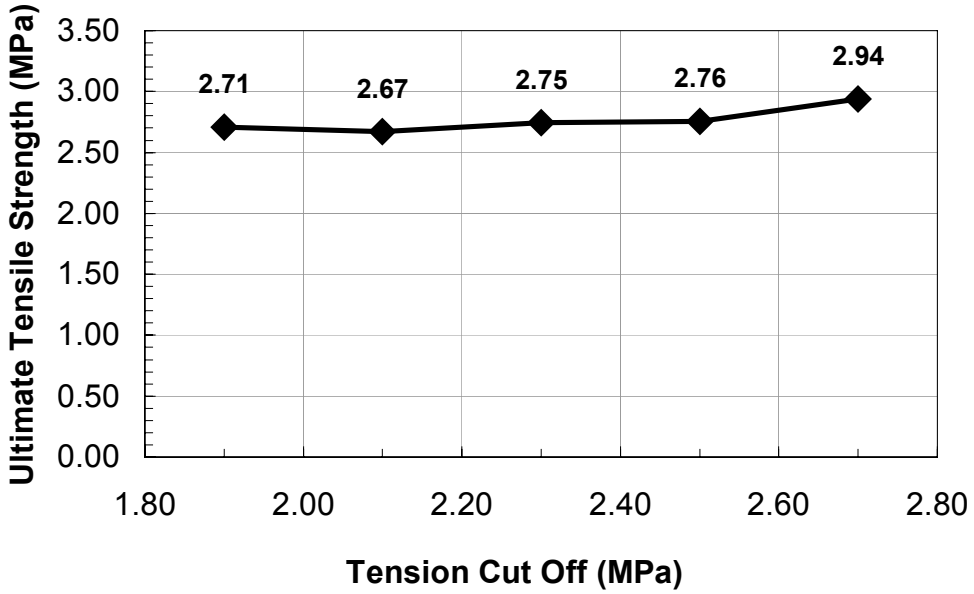

Figure 4-12. Sensitivity of the parameter tension cutoff defined in mastic to the ultimate tensile strength.

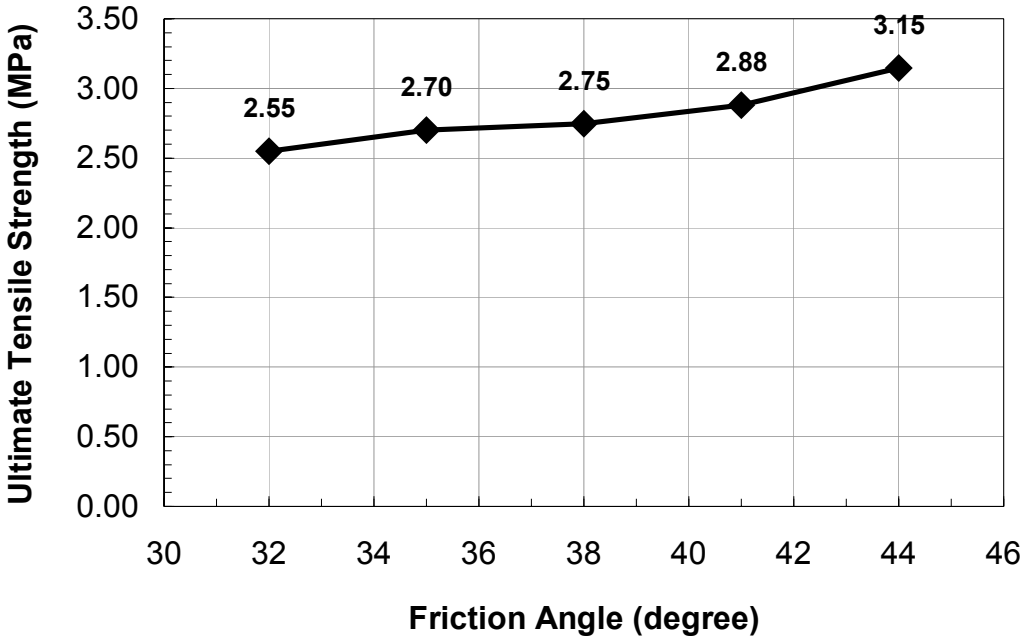

Figure 4-13. Sensitivity of the parameter friction angle defined in mastic to the ultimate tensile strength.

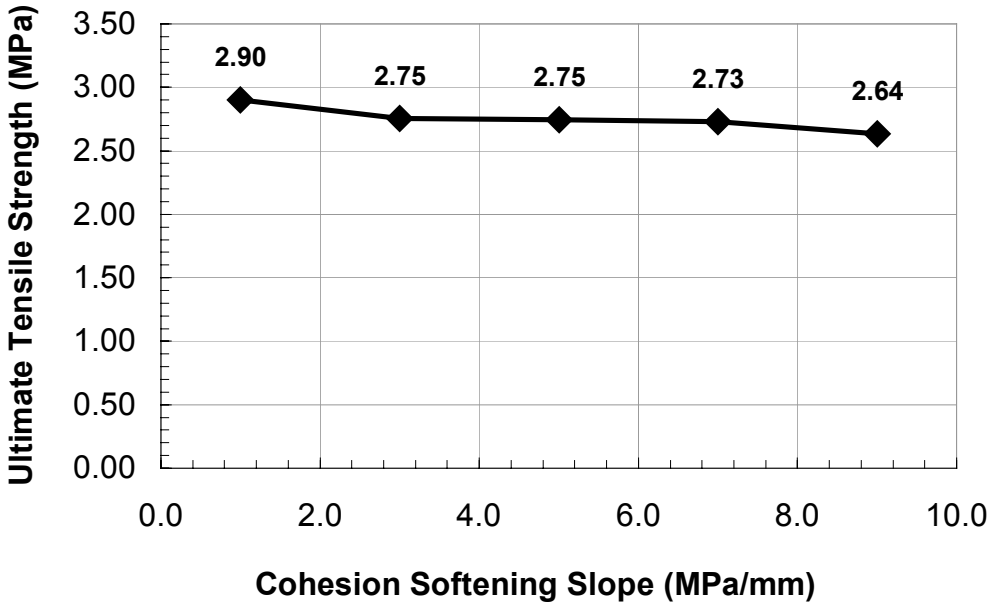

Figure 4-14. Sensitivity of the parameter cohesion softening slope defined in mastics to the ultimate tensile strength.

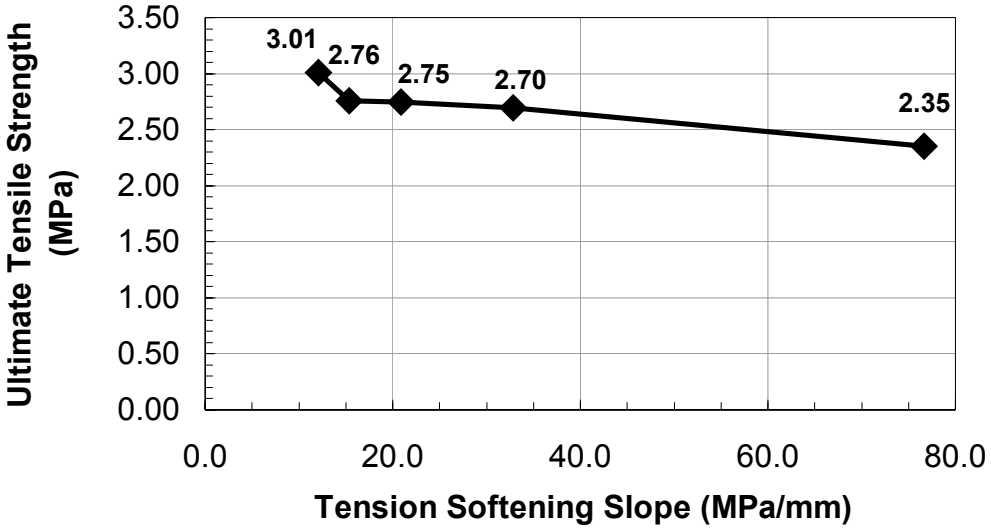

Figure 4-15. Sensitivity of the parameter tension softening slope (Linear Model) defined in mastic to the ultimate tensile strength.

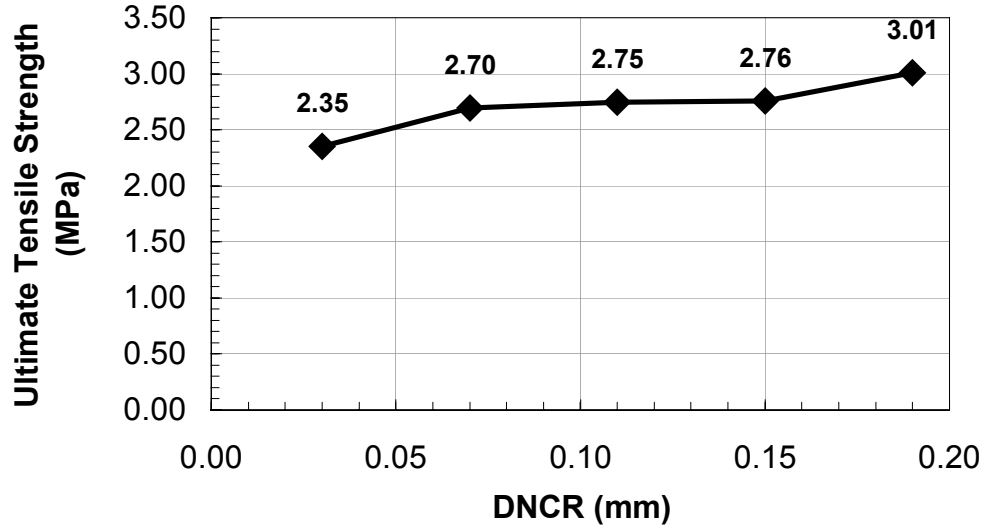

Figure 4-16. Sensitivity of the parameter opening crack limit defined in mastic to the ultimate tensile strength

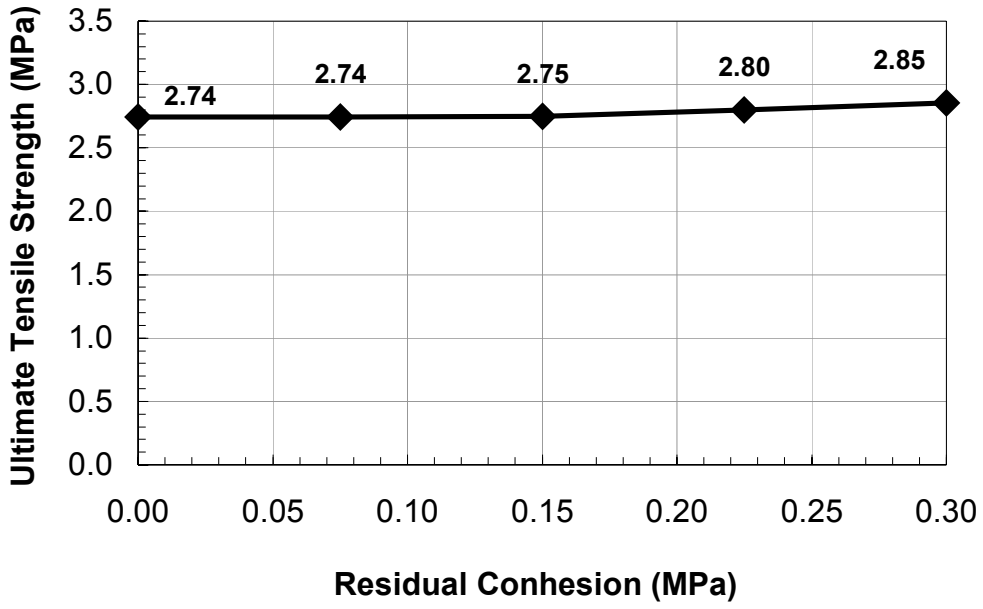

Figure 4-17. Sensitivity of the parameter residual cohesion defined in mastic to the ultimate tensile strength.

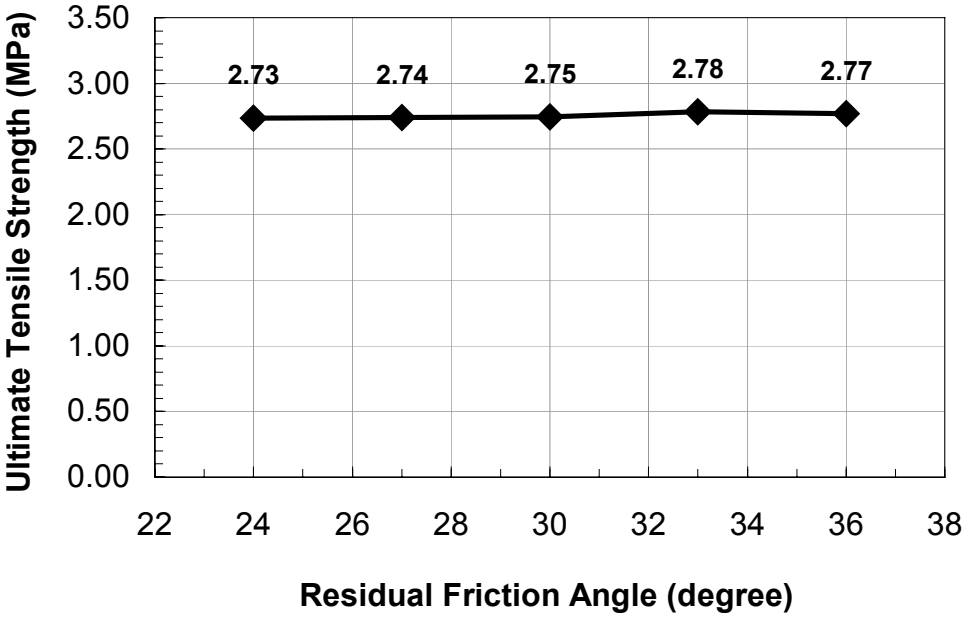

Figure 4-18. Sensitivity of the parameter residual friction angle defined in mastic to the ultimate tensile strength.

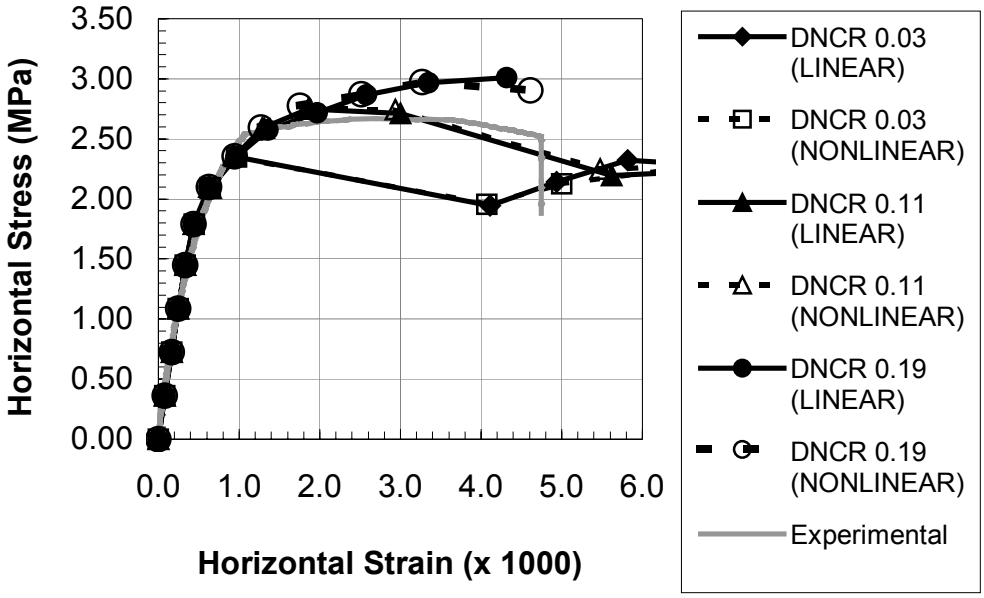

A

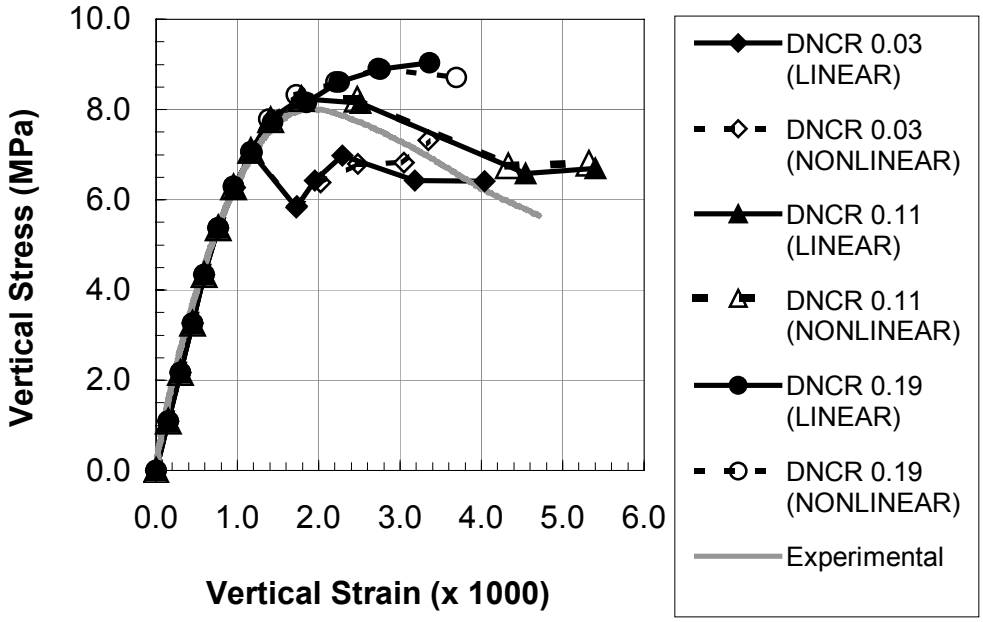

B

Figure 4-19. A comparison of stress-strain response between using a Linear (default) and Nonlinear (still in experiment) tension - softening model for the range of opening crack limit D_{NCR} 0.03 – 0.19 mm: A) Horizontal stress-strain response at center of specimen and B) Vertical stress-strain response at center of specimen.

4.7 Sensitivity Analysis of Material Parameters Defined for Internal Fracture Paths

4.7.1 Numerical Experiment

This part of the study focused on the identification of the sensitivity of the predicted ultimate tensile strength to the changes in material strength parameters defined for internal aggregate fracture paths. In the experiment, the same Voronoi tessellation scheme, previously used, with a particle size of 6.8 mm was filled with internal fracture paths to simulate faults in the aggregates. The same parallel crack growth rule was also used throughout, and the numerical model was first calibrated using the experimental stress- strain curves from the Nova Scotia mixture. Material parameters for the mastic defined in Table 4-11 were kept the same from the previous study while calibrating material parameters for internal fracture paths of aggregate. Then each of the internal fracture path strength parameter was changed to higher or lower values from the calibrated parameters to observe the sensitivity of the predicted stress-strain responses. All details of the models and material parameters used for the sensitivity analysis of the internal fracture paths are listed in Table 4-13 though Table 4-16.

4.7.2 Numerical Results

Figure 4-20 shows the effects of cohesion (C_o) and tension cutoff (T_o) on the predicted ultimate strength. It can be seen that an increase of cohesion and tension cutoff from 4.5 to 5.5 MPa increases the strength of the specimen. Later increasing of both parameters to 8.5 MPa does not improve the strength. Figure 4-21 shows the effect of the opening crack limit (D_{NCR}) on the ultimate tensile strength. Too small D_{NCR} 0.01 mm cause brittle failure of specimen and higher D_{NCR} 0.04, 0.07, 0.10, and 0.13 mm improves the strength.

Figures 4-22 through 4-25 show the effects of other parameters, friction angle (ϕ_o), cohesion-softening slope (C_{soft}), residual cohesion (C_R), and residual friction angle (ϕ_R) on the ultimate tensile strength. The ultimate tensile strength was found to be insensitive to these parameters.

4.8 Summary of Sensitivity Analysis

Numerical experiments of material parameters for the mastic and internal fracture paths revealed that the tensile strength of an IDT specimen was preliminary controlled by the mastic, which was the weakest link in specimen. The tensile strength of specimen was most sensitive to the parameters controlling strength (cohesion C_o, friction angle ϕ_o and tension cutoff T_o). Parameters that control rate of softening (cohesion softening slope C_{soft}, tension softening slope T_{soft} and opening crack limit D_{NCR}) also affect the strength of specimen. The residual parameters (residual cohesion C_R and residual friction angle ϕ_R) have the least effects on the strength of. Even though the last two residual parameters did not have a significant impact on strength, they do provide the smoothness for both ascending and descending curves of stress strain responses.

When aggregate has internal fracture paths, the strength of the specimen is slightly weakened by the aggregate breakdown. In studies, low aggregate toughness defined by cohesion and tension cutoff of 4.5 MPa (or 1.9 times that of mastic strength) decreased the specimen strength. However, when aggregate is reasonable tough 6.0 to 8.5 MPa (or 2.5 to 3.5 times that of mastic strength), the toughness does not affect the strength of the specimen.

Table 4-13. Modeling matrix for the parametric study of internal fracture paths

Component	Description
Tessellation	Voronoi with internal fracture path
Crack growth rule	Parallel
Equivalent aggregate size (mm)	6.8
Exterior boundary elements	152
Potential crack elements for mastic	1408
Potential crack elements for fracture path in aggregate	2717

Table 4-14. Global linear elasticity parameters for the parametric study of internal fracture paths

Parameter	Value
Young modulus (MPa)	7500
Poisson ratio	0.35

Table 4-15. Local material parameters (calibrated material parameters) for the parametric study of internal fracture paths

Potential crack element	T_o (MPa)	D_{NCR} (mm)	T_{soft} (MPa/mm)	C_o (MPa)	C_R (MPa)	C_{soft} (Mpa/mm)	ϕ_o (degree)	ϕ_R (degree)
Mastic	2.30	0.11	20.91	2.40	0.15	5.00	38	30
Internal fracture path	6.50	0.07	92.86	6.50	0.15	1.00	40	32

Table 4-16. Varying parameters from the calibrated fracture path shown in Table 4-15 for the parametric study of internal fracture paths

To (MPa)	D_{NCR} (mm)	Co (MPa)	C_R (MPa)	Csoft (Mpa/mm)	ϕ_o (degree)	ϕ_R (degree)
4.50	0.01	4.50	0.000	0.10	35.0	27.0
5.50	0.04	5.50	0.075	0.50	37.5	29.5
6.50	0.07	6.50	0.150	1.00	40.0	32.0
7.50	0.10	7.50	0.225	5.00	42.5	34.5
8.50	0.13	8.50	0.300	10.00	45.0	37.0

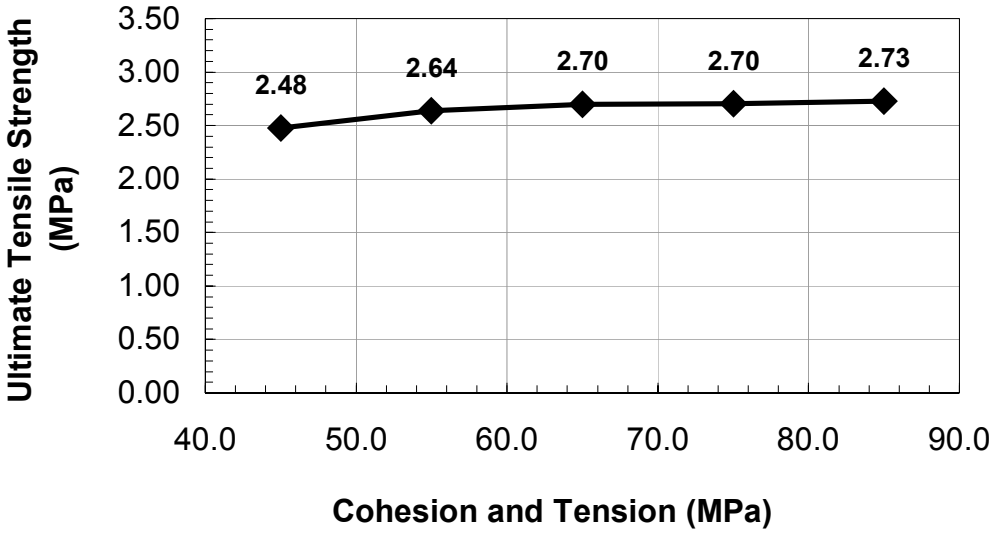

Figure 4-20. Sensitivity of both parameters cohesion and tension cutoff defined in fracture path of aggregate to the ultimate tensile strength.

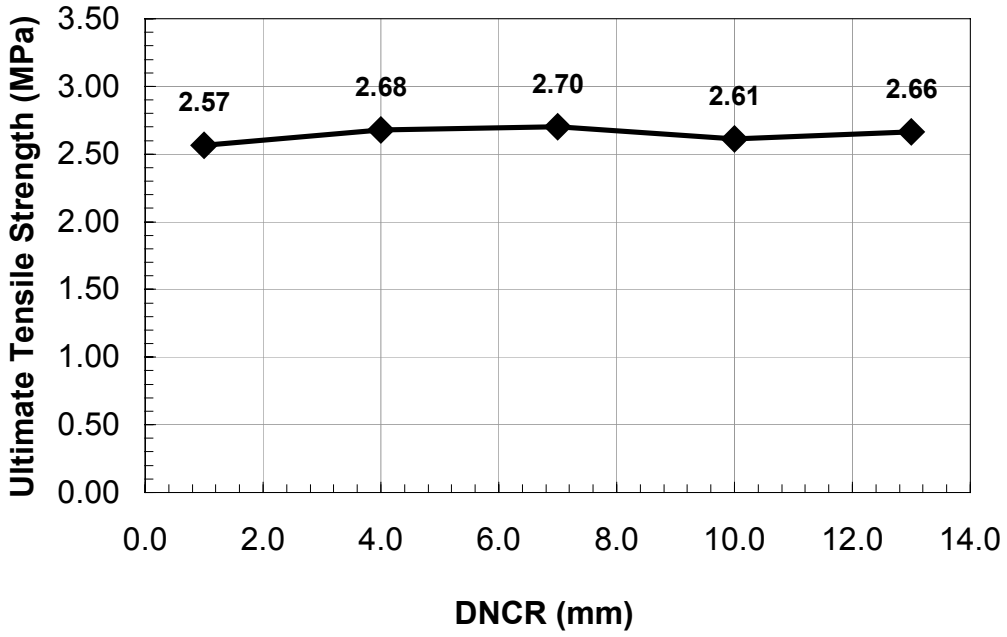

Figure 4-21. Sensitivity of opening crack limit defined in internal fracture path of aggregate to the ultimate tensile strength.

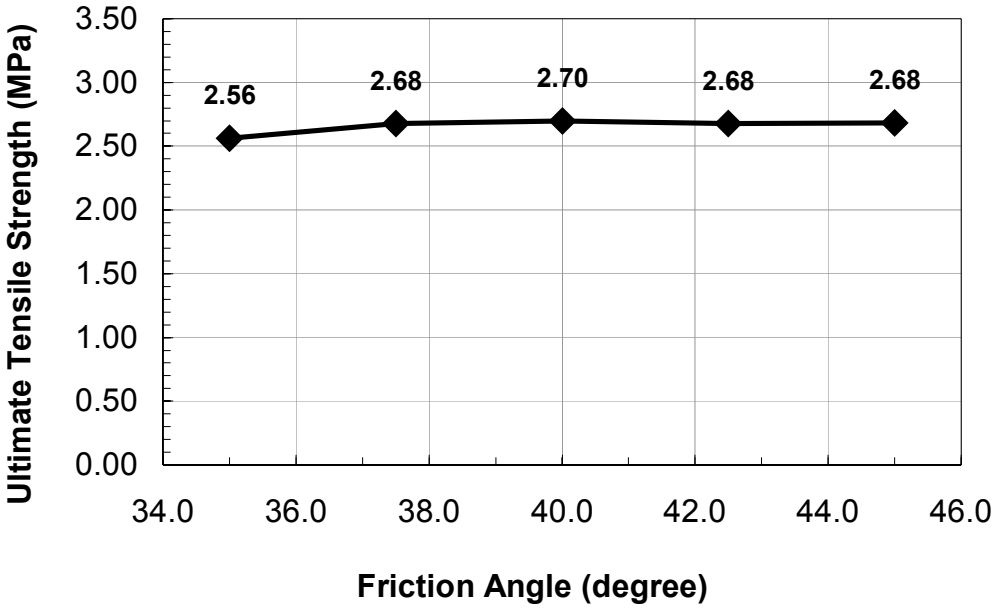

Figure 4-22. Sensitivity of friction angle defined in internal fracture path of aggregate to the ultimate tensile strength.

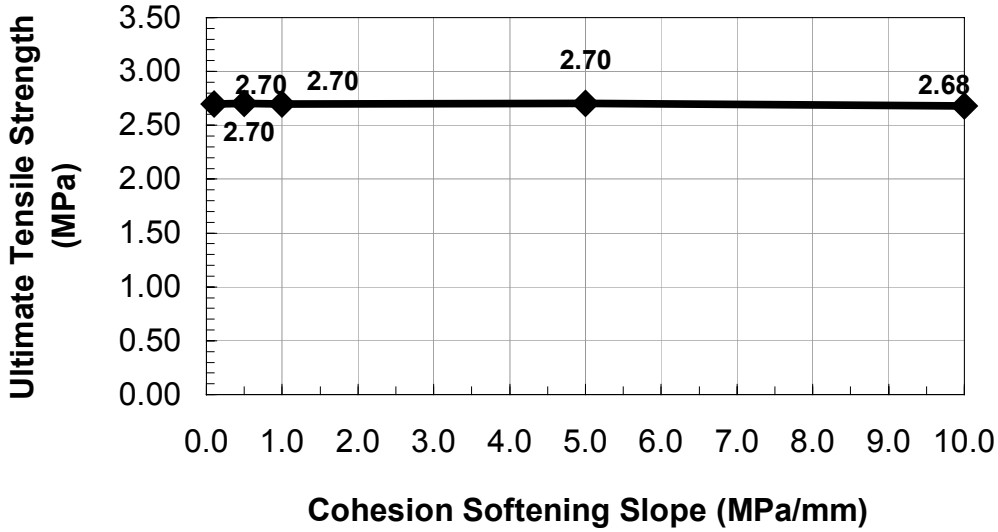

Figure 4-23. Sensitivity of cohesion softening slope defined in internal fracture path of aggregate to the ultimate tensile strength.

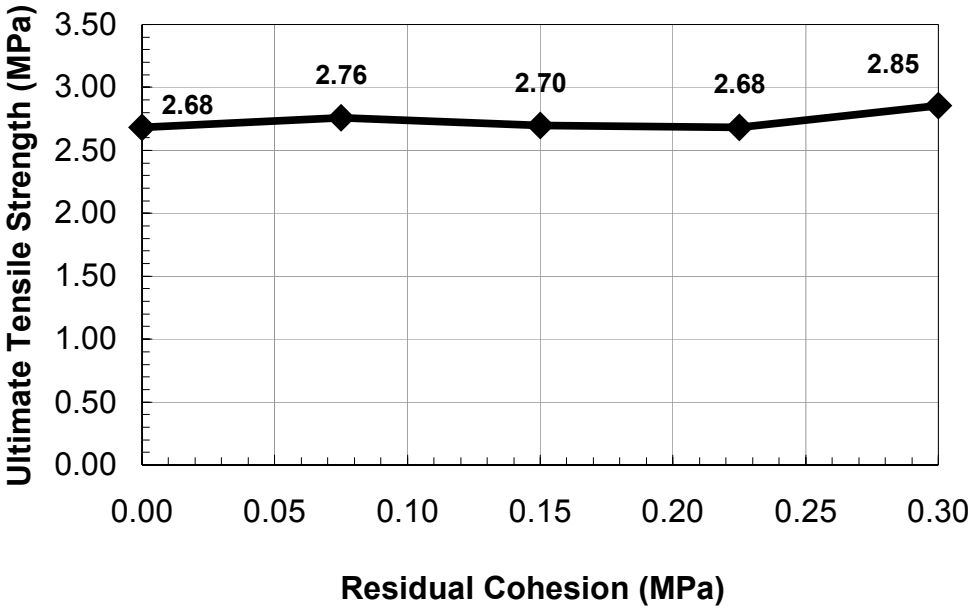

Figure 4-24. Sensitivity of residual cohesion defined in internal fracture path of aggregate to the ultimate tensile strength.

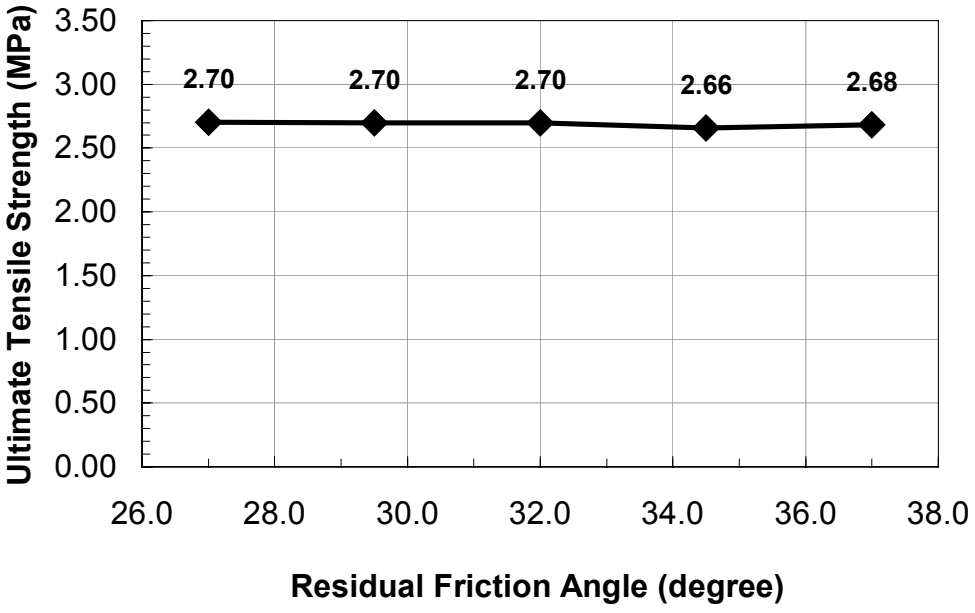

Figure 4-25. Sensitivity of residual friction angle defined in internal fracture path of aggregate to the ultimate tensile strength.

4.9 Recommendations for a Successful Numerical Simulation of IDT Strength Test

This section summarizes and proposes a standard procedure for successfully model Superpave IDT strength test with the displacement discontinuity boundary element method.

- Select "reasonable" IDT test results. The IDT strength test that yields extremely high or low values of Poisson ratio (i.e. less than 0.1 or greater than 0.4) may show a sign of nonisotropic material behavior and should be disregarded.
- Select "reasonable" load-deformation test results from the Superpave IDT test. A large discrepancy of stress strain curves obtained from each face of an IDT sample may reveal unsymmetrical aggregate structure in a specimen or highly nonhomogeneous behavior at the location of strain gauges

Numerical analysis starts with creating an IDT numerical model using exterior boundary elements for the edge of specimen and filling the inside with potential crack elements, thus forming Voronoi tessellations or Voronoi tessellations with internal fracture paths. With a suitable set of material parameters for the mastic and fracture paths in the aggregate, the predicted stress strain curves and crack patterns can match the experimental results. The steps for numerical simulation of the IDT strength test can be summarized as follows:

1. The first trial Young modulus (E) for numerical analysis can be approximated by a secant modulus at half ultimate strength $Es = \frac{1}{\varepsilon_x}\left(\sigma_x - \nu\sigma_y\right)$. Subsequent trial values could be adjusted slightly higher or lower, such that it yields the best fit to the ascending portion of the vertical compressive and horizontal tensile stress strain curves.
2. The Poison ratio can be obtained directly from IDT strength test. Acceptable Poisson ratios for asphalt concrete should vary between 0.15 and 0.35. Extreme values such as less than 0.1 or greater than 0.4 should not be used.
3. Use Voronoi tessellation with parallel crack growth rule to calibrate material parameters for the mastic.

4. The particle size around D_{40} to D_{60} of gradation is recommended for consistent results. Using coarser aggregate size is also allowed to reduce computing time since the size effect is not very strong.

5. Approximate material parameters for the mastic:

   a. For the first trail, cohesion (C_o) and tension cutoff (T_o) can be set to the ultimate tensile strength of a given sample. On subsequent trials, cohesion and tension cutoff may be adjusted slightly, according to the best fit to the vertical and horizontal stress strain curves.

   b. Friction angle (ϕ_o) around 38 to 40 degrees and opening crack limit (D_{NCR}) between 0.10 to 0.12 mm have been found to be reasonable values for asphalt mixture.

   c. A linear tension softening model T_{soft} must be defined equal to T_o / D_{NCR}.

   d. Other parameters for mastics such as residual friction angle (ϕ_R), residual cohesion (C_R) and cohesion-softening slope (C_{soft}) are chosen such that the predicted post peak responses fit the experimental post peak responses. The suggested values for the first trial are ϕ_R 30 degree, C_R = 0.10 MPa and Csoft = 1.0 MPa/mm.

6. Replace Voronoi tessellation with its dual Voronoi tessellation with internal fracture paths and calibrate material parameters for fracture paths within the aggregates.

7. Material parameters for internal fracture paths within aggregates (in case the strength of the aggregate is not known, it is assumed that the aggregate is reasonable tough)

   a. Cohesion (C_o) and tensile strength (T_o) can be set to any high values about 2.5 to 3.5 times of those used for mastic strength.

   b. Friction angle (ϕ_o) of 40 degree and D_{NCR} between 0.03 - 0.07 mm have been found to be good values for fracture paths inside aggregate.

   c. A linear tension softening slope T_{soft} must be set to T_o/D_{NCR}.

   d. Other parameters for internal fracture paths such as residual friction angle (ϕ_R), residual cohesion (C_R) and cohesion softening slope (C_{soft}) are chosen such that the predicted post peak responses fit to the experimental post peak responses. The suggested values for the first trial are ϕ_R = 30 degree, C_R = 0.10 MPa and Csoft = 1.0 MPa/mm.

8. For known soft aggregates the exact values for the material parameters can be used.

9. Adjust material parameters until the predicted stress strain curves fit to the experimental stress strain curves for both the vertical and horizontal directions.

4.10 Summary

From the numerical studies conducted in this Chapter, it can be concluded that the appropriate tessellation scheme to represent the aggregate structure in the Superpave IDT strength test was a Voronoi tessellation scheme with internal fracture paths. This tessellation scheme predicted the stress strain responses closest to the experimental results. The internal fracture paths allowed the aggregates to break down at high loads, which realistically simulate the cracking behavior of IDT specimen observed in laboratory.

The study to identify the appropriate crack growth rule for the indirect tension strength test resulted in the recommendation of using the parallel crack growth rule. Both parallel and sequential methods predicted approximately the same stress strain responses and crack patterns, but the parallel consumed much less computing time than the sequential did. Furthermore, it is highly possibly that several cracks in a specimen can occur simultaneously for fast loading test.

The parametric studies of the aggregate size, material parameters for mastics, and material parameters for internal fracture path revealed that the primary factor that controlled the strength of IDT specimen were the strength of mastics. The secondary factor was the strength of aggregate. The least important factor was the aggregate size. Even though the aggregate size was not really important for the strength of specimen, from a calibration point of view, the larger the aggregate size the more difficult it is to tune the material parameters to fit the experimental results and the smaller the aggregate size, the longer the computing time. For the gradations studied, it was found that an

optimal aggregate size around 40-60% passing of gradation (D_{40} - D_{60}) yields the most consistent results with a reasonable amount of computational time.

CHAPTER 5
EVALUATION OF TENSILE STRENGTH AND FRACTURE ENERGY DENSITY

5.1 Overview

Tensile strength at fracture and fracture energy density have identified in previous studies (Sedwick, 1998 and Garcia, 2002) to be related to the fracture resistance of mixtures. The Superpave tensile strength is referred to as the strength at the fracture point (Roque (1997) and Buttlar et al.,(1997)). The strength at this point is normally slightly lower than the tensile strength at ultimate load. Another parameter, the fracture energy density at the center of the IDT specimen, has also been used to evaluate the cracking resistance of mixtures. The fracture energy can be obtained by integrating the area under tensile stress-strain curve up to the point of fracture.

During Superpave IDT strength test, load is recorded as well as vertical and horizontal deformations at strain gauges. To account for three-dimensional effects, bulging correction factors C_{bh} and C_{bv} shown in Table 5-1 are applied to correct the measured horizontal and vertical deformations to the deformations in flat planes

$$H_{corrected} = H_{measured} C_{bh} \tag{5-1}$$

$$V_{corrected} = V_{measured} C_{bv} \tag{5-2}$$

Table 5-1. Correction factors accounting for bulging effect

D = 4" or 6"	Poisson's ratio	Diameter - to - Thickness ratio (t/D)				
	ν	0.167	0.333	0.500	0.625	0.750
C_{BX}	0.20	0.9816	0.9638	0.9461	0.9358	0.9294
	0.35	0.9751	0.9518	0.9299	0.9179	0.9108
	0.45	0.9722	0.9466	0.9234	0.9111	0.9040
C_{BY}	0.20	0.9886	0.9748	0.9677	0.9674	0.9688
	0.35	0.9808	0.9588	0.9479	0.9473	0.9493
	0.45	0.9759	0.9492	0.9361	0.9358	0.9380

The corrected horizontal and vertical deformations are then divided by the gauge length GL to obtain the average strains, and again the strain center correction factors $C_{eh} = 1.072$ and $C_{ev} = 0.977$ are applied to change the average strains to the strains at the center of specimen

$$\varepsilon_{h\_corrected} = \frac{H_{corrected}}{GL} C_{eh} \tag{5-3}$$

$$\varepsilon_{v\_corrected} = \frac{V_{corrected}}{GL} C_{ev} \tag{5-4}$$

In the same way as strains, the corresponding stresses in the horizontal and vertical directions evaluated at center of specimen can be computed by two-dimensional plane stress formulas and are then corrected with the center stress correction factors $C_{\sigma h}$ and $C_{\sigma v}$ shown in Table 5-2 to convert these stresses in a plane to the stresses on the surfaces of 3D specimen

$$\sigma_{h\_corrected} = \frac{2P}{\pi DT} C_{\sigma h} \tag{5-5}$$

$$\sigma_{v\_corrected} = \frac{6P}{\pi DT} C_{\sigma v} \tag{5-6}$$

Fracture point in specimen can be detected by monitoring the deformation differential ($V_{corrected} - H_{corrected}$) recorded at each load step and marking the point when it

starts to deviate from the smooth curve. Corresponding to the fracture point, the recorded applied load and the measured horizontal and vertical deformations are used to calculate the tensile strength and fracture energy density as previously described.

Table 5-2. Correction factors accounting for stress at center of specimen

D = 4"or 6"	Poisson's ratio	Diameter – to – Thickness ratio (t/D)				
	ν	0.167	0.333	0.500	0.625	0.750
$C_{\sigma xCTR}$	0.20	0.9471	0.9773	1.0251	1.0696	1.1040
	0.35	0.9561	1.0007	1.0871	1.1682	1.2321
	0.45	0.9597	1.0087	1.1213	1.2307	1.3171
$C_{\sigma yCTR}$	0.20	-0.9648	-0.9754	-0.9743	-0.9693	-0.9611
	0.35	-0.9732	-0.9888	-0.9844	-0.9710	-0.9538
	0.45	-0.9788	-0.9971	-0.9864	-0.9646	-0.9395

5.2 Numerical Model V.S. Asphalt Mixtures

The displacement discontinuity boundary element method assumes the material to be linear elastic until fracture. When cracks appear in the specimen, the linear elastic behavior still remains but with a plastic failure and localization in the crack.

For this part of the study, three mixtures, Nova Scotia, NW39_1C and I95SJN_BWP described in Table 5-3 were chosen. These mixtures range from having a predominantly ductile failure mode (Nova Scotia mix) to a very brittle failure mode (I95SJN_BWP) to evaluate the capabilities of the displacement discontinuity method of simulating very different mixture responses. The material properties obtained from IDT strength tests of three mixtures are listed in Table 5-4.

In this study, a single "representative" sample was selected out of the three samples tested for each mixture, based on the closeness of the measured load-deformation responses at both sides of the sample. In the case of the Nova Scotia and NW39_1C mixtures, the middle sample was selected, but for the I95SJN_BWP the upper bound sample was selected. Once a "representative" sample for each mix was selected, the

measured load and deformations were used to calculate vertical and horizontal stress-strain curves on the faces of the specimen as described in the previous section. Then the averaged stress strain-curves from both faces were used for comparisons to the numerical simulation.

Table 5-3. Gradation of three mixtures used in simulations

Sieve size	Percent passing		
	Nova Scotia	NW39_1C	I95SJN_BWP
25 mm (1)	100		
19 mm (3/4)	97	100	100
12.5 mm (1/2)	83	93	91
9.5 mm (3/8)	66	87	76
4.75 mm (#4)	38	62	53
2.36 mm (#8)	23	46	40
1.18 mm (#16)	18	39	36
600 μm (#30)	14	33	34
300 μm (#50)	10	27	28
150 μm (#100)	6.5	14	19
75 μm (#200)	3.5	8	5

(1) Nova Scotia was a virgin coarse-graded mix with 19 mm nominal maximum aggregate size, designed according to SuperPave™ specifications. The mixture has 7.0% air void and 5.5% design asphalt content with an asphalt binder of grade AC30.

(2) NW39-1C was a core excavated on Section 1 (cracked pavement), from Alachua County, FL, on NW39th Ave., eastbound, section limit 34th St – 24th St. The pavement was 14 years old at the time of coring. The mixture was a fine-graded mix with 12.5 mm nominal maximum aggregate size, 7.3% air void, 4.7% effective asphalt content (the recovered unknown binder has Brookfield viscosity 16000 Poises at 60 °C).

(3) I95SJN_BWP was a core excavated between wheel paths, from St. Johns County on Interstate I95, northbound, county milepost limit 26.218-34.855. The age of the pavement was 5 years old. The mixture was a fine-graded mix with 12.5 mm nominal maximum aggregate size, 4.0% air voids, 4.7% effective asphalt content (AC30 was believed to be used with the recovery Brookfield viscosity 36548 Poises at 60 °C).

Table 5-4. Material properties of three mixtures obtained from Superpave IDT tests

Mixtures	Test temp. (^oC)	Failure strain (micro strain)	Tensile strength (MPa)	Fracture energy density (KJ/m^3)	Poisson ratio	D_0 (1/GPa)	D_1 (1/Gpa* sec)	m
Nova Scotia	0	618	2.05	0.83	0.35	0.0645	0.0271	0.567
NW39_1C	10	786	2.70	1.38	0.30	0.0521	0.0192	0.524
I95SJN_BWP	-10	590	3.19	1.44	0.22	0.0936	0.0014	0.574

5.3 Numerical Simulation of Three Mixtures

Modeling matrix of the displacement discontinuity models for simulating three mixtures, Nova Scotia, NW39_1C and I95SJN_BWP are shown in Table 5-5. Based on the size effect study of Voronoi particles in Chapter 4, Voronoi particles with average diameters of 8.1 mm were used for the Nova Scotia coarse mix, and slightly smaller particles 6.8 mm for NW39_1C fine mix and 6.6 mm for I95SJN_BWP fine-graded mix. The numbers of exterior boundary elements for constructing the edge of three specimens were 152, of those, 8 elements each were used for simulating fix condition at the bottom and displacement control at the top. The displacement control for all three mixtures was divided into 20 equal load steps for the total vertical displacement of 0.35, 0.30 and 0.19 respectively. The number for potential crack elements, simulating mastics and internal fracture paths inside Voronoi particles are provided in Table 5-5.

Table 5-6 shows global material parameters (Young modulus and Poisson ratio) for numerical models simulating three mixtures. Poisson ratios were obtained directly from IDT strength test. The secant modulus at 50 percent of the ultimate load was found to be a good value for the Young modulus in the numerical model. Other local material parameters for mastics and internal fracture paths for the three numerical models in Table 5-7 were determined by numerical tuning.

From the sensitivity analysis presented in Chapter 4, it was found that cohesion C_o and tension cutoff T_o of the mastic control the tensile strength of the specimen. Therefore, by tuning these two parameters, the predicted ultimate load in the stress-strain curves can fit to the ultimate load of given stress-strain curves. The residual strength of the mastic was also used to provide additional strength when the material damages. They provided the fit to the stress-strain responses in the post peak region of the stress-strain curves. Other local parameters for the mastic and fracture path in the aggregates are less important; they can be used to adjust the predicted stress strain curves to have the best fit of given stress-strain curves. The complete calibrated local material parameters that make numerical models fit to the test results are listed in Table 5-7. Once the numerical models fit the test results, the tensile strength at fracture and fracture energy density were evaluated according to SHRP method described earlier.

Table 5-5. Modeling matrix for three mixtures used:

Mixtures	Specimen size (diameter x thickness) (mm x mm)	Equivalent Voronoi diameter (mm)	Number of exterior boundary elements	Number of potential crack elements for mastic	Number of potential crack elements for internal fracture paths	Total vertical deformation at load plate for 20 load step (mm)
Nova Scotia	150.0 x 50.3	8.1	152	978	1,791	0.350
NW39_1C	150.6 x 28.2	6.8	152	1,409	2,651	0.325
I95SJN_BWP	143.5 x 53.6	6.6	152	1,249	2,287	0.190

Table 5-6. Global linear elasticity parameters for three mixtures used

Mixtures	Young modulus (MPa)	Poisson ratio
Nova Scotia	7,250	0.35
NW39_1C	8,500	0.30
I95SJN_BWP	13,250	0.22

Table 5-7. Local material parameters for three mixtures used

Mixtures	Potential crack elements	T_o (MPa)	D_{NCR} (mm)	T_{soft} (MPa/ mm)	C_o (MPa)	C_R (MPa)	C_{soft} (Mpa/ mm)	ϕ_o (degree)	ϕ_R (degree)
Nova Scotia	Mastic Internal fracture path	2.30	0.10	1.0	2.50	0.15	1.0	38	30
		6.25	0.05	1.0	6.25	0.10	1.0	40	30
NW39_1C	Mastic Internal fracture path	3.05	0.07	1.0	3.20	0.10	1.0	35	20
		8.00	0.05	1.0	8.00	0.10	1.0	40	30
I95SJN_BWP	Mastic Internal fracture path	4.50	0.03	1.0	4.90	0.10	1.0	35	20
		9.00	0.03	1.0	9.00	0.10	1.0	40	30

5.4 Numerical Test Results

The predicted stress strain curves of three mixtures (Figure 5-1) agreed well with the experimental results. The predictions matched both horizontal tensile and vertical compressive stress strain curves up to the peak and they partially captured the post peak responses.

Figure 5-2 shows the deformation differential of three mixtures: Nova Scotia, NW39_1C and I95SJN_BWP. The fracture points marked in Figure 5-1A were determined at the peaks of the curves where the deformation differentials start to drop. The corresponding tensile strength at fracture point is shown in Figure 5-3.

The differences between the predicted values and the average values for Nova Scotia, NW39_1C and I95SJN_BWP were 5.3%. 5.6% and 12.5% respectively. Figure 5-4 compares the predicted fracture energy densities to the trim mean average values of the mixes (Table 5-4). The trim mean average value of a given mix was calculated by excluding the highest and the lowest of the reported values on 6 faces of the 3 samples and average the remaining four. The differences between the predicted values and the

trim mean average values for Nova Scotia, NW39_1C and I95SJN_BWP were -3.6%, 0.7% and –31.2% respectively.

The large discrepancy of the I95SJN_BWP was likely primary due to the variability in the experimental test results. The test result of mix I95SJN_BWP samples 1 to 3 had tensile strengths of 3.75, 3.38 and 2.45 MPa respectively and fracture energy densities reported on each face of sample 1 to 3 were (1.56, 1.68), (0.70, 1.33), and (1.20, 2.38) KJ/m^3 respectively. Overall, the method yields a good approximation for tensile strength at fracture and fracture energy density when the material variability is small and becomes less reliable when the variability is high.

Figure 5-5 shows crack patterns of three mixtures at three critical load steps: A) crack initiation, B) crack at fracture points and C) major opening cracks at final load step. All three samples have the same crack pattern that several micro cracks randomly initiate in the tension zone and coalesce to form a major opening crack, which can be observed in laboratory.

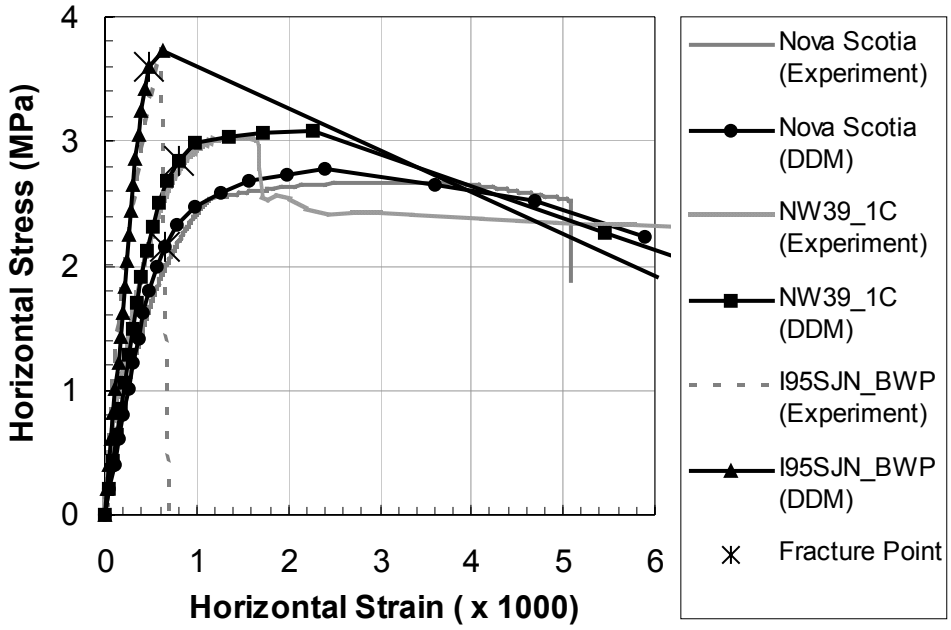

A

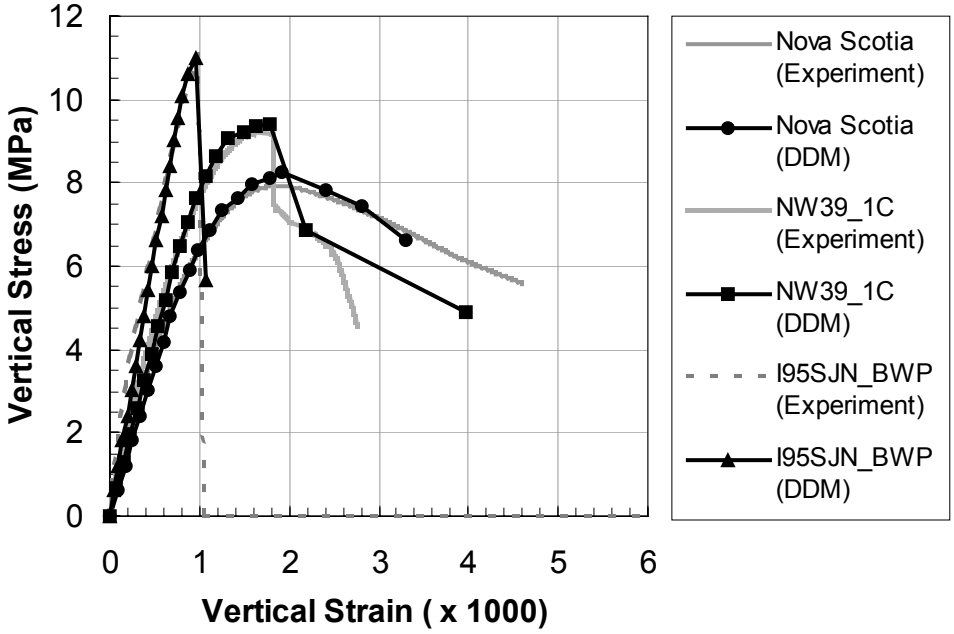

B

Figure 5-1. Comparison of predicted and measured horizontal and vertical stress-strain curves for three mixtures: Nova Scotia, NW39_1C and I95SJN_BWP. A) Horizontal stress strain responses at center of specimen and B) Vertical stress strain responses at center of specimen.

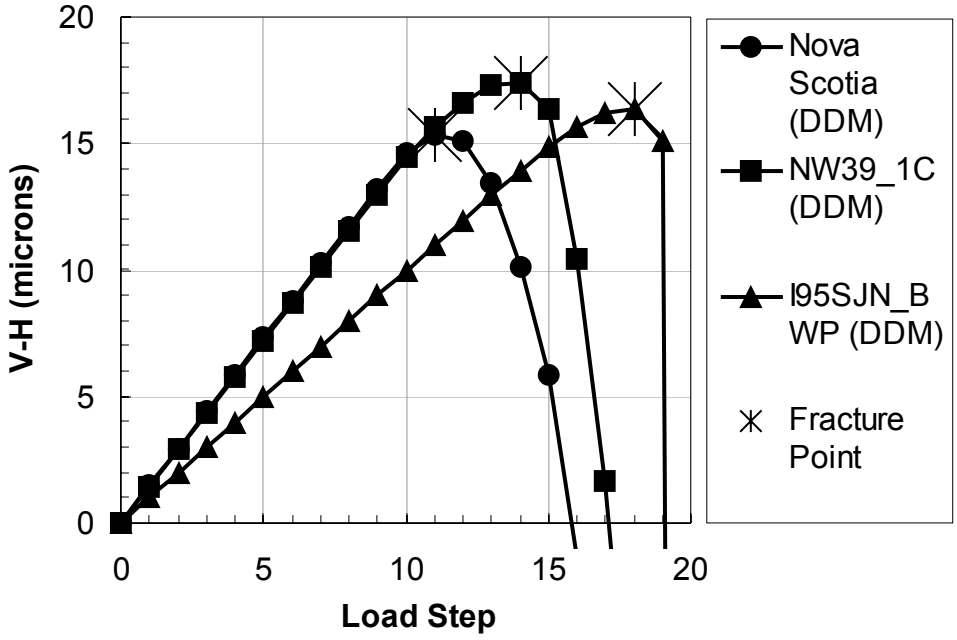

Figure 5-2. Simulated deformation differentials for the Nova Scotia, NW39_1C and I95SJN_BWP mixtures.

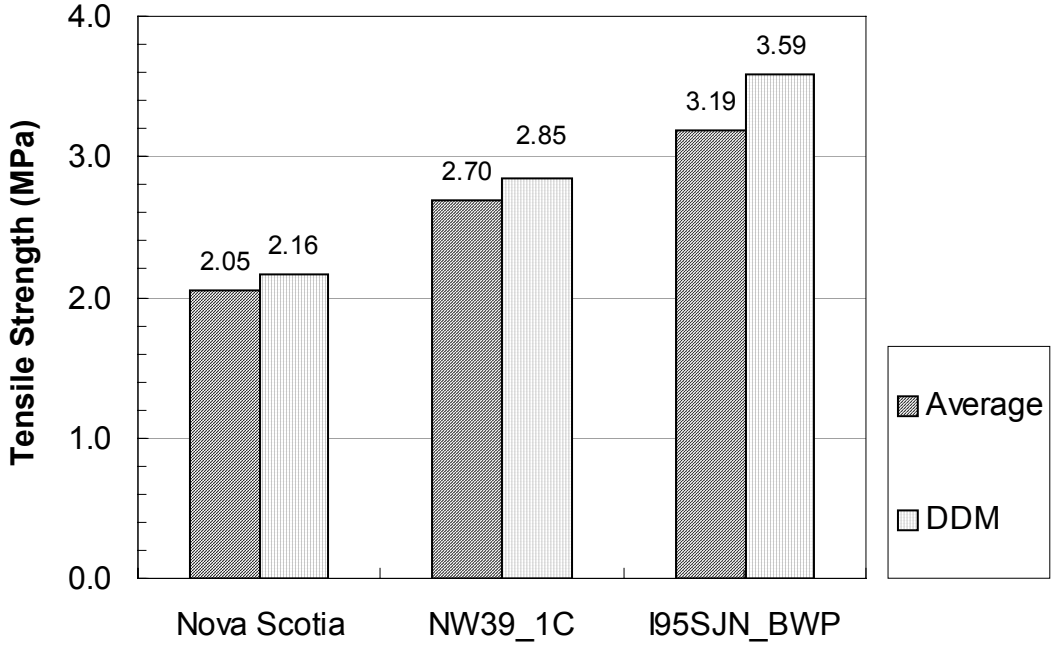

Figure 5-3. Tensile strength at fracture for three mixtures (Nova Scotia, NW39_1C and I95SJN_BWP). The average value of each mixture was compared to the tensile strength predicted by displacement discontinuity method (DDM).

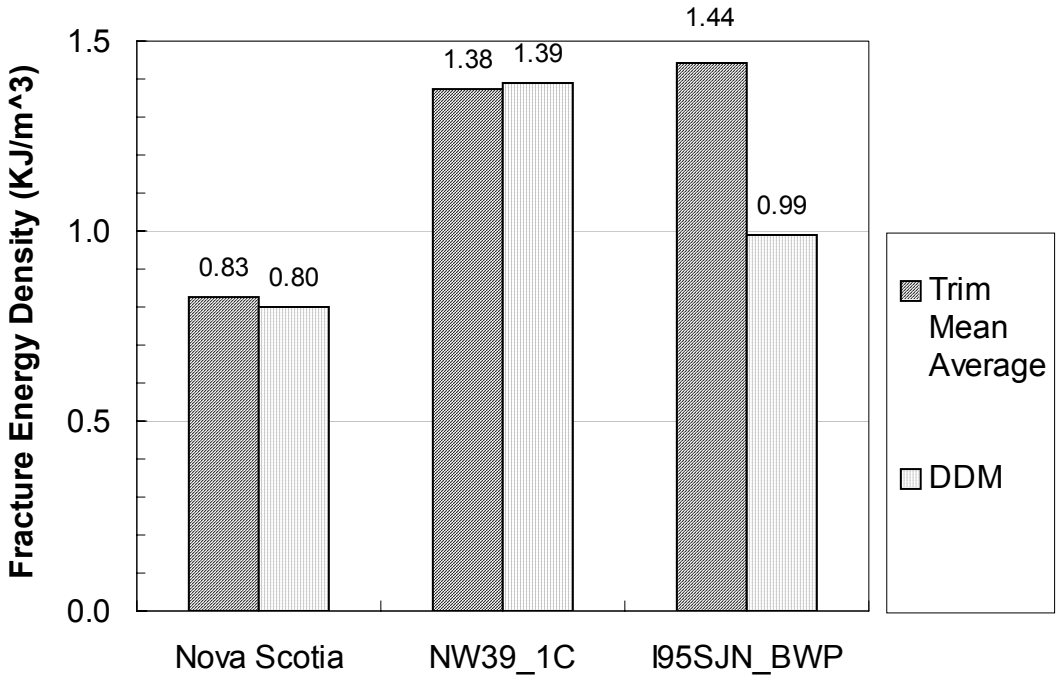

Figure 5-4. Fracture energy density at center of specimen for three mixtures (Nova Scotia, NW39_1C and I95SJN_BWP). The trim mean average value of each mixture was compared to the fracture energy density predicted by displacement discontinuity method (DDM).

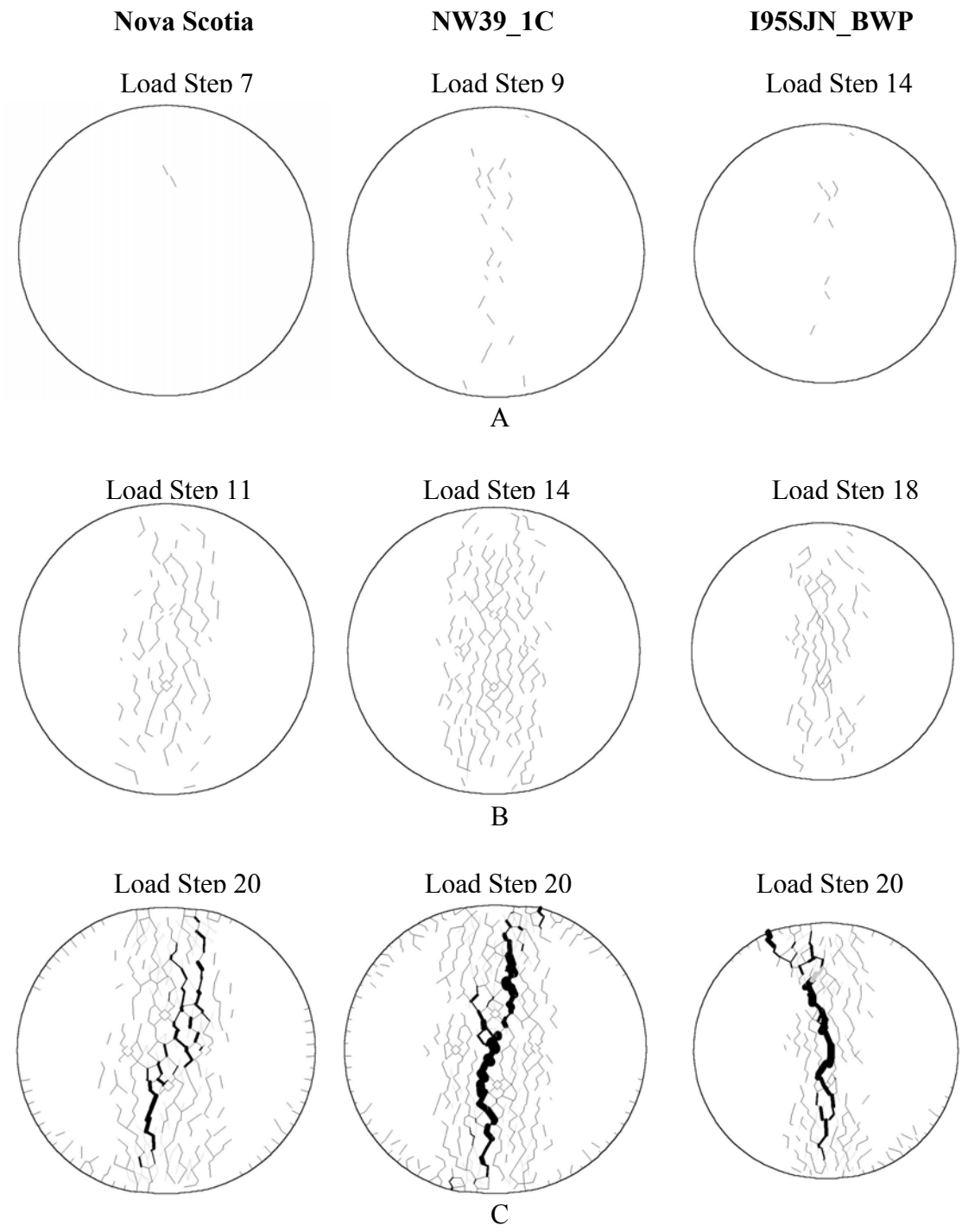

Figure 5-5. Predicted crack patterns for the three mixtures (Nova Scotia, NW39_1C and I95SJN_BWP) at three load steps: A) Crack initiation in specimen (first cracks that appear in specimen), B) Crack pattern at fracture point and C) Cracks at the final load step.

5.5 Conclusions

Explicit fracture modeling with the displacement discontinuity boundary element method successfully simulated the cracking behavior of three asphalt mixtures and evaluated their tensile strength and fracture energy density. It can be concluded, according to three mixtures demonstrated here, that the explicit fracture model with displacement discontinuity elements has the potential to simulate the cracking behavior and reasonably evaluate tensile strength and fracture energy density.

CHAPTER 6
SUMMARY, CONCLUSIONS AND RECOMMENDATIONS

6.1 Summary

Several studies using the displacement discontinuity boundary element method were conducted to identify the most appropriate set of components for a numerical model that can realistically simulate the Superpave IDT strength test. Parametric studies were also performed to identify the key factors that control the cracking behavior of asphalt mixtures. Finally, the method was applied to evaluate the fracture behavior of mixtures. A summary of the findings obtained from each study is listed below:

- The most suitable tessellation scheme to represent aggregate structure was the Voronoi with internal fracture paths. Voronoi tessellations alone can also yield a reasonable results but it was found difficult to calibrate material parameters to fit the experimental stress strain curves, especially at the peak and in the post-peak part of the stress-strain curves. Deluanay tessellation schemes were found unsuitable to represent aggregate structure because the resulting cracked structure causes floating regions, which sometimes lead to instability at strain gauge locations.

- The mastic properties are key to controlling the cracking behavior of asphalt mixtures. At the beginning, the initiation and propagation of microcracks in the mastic weakens the aggregate structure and causes compression softening in the stress-strain curve. As the number of active cracks and their sizes increase, the sample stiffness decreases rapidly. The strength is terminated when the random major cracks appear in the mastic. The material parameters defined for the mastic that are directly related to the strength of the specimen are cohesion, tension cutoff and friction angle. The rate of cohesion softening, tension softening and opening crack limit also affected the strength of specimen. The residual cohesion and residual friction angle had little effect to the strength of specimen, but they do control the post peak behavior of stress strain responses.

- Toughness of rock represented by the strength of the fracture paths inside aggregates is not sensitive to the specimen strength as long as it is about 2-3 times larger than the mastic strength. The break down of aggregate at high load levels

yields a smooth compression softening curve near the peak of the vertical compression stress strain curve.

- In the numerical experiments, using different uniform aggregate size revealed a small size effect on the strength of specimen. Smaller aggregate sizes yield more distributed cracks and cause softer responses than the larger aggregate sizes.

- The current version of DIGS that uses Mohr-Coulomb type of failure can simulate the Superpave IDT strength test and evaluate its mixture properties with acceptable accuracy.

6.2 Conclusions

Based on the finding previously discussed, the following conclusion were made:

- The displacement discontinuity boundary element method with tessellation scheme can simulate the Superpave IDT strength test.

- Voronoi tessellation with internal fracture paths is the best representative of aggregate structure.

- The parallel crack growth rule is suitable for simulating the Superpave IDT strength test because it is more economical than the sequential crack growth rule.

- The factors that control the strength of a Superpave IDT specimen ranked from the most to the least are strength of mastic, strength of fracture path in aggregates, and aggregate size.

6.3 Recommendations

Based on the findings and conclusions of numerical experiments the following recommendations are made:

- From the numerical studies, the mastic, which is the weakest link in the specimen, plays the most important role in cracking behavior in the Superpave IDT test. The mastic in a numerical model refers to the apparent strength of the mastic in the presence of air voids. The improvement of mastic properties will directly result in the increase of cracking resistance.

- Despite the success of the numerical modeling, the simulations were merely the results of the assumptions made in the models. Whether the assumptions are reasonable may require the development of testing procedures to more directly obtain values for the micromechanical parameters used.

- Other failure laws that can simulate viscoplastic and cyclic loading should be developed so that the method will yield more useful applications.

- The incorporation of multi-region boundary element codes into DIGS that can simulate layered pavement is recommend for future research. These will provide analytical tools to simulate and observe cracking behavior of specific mixtures in a pavement.

APPENDIX
USER MANUALS FOR PRE/POST PROCESSOR (DDM)

A.1 Introduction

This user manual explains how to use PRE/POST processor DDM with the program Discontinuity Interaction and Growth Simulation DIGS and Delaunay Voronoi Tessellation Generator DVT. DDM is a graphic user interface operates under window environment. It can read and write codes to the files associated with DIGS and DVT. Three file types (*.IN, ._SG and .DAT) are involved with PRE processor and other three file types (*.OUT, *.REQ and *.RPT) are involved with POST processor. DIGS is a two-dimensional (plane strain) stress analysis computer code that can be used to solve crack, fault and tabular stope interaction and intersection problems. The code is based on the displacement discontinuity boundary element method and employs linear-variation shape functions in the element. DVT is a mesh generator for Delaunay and Voronoi tessellation. The result of meshing can be used to simulate granular structure of the desired material.

Input file (*.IN) contains information of meshing parameters and boundary definition of the regions to be meshed. The IN file is used with the DVT to generate two segment files (*._SG): Delaunay (*.DSG) and Voronoi with internal fracture path (*.VSG). Segment file contains definitions of 'Line' segments that describe geometry of the problem to be solved. User can use PRE processor to open these two segment files, edit segment definitions and save them to other segment file names (*._SG) for later used. It is required by the PRE processor that the segment file must have its last two

letters ‘SG’ in the extension. Data file (*.DAT) contains essential information (background material properties, primitive stress fields, boundary conditions, load step, segment file name and request output report) to run boundary element analysis with DIGS. Even though, segment definitions can be explicitly defined within the DAT file, the PRE processor does not recognize that format. Users must complexly define the geometry of the problem in a segment file and attach its name to the DAT file. Output file (*.OUT) contains the results from boundary element analysis. POST processor can open this file to view the result graphically. Users can also request specific output variables at desired load steps by writing command codes in the request file (*.REQ) and reporting them to the report file (*.RPT).

A.2 Coordinate Systems

The DIGS code assumes that all discontinuity positions are defined with respect to a global Y-Z coordinate system as depicted in Figure A-1. The X-axis is assumed to point into the plane of the diagram and all displacements in the X-direction are assumed to be zero (i.e. plane strain with respect to the Y-Z plane).

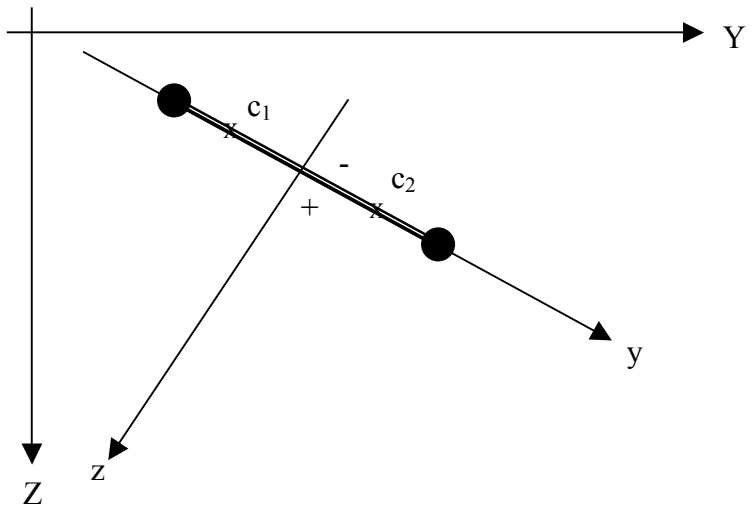

Figure A-1. Global (Y-Z) and local (y-z) coordinate systems used by DIGS.

Each defined element is flat and has a local y-z coordinate system as shown in Figure A-1. The ends of the element are marked "o" and discontinuity values are computed at two collocation points (c_1 and c_2) within the element, marked "x". The local element axis system implies an orientation of the element with the positive (+) side in the positive z direction and the negative (-) side in the opposite direction. No continuity conditions on the discontinuity slip or opening values are enforced between adjoining elements. It is important that elements should not be defined to intersect one another but may be defined to be connected at their end points.

A.3 Text Files Associated with PRE/POST Processor

There are total 6 files (*.IN, *._SG, *.DAT, *.OUT, *.REQ and *.RPT) associated with PRE/POST Processor. The following 6 subsections will explain the structure and command codes used in each file.

A.3.1 Input File (*.IN File)

The IN file is an input text file containing computer codes for the program DVT to generate two tessellations: Delaunay and Voronoi with internal fracture path. The computer codes are written in fixed field format. That mean users have to write the codes within a specific range of columns. The structure of IN file consists of 3 coding blocks as following.

- Random point generation
- Seed triangle for creating tessellation
  -End of region definition ('R/')
- Boundary definitions
  -End of boundary line definition ('B/')
  -Comments (optional)

To explain the code for each field, the Fortran format 'A*n*' is used for characters, 'I*n*' for integer values, 'F*n*' for floating point numeric values where *n* denotes the length of the record field.

Random Point Generation (defined in one line)

Field 1 (A3): Random point generation code = 'RMG'

Field 2 (I8): Nominal number of points to be generated. Suppose there is an area A to be generate with the nominal mesh length g. The nominal number of point is $N = A/g^2$. However, it should set the number of point to be slightly greater than N, say 1.5*N.

Field 3 (I8): Random number seed. It is an arbitrary number used as a start sequence in the FORTRAN random number routine.

Field 3 (I8): Minimum point spacing constraint. When the random points are generated, they are never allowed to be closer to one another than this minimum distance. This prevents coincident points or very closely spaced points leading to very irregular mesh triangle generation.

Field 4 (F8): Start y-coordinate of a rectangular area (Left) for random point to be generated.

Field 5 (F8): Start z-coordinate of a rectangular area (Top) for random point to be generated.

Field 6 (F8): End y-coordinate of a rectangular area (Right) for random point to be generated.

Field 7 (F8): End z-coordinate of a rectangular area (Bottom) for random point to be generated.

Field 8 (F8): Subtended angle for Voronoi edge condensation. In the Voronoi polygon generation, each random point forms the so-called geometric center of the polygon. Joining a set of lines from the center to each vertex of the polygon, defines a set of triangles with a common vertex at the center. If the angle formed between the sides of any triangle emanating from the central vertex is less than the specified tolerance, then the other two points of the triangle are condensed to one point. This effectively eliminates very short mesh lengths in the Voronoi construction (but of course destroys the Voronoi diagram strict properties).

Seed Triangle for Construction of Tessellation (defined in one line)

Field 1 (A1): Seed triangle code = 'S'

Field 2 (I8): Seed triangle vertex component y1

Field 3 (I8): Seed triangle vertex component z1

Field 4 (I8): Seed triangle vertex component y2

Field 5 (I8): Seed triangle vertex component z2

Field 6 (I8): Seed triangle vertex component y3

Field 6 (I8): Seed triangle vertex component z3.

The triangle will be used as a starter to form Delaunay tessellation and construct its dual mesh Voronoi. It is important to place the triangle in the region where tessellation to be generated.

End of Region Definition (defined in one line)

Field 1 (A2): End of region definition = 'R/'

Boundary Definition (defined as many lines as needed)

Field 1 (A3): Boundary definition code = 'BLB' or 'BCB'

BLB : B = ‘boundary’ definition; L = ‘line’ type; B = ‘color’ code stored in output record.

BCB : B = ‘boundary’ definition; C = ‘circle’ type; B = ‘color’ code stored in output record.

DDM recognizes only two boundary definition codes ‘BLB’ and ‘BCB’. The color code ‘B’ is not used in the PRE/POST processor but must be defined as part of the boundary definition code.

Field 2 (I8): Number of elements along the boundary line.

Field 3 (F8): Minimum distance a random point is allowed from the boundary. Too small distance may result in generated mesh crossing the boundary line.

Field 4 (F8): Start y-coordinate of the line (for boundary definition code ‘BLB’) or Start y- coordinate of the center (for boundary definition code ‘BCB’)

Field 5 (F8): Start z-coordinate of the line (for boundary definition code ‘BLB’) or Start z-coordinate of the center (for boundary definition code ‘BCB’)

Field 6 (F8): End y-coordinate of the line (for boundary definition code ‘BLB’) or End y-coordinate on the circumference (for boundary definition code ‘BCB’)

Field 7 (F8): End z-coordinate of the line (for boundary definition code ‘BLB’) or End z-coordinate on the circumferences (for boundary definition code ‘BCB’)

<u>End of Boundary Line Definition (defined in one line)</u>

Field 1 (A2): End of boundary line definition = ‘B/’

Comment Record (defined as many lines as needed)

Any record starting with the characters '**' is ignored and treated as a comment. In the IN file, comments can only be placed after the end of boundary line definition ('B/'). Placing comments among the lines of codes will cause errors.

Example 1: Square Plate with a Circular Hole (PLATE_H.IN)

Figure A-2 shows a square plate that has a size of 100x100 mm. The boundary region consists of four 'Line' segments and a 'Circular' segment. 'Linear' and 'Circular' segments are each divided into 10 elements. Points used for constructing of tessellation are randomly seeded from the 'Left Top' corner (-50, -50) to the 'Right Bottom' corner (50, 50) of the model with these parameters: nominal number of points = 1000, random number seed = 1, minimum point spacing constraint = 10, subtended angle for Voronoi edge condensation = 15. An initial triangle with the coordinates (30,0), (40,0) and (35, 10) are placed between the inner circle and the outer square. The mesh generation is not allowed to go closer than 5 mm to the 'Line' segment and 10 mm to the 'Circular' segment.

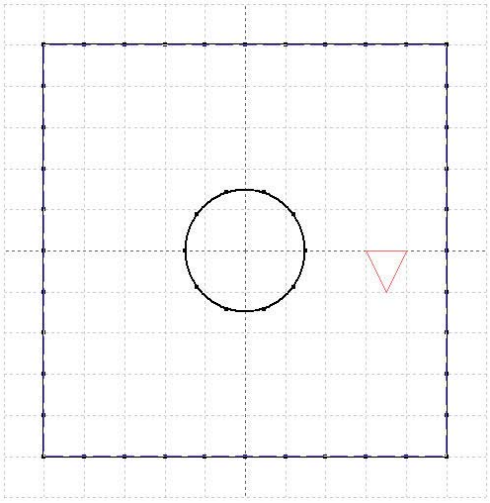

Figure A-2. Square plate with a circular hole for the input file.

The following codes in PLATE_H.IN can be used with DVT.exe to generate Delaunay tessellation and Voronoi tessellation with internal fracture path.

PLATE_H.IN

```
RMG    1000       1      10     -50     -50      50      50      15
S        30       0      40       0      35      10
R/
BLB      10       5     -50     -50      50     -50
BLB      10       5      50     -50      50      50
BLB      10       5      50      50     -50      50
BLB      10       5     -50      50     -50     -50
BCB      10      10       0       0       0      15
B/
***
*** use DVT.exe to generate tessellation
```

A.3.2 Segment File (*._SG)

The segment file is a text file containing definition of segments that describe geometry of the problem. The DVT uses the IN file to generate two segment files named Dealuanay tessellation file (*.DSG) and Voronoi with internal fracture path tessellation file (*.VSG). The computer codes of these two files are written in fixed field format. The structure of the segment file consists of several lines of segment definitions, which its codes are as follows.

Segment Definition (defined as many lines as needed)

Field 1 (A1): Segment type code

= ‘S’ for ordinary boundary segment

= ‘?’ for potential crack segment

Field 2 (A1): A letter code refers to boundary condition code for ordinary boundary segment or material constitutive code for potential crack segment.

Field 3 (I4): Segment number

Field 4 (I4): Number of elements per segment

Field 5 (F8): Start y-coordinate for a line segment

Field 6 (F8): Start z-coordinate for a line segment

Field 7 (F8): End y-coordinate for a line segment

Field 8 (F8): End z-coordinate for a line segment

Field 9: The remaining codes are not used by the program.

Example 2: Square Plate with a Circular Hole (PLATE_H.DSG and PLATE_H.VSG)

Figure A-3 below shows the result of using DVT with PLATE_H.IN to generate Delaunay and Voronoi with internal fracture path tessellations. The segment files PLATE_H.DSG and PLATE_H.VSG can be included in a DAT file to describe the plate geometry and tessellation used in a problem.

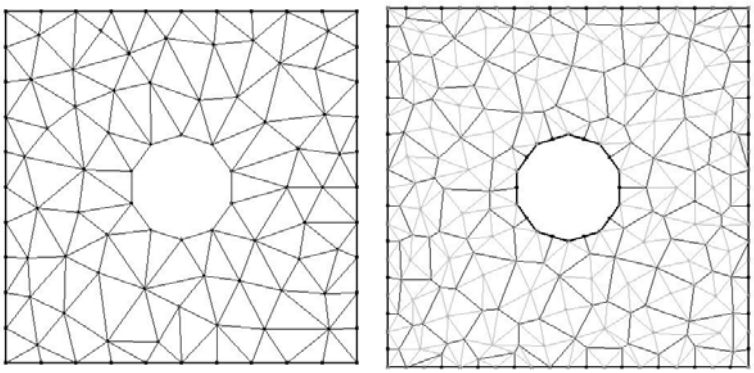

A B

Figure A-3. Square plate with a circular hole for the segment files: A) Delaunay tessellation (PLATE_H.DSG) and B) Voronoi with internal with fracture path (PLATE_H.VSG).

Here are the samples of codes written in the segment files (PLATE_H.DSG and PLATE_H). The segment files can then be attached to the DAT file to run the boundary element analysis with DIGS.

PLATE_H.DSG

```
SM   1   1  30.000    .000  40.000    .000     0.0     0.0           G   T T
SM   2   1  40.000    .000  35.000  10.000     0.0     0.0           G   T T
SM   3   1  35.000  10.000  30.000    .000     0.0     0.0           G   T T
SB   4   1 -50.000 -50.000 -40.000 -50.000     0.0     0.0           B   T T
SB   5   1 -40.000 -50.000 -30.000 -50.000     0.0     0.0           B   T T
SB   6   1 -30.000 -50.000 -20.000 -50.000     0.0     0.0           B   T T
.
.
.
SM 248   1 -50.000 -10.000 -44.795  -8.764     0.0     0.0           G   T T
SM 249   1 -50.000 -30.000 -42.834 -30.814     0.0     0.0           G   T T
SM 250   1 -50.000 -50.000 -40.659 -43.330     0.0     0.0           G   T T
```

PLATE_H.VSG

```
SV   1   1 -50.000 -50.000 -45.000 -50.000     0.0     0.0           W   T T
SV   2   1 -45.000 -50.000 -40.000 -50.000     0.0     0.0           W   T T
SV   3   1 -40.000 -50.000 -35.000 -50.000     0.0     0.0           W   T T
.
.
.
?V 711   1  33.368  20.420  24.491  22.315     0.0     0.0           W   T T
?V 712   1  33.368  20.420  34.769  27.095     0.0     0.0           W   T T
?V 713   1  33.368  20.420  39.906  23.158     0.0     0.0           W   T T
```

A.3.3 Data File (*.DAT)

The DAT file is a text file that contains command codes describing background material, primitive stress fields, boundary conditions, material constitutive models, load steps and output reports. The codes are written in fixed field format. The structure of the DAT file consists of 4 coding blocks.

- General parameters for background material and primitive stress fields
- Boundary conditions
- Material constitutive models for potential crack segments
- Processing steps (or load step)
  - Processing step element report requests
  - Processing step field point report requests

  - Comments (optional) can be placed at any locations between each coding bock.
  - End of Data file marked with '//'

General Parameters for Background Material and Primitive Stress Fields
(defined in one line)

Field 1 (A1): Record type character = 'P'

Field 2 (A1): Symmetry control character

= 'R' – No symmetry, infinite region

= 'H' – Half-space problem in region $z \geq 0$, enforcing a stress-free surface on $z = 0$

= 'Y' – Symmetry with respect to the y-axis ($z = 0$)

= 'Z' – Symmetry with respect to the z-axis ($y = 0$)

= 'D' – Double symmetry with respect to both the y-axis and the z-axis

= 'A' – Anti-symmetry through the origin $y = 0, z = 0$

Field 3 (F8): Young's modulus (MPa)

Field 4 (F8): Poisson's ratio

Field 5 (F8): Stress gradient, with respect to the *z* – direction, of the *yy* stress component of the primitive stress field (MPa / m)

Field 6 (F8): Stress gradient, with respect to the *z* – direction, of the *zz* stress component of the primitive stress field (MPa / m)

Field 7 (F8): Constant *yy* component of the primitive stress field

Field 8 (F8): Constant *yz* component of the primitive stress field

Field 9 (F8): Constant *zz* component of the primitive stress field

Boundary Conditions (defined as many lines as needed)

Field 1 (A1): Record type character = 'C'

Field 2 (A1): Single character for boundary condition code.

Field 3 (A1): Format selection character for explicit boundary condition interpretation (Set character = 'C')

Field 4 (A1): Shear boundary condition indicator; set character = 'S'

Field 5 (A1): Shear boundary condition type selection code:

= 'T' – local shear traction component specification

= 'D' – local shear discontinuity component specification

= '+' – local *y* displacement component specification on '+' side of element

= '-' – local *y* displacement component specification on '-' side of element

Field 6 (F10): Numerical value of selected shear boundary condition at collocation point 1

Field 7 (F10): Numerical value of selected shear boundary condition at collocation point 2

Field 8 (A1): Normal boundary condition indicator; set character = 'N'

Field 9 (A1): Normal boundary condition type selection code:

= 'T' – local normal traction component specification

= 'D' – local normal discontinuity component specification

= '+' – local *z* displacement component specification on the '+' side of element

= '-' – local *z* displacement component specification on the '-' side of element

Field 10 (F10): Numerical value of selected normal boundary condition at collocation point 1

Field 11 (F10): Numerical value of selected normal boundary condition at collocation point 2

Material Constitutive Model for Potential Crack Segments (defined as many lines as needed)

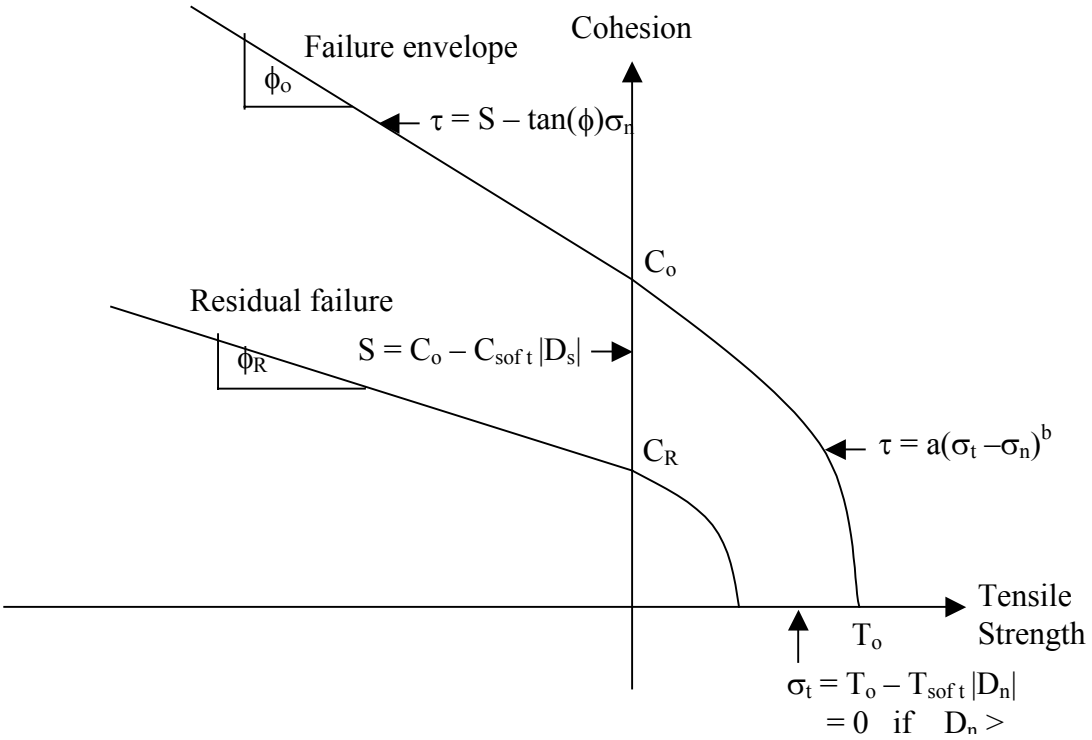

Figure A-4. Mohr Coulomb type of failure.

Field 1 (A1): Record type character = 'C'

Field 2 (A1): Single character for a material constitutive code.

Field 3 (A1): Format selection character for constitutive model

(Set character = blank). The constitutive definition is applied to *both* collocation points in any discontinuity segment that refers to this definition.

Field 4 (F5): Crack width (must be set = 0 for crack or fault definition)

Field 5 (F6): Initial intact cohesion, C_o (MPa)

Field 6 (F6): Initial intact friction angle, ϕ_o (Degree)

Field 7(F6): Initial sliding dilation angle, ψ_o (Degree)

Field 8(F6): Residual cohesion, C_R (MPa)

Field 9(F6): Residual friction angle, ϕ_R (MPa)

Field 10(F6): Reverse dilation angle relative to initial sliding direction, ψ_R (Degree)

Field 11(F6): Tension cut off, T_o (MPa)

Field 12(F6): Opening crack limit over which tensile strength is lost, D_{NCR} (This defines implicitly the tension softening slope, $T_{soft} = T_o/D_{NCR}$, with respect to the opening crack limit.

Field 13(F6): Cohesion softening slope, C_{soft} (MPa / mm)

Field 14(F6): Tension softening slope, T_{soft} (MPa / mm). Note that the specification of *both* D_{NCR} and T_{soft} is redundant. This arises from the possible provision of a non-linear tension-weakening law not described here. The non-linear model is still in experimental process.

Field 15(F9): Parameter LAMDA. It is a exponent in tension weakening law controlling residual tensile strength as a function of crack opening. LAMDA = 1 for linear tension weakening (default)

Field 16 (F8): Viscoelastic parameter 1, VP1 (mm/(s.MPa)). It is proportionality constant in relaxation creep law or may be ignored if creep not being simulated.

Field 16 (F8): Viscoelastic parameter 2, VP2. It is an exponent in creep law or ignored if creep not simulated.

Processing Step (defined as many lines as needed)

Field 1 (A1): Processing step header specification ('!')

Field 2 (A1): Single character for determining crack grow rule

'P' = parallel crack growth rule for each incremental growth step

'I' = incremental (or sequential) crack growth rule for each incremental growth step

Field 3 (A4): Step identification name

Field 4 (F6): Message skip interval for reporting iteration convergence status (≥ 1)

Field 5 (F6): Maximum number of crack growth search increments per time step interval (≥ 0)

Filed 6 (F6): Number of time steps associated with the current processing step (≥ 0)

Field 7 (F6): Time step size in chosen "time" units

Field 8 (F6): Stress tolerance for solution iteration (MPa)

Field 9 (F6): Field not used – set to zero

Field 10 (F6): Maximum number of iterations allowed in each solution cycle

Field 11 (F6): Iteration relaxation factor, ω (suggest $\omega = 0.4$)

Field 12 (A2): Step “color” code character

Field 13 (A2): Selection code for iterative solution routine, right justified

= ‘#’ - Lanczos-1-Delayed

= ‘%’ - Lanczos-2 scheme

= ‘G’ - Gauss-Seidel

= ‘J’ - Jacobi

Processing Step Element Report Request (defined as many lines as needed within the current processing step)

Field 1 (A1): Record type character = ‘R’

Field 2 (A1): Report type code

= ‘A’ – report only active elements.

= ‘X’ – report all elements.

= ‘S’ – report energy release

Field 3 (A4): Segment selection mask code – this field is optional and can be used to select element reports on segments that match non-blank characters in the mask code

Processing Step Field Point Report Request (defined as many lines as needed within the current processing step)

Field 1 (A1): Record type character = ‘R’

Field 2 (A1): Report type code

= ‘C’ – report stress component in Cartesian coordinates

= ‘G’ – report stress components in principal directions

Both ‘C’ and ‘G’ report displacement components in global Cartesian coordinates

Field 3 (F4): Number of field points in Y-axis direction

Field 4 (F4): Number of field points in Z-axis direction

Field 5 (F4): Origin field point coordinate Y_o

Field 6 (F4): Origin field point coordinate Z_o

Field 7 (F4): Angle of a line of field points, in degrees, measured positive from global Y-axis towards global Z-axis

Field 8 (F4): Incremental distance between field points in Y direction

Field 9 (F4): Incremental distance between field points in Z direction

End of Input Data Marker (defined in one line)

Field 9 (A2): Record type character = '//'.

Comment record (defined as many lines as needed)

Any record starting with the characters '**' is ignored and treated as a comment.

Example 3: Square Plate with a Circular Hole (PLATE_H.DAT)

A square plate with a circular hole shown in Figure A-5 is subjected to uniaxial tension. The elastic background material has Young's Modulus = 6000 MPa and Poisson's ratio = 0.2. Five boundary condition codes (T, D, B, C and A) are defined for ordinary boundary segments on the edges of square plate and the inner circle. Two material constitutive codes (M and V) are defined for potential crack segments that form Voronoi with internal fracture path tessellation. All segments used for this problem are defined in the segment file PLATE_H2.VSG, which was created by using the PRE processor to edit boundary condition codes for ordinary boundary element and material constitutive codes for potential crack elements in the PLATE_H.VSG.

The square plate is fixed at the bottom and pulled upward 0.05 mm for 5 load steps. In the first load step LD00, request energy release report (RS) and all element report (RX). In subsequent load steps (LD01, LD02, LD03, LD04 and LD05), request energy

release report (RS), active element report (RA), ‘Linear’ field point report in principal direction (RG) and ‘Matrix’ field point report in Cartesian coordinate (RC).

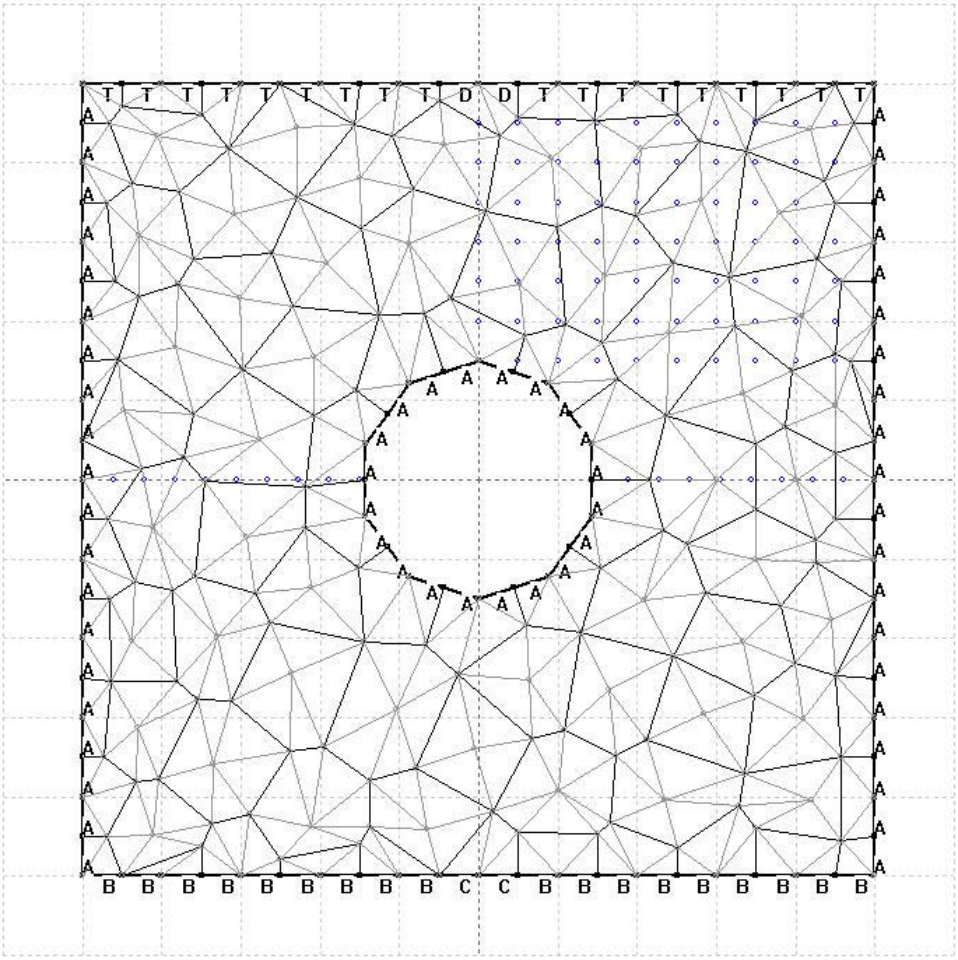

Figure A-5. Square plate with a circular hole for the data file.

Here are the codes written in PLATE_H.DAT file for this problem.

PLATE_H.DAT

```
*****************************************************************************
***                              DAT file                                 ***
*****************************************************************************
**
**...GENERAL PARAMETERS
**       YM       PR       GY       GZ      CYY      CYZ      CZZ      CPP     PPGR
PR     6000      0.2        0        0        0        0        0        0        0
```

```
VTCST          0          0N+      -0.01      -0.01
VDCS+          0          0N+      -0.01      -0.01
CBCST          0          0N+          0          0
CCCS+          0          0N+          0          0
CACST          0          0NT          0          0
**
**   WID   COH   FRN   DIL  FCOH  FFRN  RDIL  TCUT  DNCR CSOFT TSOFT#   LAMDA VP1   VP2
CM     0     3    35     0   0.1    20     0     3  0.05    60    60         1   0     1
CV     0     6    35     0   0.1    20     0     6  0.02   300   300         1   0     1
**
**STEP MSKIP MXINC MXSTP TSTEP  TTOL  DTOL MAXIT   SOR C S
!PLD00    10    10     1     1 0.005     0   250   0.4 B #
I PLATE_H2.VSG
RX
RS
!PLD01    10    10     1     1 0.005     0   250   0.4 B #
RA
RS
RG  10   1      15       0       0  3.8889       0
RC  11   8       0     -50       0       5       5
!PLD02    10    10     1     1 0.005     0   250   0.4 B #
RA
RS
RG  10   1      15       0       0  3.8889       0
RC  11   8       0     -50       0       5       5
!PLD03    10    10     1     1 0.005     0   250   0.4 B #
RA
RS
RG  10   1      15       0       0  3.8889       0
RC  11   8       0     -50       0       5       5
!PLD04    10    10     1     1 0.005     0   250   0.4 B #
RA
RS
RG  10   1      15       0       0  3.8889       0
RC  11   8       0     -50       0       5       5
!PLD05    10    10     1     1 0.005     0   250   0.4 B #
```

```
RA
RS
RG  10   1      15       0       0  3.8889       0
RC  11   8       0     -50       0       5       5
//
```

A.3.4 Output File (*.OUT)

The OUT file contains the analysis result obtained from DIGS. The OUT file first echoes the information in the DAT file and subsequently reports the requested output variables at elements and field points for each load step. The output variable names will be explained in three subsets:

- Output variables at element (requested with command code 'RX' or 'RA')
- Output variable at field point (requested with command code 'RC')
- Output variables at field point (requested with command code 'RG')

Output Variables at Element (Requested with Command Code 'RX' or 'RA')

The output variables below are reported at two collocation points (YC, ZC) for each element being requested.

ANG = Angle (degree) measured from Y-axis to Z-axis

TYY+ = Local tangential stress yy component (MPa) on positive side

TYY- = Local tangential stress yy component (MPa) on negative side

TYZ = Local shear stress yz component (MPa)

TZZ = Local normal stress zz component (MPa); tension positive

COH = Cohesion strength (MPa)

DY = Sliding crack displacement (mm*1000)

DZ = Opening crack displacement (mm*1000)

FW/DL = Either Fill Width (ignore - for mining applications) or crack dilation (mm*1000) - crack opening induced by sliding if a dilation angle is specified.

UY+ = Local displacement in y direction (mm*1000) measured on positive side

UZ+ = Local displacement in z direction (mm*1000) measured on positive side

CODE = A letter code (either boundary condition code or material constitutive code for the element being reported.

Output Variables at Field Point (Requested with Command Code 'RC')

MAJOR = Major principal stress (MPa); tension positive

MINOR = Minor pricipal stress (MPa) ; tension positive

MAJ.ANG = Major angle (degree) measured from Y-axis to Z-axis

UY = Global displacement in Y-direction (mm*1000)

UZ = Global displacement in Z-direction (mm*1000)

DMC = Distance to a Mohr-Coulomb envelope (MPa)

SED = Strain energy density (MPa)

Output Variables at Field Point (Requested with Command Code 'RG')

TYYB = Normal stress YY component (MPa) in global Cartesian coordinate.

TYZB = Shear stress YZ component (MPa) in global Cartesian coordinate.

TZZB = Normal stress ZZ component (MPa) in global Cartesian coordinate

UYB = Displacement in Y-direction (mm*1000) in global Cartesian coordinate

UZB = Displacement in Z-direction (mm*1000) in global Cartesian coordinate

ESS = Excess shear stress (MPa). This is the absolute shear stress across an element minus the frictional resistance (friction coefficient*normal stress).

A.3.5 Request File (*.REQ)

The REQ file is a text file containing request command codes to report output variables at each load step to the report file (*.RPT). The request command codes are written in free field format; separate each field with comma ",". If more than one line of request command code is needed, place a comma "," at the end of the line before continuing to the next line. The structure of REQ file consists of any of these coding blocks (not in particular order).

- Request output variables at elements
- Request output variables at field points (Cartesian coordinate 'RC')
- Request output variables at field points (Principal coordinate 'RG')

Request Output Variables at Elements

['EL']

[Number of load step requested], [number of lines defining load step names]

[Load step names (separate load step name with comma ",")

. {Continue to next line if needed}

.

]

[Number of elements requested], [number of lines defining element numbers]

[Element numbers (separated element number with comma ",")

. {Continue to next line if needed}

.

]

[Number of output variable names requested], [Number of lines defining output variable names]

[Output variable names such as YC, ZC, ANG, TYY+, TYY-, TYZ, TZZ, COH, DY, DZ, FW/DL, UY+, UZ+, CODE (separated by comma ‘,’)

. {Continue to next line if needed}

.

]

Request Output Variables At Field Points (Cartesian Coordinate ‘RC’)

[‘RC’]

[Number of load steps requested], [number of lines defined load step names]

[Load step names (separate load step name with comma)

. {Continue to next line if needed}

.

]

[Number of coordinates requested]

[Coordinate Y1, Coordinate Z2]

.

[Coordinate Yn, Coordinate Zn]

[Number of output variable names requested], [Number of lines defining output variable names]

[Output variable names such as TYYB, TYZB, TZZB, UYB, UZB, ESS (separated with comma)

. {Continue to next line if needed}

]

Request Output Variables at Field Points (Principal Coordinate ‘RG’)

[‘RG’]

[Number of load steps], [number of lines defining load step names]

[Load step names (separate load step name with comma)

. {Continue to next line if needed}

.

]

[Number of coordinates requested]

[Coordinate Y1, Coordinate Z2]

[Coordinate Y2, Coordinate Z2]

.

.

[Coordinate Yn, Coordinate Zn]

[Number of output variable names requested], [Number of lines defining output variable names]

[Output variable names such as MAJOR, MINOR, MAJ.ANG, UY, UZ, DMC, SED (separated with comma)

. {Continue to next line if needed}

.

]

Example of request file (*.REQ)

```
EL                        -Request output variables at DD elements
4, 1                      -4 load steps defined in 1 line
L010, L020, L030, L040    -Load step name (CAPITAL)
8, 1                      -8 number of elements defined in 1 line
1, 2, 3, 4, 5, 6, 7, 8    -Element numbers
4, 1                      -4 output variables defined in 1 line
YC, ZC, TYZ, TZZ          -Name of output variables (CAPITAL)
RG                        -Request output variables at field points
8, 2                      -8 load steps defined in 2 line
L010, L020, L030, L040,   -Load step names and use "," at the end of
L050, L060, L070, L080    -line to continue to next line
3                         -3 coordinates
-75.000, 0.000            -Coordinate (Y1,Z1)
-72.000, 0.000            -Coordinate (Y2,Z2)
-69.000, 0.000            -Coordinate (Y3,Z3)
5, 2                      -5 output variables defined in 2 line
MAJOR, MINOR, MAJ.ANG,    -Name of output variables (CAPITAL) and use
UY, UZ                    -"," at the end of line to continue next line
//                        -"//" for ending request
```

Note that *"-" at each line is used for the explanation purpose. Users should not use in the REQ file.*

A.3.6 Report File (*.RPT)

The RPT file is a result of using the request file (*.REQ) to request the output variables stored in the POST processor. The requested output variables are written in fixed field format, convenient to be opened with Spreadsheet program such as Excel.

A.4 The PRE/POST Processor (DDM)

PRE/POST processor was developed to help users create input and read output files. It assumes that users are familiar with window applications. Therefore, the manual will briefly explain only the functionality of the selections on menu bar and special features. In addition to the menu bar, the commonly tasks used in the program are provided in the tool bar for convenience.

PRE/POST processor provides a temporary workspace for several files (*.IN, *._SG, *.DAT, *.OUT). For each file opened, the information from that particular file will be loaded to the temporary workspace available for user to edit and save it back to the file where it belongs.

A.4.1 Symbols and Terminologies

[Menu] -> [Submenu] refers to the processes that the user selects a menu from a menu bar and then select one of its submenu.

<Key or Event> refers to a particular key on keyboard or an event acted by mouse. For example <Shift> + <Left Click> refers to the event that user hold <Shift> key and press <Left Click> on the mouse.

“Entity” here refers to one of these 4 objects (‘Line’ segment, ‘Circular’ segment, ‘Linear’ field point and ‘Matrix’ field point). These entities can be create, edit, and delete within the PRE processor.

“Highlight” (with pink color) happens when placing cursor over an entity. It indicates that the highlighted entity is temporarily selected. The selected entity can be processed with other commands by <Right Click> to open the cursor menu that contains Cut, Copy, Paste, Move, Send to Back, Edit Segment, Break Segment, Flip and Delete.

"Dark Highlight" (with dark pink color) happens when placing cursor over an entity and press <Shift> + <Left Click>. It indicates that the highlighted entity is permanently selected. When moves cursor away from the highlighted entity, the color of entity will appear dark pink. Users can add more selected entities by repeating the processes; place cursor over the desired entity and press <Shift> + <Left Click>.

A.4.2 Menu Bar

Figure A-6 shows the PRE/POST processor menu bar. It consists of File, Edit, View, Tessellation, Geometry, Field Point, Boundary, Material, Load Step, Display and Help. The common tasks available in menu bar are also provided in tool bar for convenience.

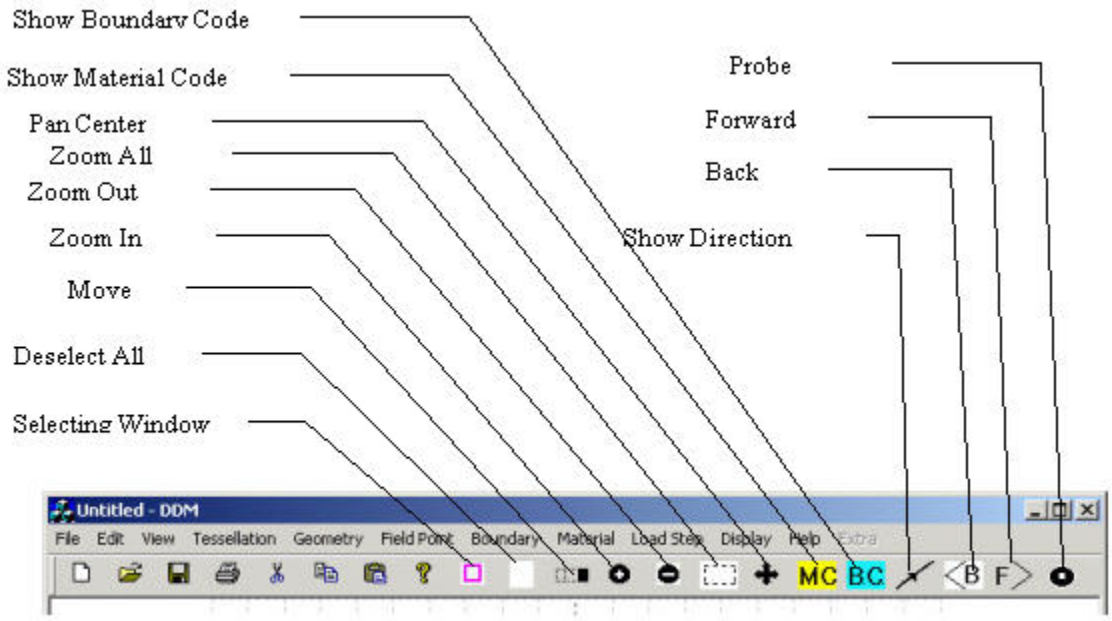

Figure A-6. The DDM menu bar.

[File]

Menu [File] has 5 submenus [New], [Open], [Save All], [Save As] and [Exit].

[File] -> [New] 

Pop up ‘Warning Dialog Box’ asking the user to save the opened files before creating new information in workspace. If select [Yes], the program will save all opened files (*.IN, *._SG and *.DAT). If select [No], the program will not save any information before working with new workspace. If select [Cancel], nothing happens.

[File] -> [Open] 

Pop up ‘Open Dialog Box’ asking the user to open one of these 4 file types (*.IN, *._SG *.DAT and *.OUT). The program will read information from each file and fill that information in workspace. The graphical information such as segments will be displayed graphically in window screen while non-graphical information such as boundary conditions will be placed in a particular dialog box such as ‘Boundary Condition Dialog Box’. The user can modify and save the information to the existing file or to the new file.

[File] -> [Save All] 

Pop up ‘Save As Dialog Box’ asking the user to save or not to save three file types (*.IN, *._SG *.DAT). The PRE processor can open up to 4 different files (*.IN, *._SG *.DAT and *.OUT) at the same time for convenience reason. The information of first three files that associate with the PRE processor will be saved to the files where it belongs.

[File] -> [Save As]

Pop up ‘Save As Dialog Box’ asking the user to save or not to save one of these 3 files (*.IN, *.XSG *.DAT).

[File] -> [Exit]

Pop up ‘Warning Dialog Box’ asking the user to save files before leaving the program. User has the last chance to save or not to save the information on workspace.

[Edit]

Menu [Edit] has 13 submenus [Selecting Window], [Select Element Group], [Deselect All], [Cut], [Copy], [Paste], [Move], [Send to Back], [Edit], [Break Segment], [Flip], [Delete] and [Clear].

[Edit] -> [Selecting Window] 

Turn on/off ‘Selecting Window’ mode. When the mode is on, the user can select several entities by pressing <Left Mouse Button> and drag to create a rectangular window crossing those entities. After releasing the mouse button, those entities will be permanently selected (dark highlighted) available for other operations to proceed.

[Edit] -> [Select Element Group]

Pop up ‘Select Element Group Dialog Box’ shown in Figure A-7 and ask the user to select element groups by specify boundary condition codes for ordinary boundary segments and/or material constitutive codes for potential crack segments. The segments that have the specified codes will be permanently selected (dark highlighted) available for other operations to proceed.

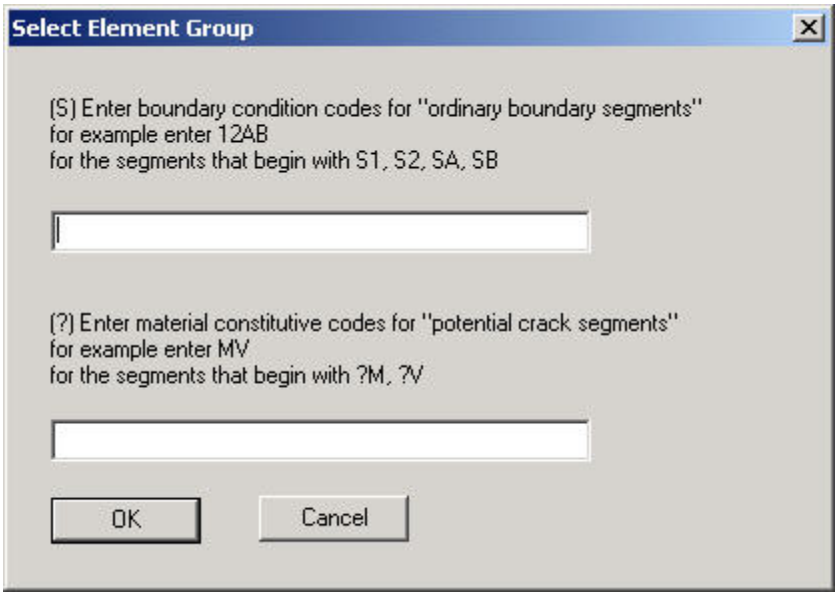

Figure A-7. Select element group dialog box.

[Edit] -> [Deselect All]

Clear the ‘selected ’status for all previous permanently selected entities and also turn off other modes (‘Move’, ‘Pan Center’, ‘Probe’ and ‘Zoom Window’).

[Edit] -> [Cut]

Remove the selected entities and place them to a temporary memory.

[Edit] -> [Copy]

Copy the selected entities to a temporary memory.

[Edit] -> [Paste]

Paste the selected entities that exist in the temporary memory at the center of the screen. All entities still remain highlighted so other operation such as ‘Move’ can continue.

[Edit] -> [Move]

Turns on/off ‘Move’ mode. When the mode is on, the user can drag the highlighted entities to any desired locations. Move mode can also be turned off by [Edit]-> [Deselect All].

[Edit] -> [Send To Back]

Send the selected entities to the back. The last drawn entities will be placed on the top of the previous drawn entities. If the user wants to select the entities that have other entities in front of them, those entities in the front must be sent to the back.

[Edit] -> [Edit]

Pop up a specific edit dialog box (‘Linear Segment Dialog Box’, ‘Circular Segment Dialog Box’, ‘Linear Field Point Dialog Box’ and ‘Matrix Field Point Dialog Box’) for each type of entity selected. If more than one entity is selected, the ‘Multiple Edit Segment Dialog Box’ will be opened. The user can then edit properties of each selected entity.

[Edit] -> [Break Segment]

Break ‘Line’ or ‘Circular’ segments into small ‘Line’ segments according to number of elements per segment specified.

[Edit] -> [Flip]

Flip the direction of the selected entities (‘Line’ segment, ‘Linear’ and ‘Matrix’ field output). Start point becomes end point and end point becomes start point.

[Edit] -> [Delete]

Delete the selected entities from the workspace.

[Edit] -> [Clear]

Clear has 9 submenus [Tessellation], [Segment], [Field Point], [Boundary Condition], [Base Material], [Cemented Material], [Step], [All Components in PRE Processor] and [All Components in POST Processor].

[Edit] -> [Clear] -> [Tessellation]

Clear the information specified in ‘Tessellation Dialog Box’.

[Edit] -> [Clear] -> [Segment]

Delete all segments (‘Line’ and / or ‘Circular’) from workspace.

[Edit] -> [Clear] -> [Field Point]

Delete all field points (‘Linear’ and / or ‘Matrix’) from workspace.

[Edit] -> [Clear] -> [Boundary Condition]

Delete all boundary conditions defined in ‘Boundary Condition Dialog Box’.

[Edit] -> [Clear] -> [Base Material]

Clear the information of background material and primitive stress field parameters defined in ‘Base Material Dialog Box’.

[Edit] -> [Clear] -> [Cemented Material]

Delete all material constitutive codes defined in ‘Cemented Material Dialog Box’.

[Edit] -> [Clear] -> [Load Step]

Delete all processing steps (load steps) defined in ‘Load Step Dialog Box’.

[Edit] -> [Clear] -> [All Components in PRE Processor]

Delete all components associated with the PRE processor (tessellation, segment, field point, boundary condition, base material, cemented material and load step).

[Edit] -> [Clear] -> [All Components in POST Processor]

Delete all components associated with the POST processor so that the new output file can be opened.

[View]

Menu [View] has11 submenus [Model Settings], [Zoom In], [Zoom Out], [Zoom Window], [Zoom All], [Pan Center], [Show Boundary Condition Code], [Show Material Constitutive Code], [Show Direction of Segment], [Tool bar], [Status Bar].

[View] - > [Model Settings]

Pop up 'Model Setting Dialog Box' shown in Figure A-8. The user can specify the 'Left Top' and 'Right Bottom' corner of the model in Y-Z coordinate, grid size, snap size, the decimal point used, turn on/off the grid and snap mode.

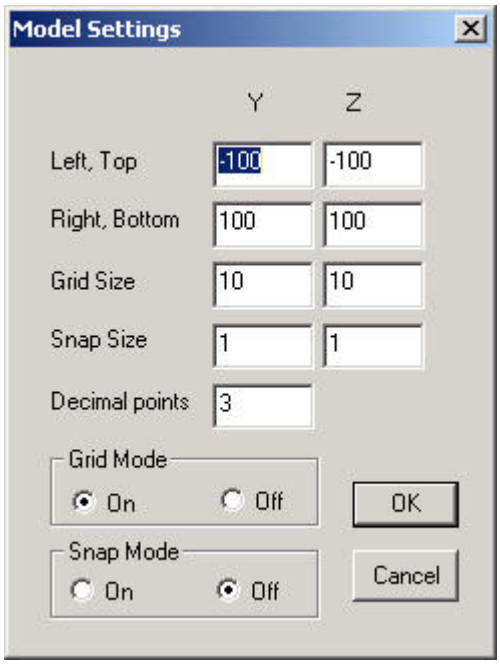

Figure A-8. Model setting dialog box.

[View] - > [Zoom In] 

Enlarge the view by 20% of the original model size.

[View] - > [Zoom Out] 

Decrease the view by 20% of the original model size.

[View] - > [Zoom Window] 

Turn on/off 'Zoom Window' mode. When the mode is on, left click and drag a rectangular window over the area of interest.

[View] - > [Zoom All]

Adjust the zoom mode to view an entire model size.

[View] - > [Pan Center] 

Turn on/off the 'Pan Center' mode. When the mode is on, right click at the location to be viewed at the centre of computer screen. 'Pan Center' mode can also be turned off by [Edit]-> [Deselect All].

[View] -> [Show Boundary Condition Code] 

Turn on/off the 'Show Boundary Condition Code' mode. When the mode is on, the ordinary boundary segments will show their boundary condition codes.

[View] -> [Show Material Constitutive Code] 

Turn on/off the 'Show Material Constitutive Code' mode. When the mode is on, the potential crack segments will show their material constitutive codes.

[View] -> [Show Direction of Segment] 

Turn on/off the 'Show Direction of Segment' mode. When the mode is on, the 'Line' segments will show their directions with arrows from the start point to the end

point and the ‘Circular’ segment will show the clockwise direction. The direction of the ‘Line’ segment can be flipped by [Edit]->[Flip], but the direction of ‘Circular’ segment cannot be flipped. The ‘BCB’ command used in the IN file always construct segments along circumference in clockwise direction. To create segment in counter clockwise direction, user may break ‘Circular’ segment to several small ‘Line’ segments along its circumference with [Edit]->[Break] and then [Edit]-> [Flip] those ‘Line’ segments.

[View] -> [Tool Bar]

Turn on/off the tool bar.

[View] -> [Status Bar]

Turn on/off the status bar.

[Tessellation]

Menu [Tessellation] has 2 submenus [Create] and [Export Segment].

[Tessellation] -> [Create]

Open ‘Tessellation Dialog Box’ shown in Figure A-9 for the user to input the data needed for generating tessellation. The information in ‘Tessellation Dialog Box’ will be saved to the input file (*.IN).

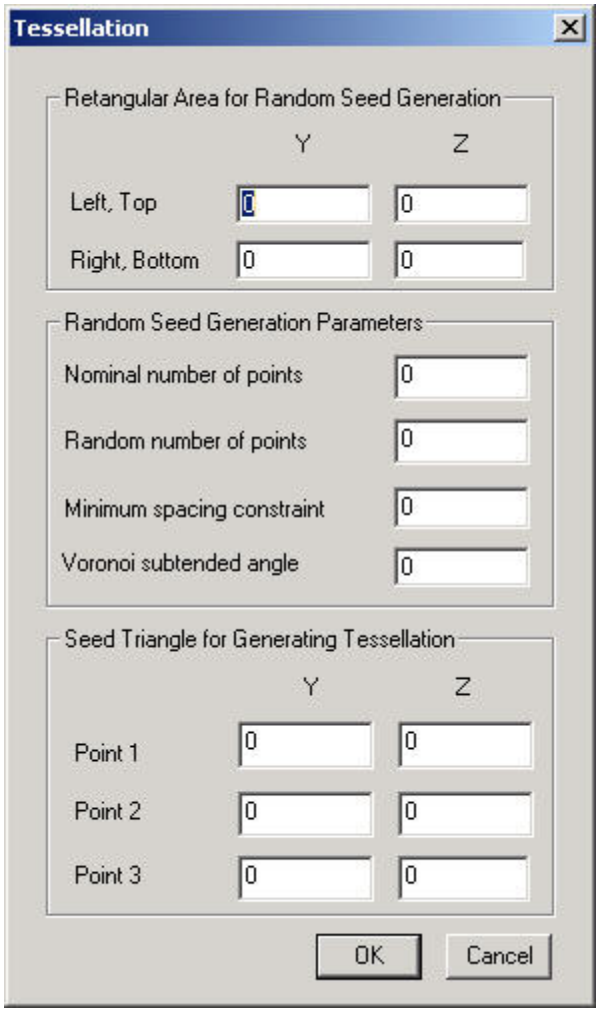

Figure A-9. Tessellation dialog box.

[Tessellation] -> [Export Segment]

Open ‘Export Segments Dialog Box’ shown in Figure A-10 for the user to export ordinary boundary segments and/or potential crack segments to the segment file (*._SG) by giving their boundary condition codes and/or material constitutive codes in the order of the segments to be written in the segment file.

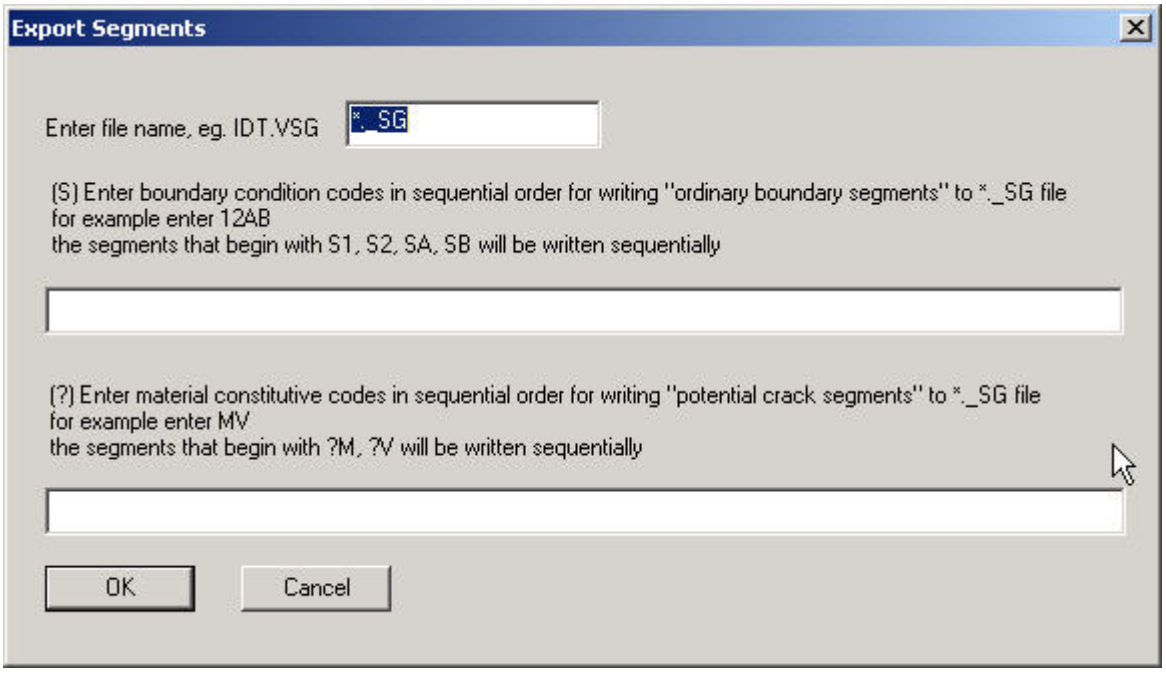

Figure A-10. Export segment dialog box.

[Geometry]

Menu [Geometry] has 2 submenus [Line] and [Circle].

[Geometry] - > [Line]

Turn on the drawing mode for 'Line' segment. Press <Left Mouse Button> and drag from the start point to the end point to create a 'Line' segment. Its properties can be edited by placing cursor over the segment and right click to open the cursor menu, then select [Edit]. Figure A-11 shows 'Line Segment Dialog Box'.

If the letter code for the segment is specified, the 'Line' segment will be saved in a segment file. A letter code refers to the boundary condition code for ordinary boundary segment and material constitutive code for potential crack segment. If the letter code is omitted, the segment will be considered as a part of the boundary regions and will be saved to the input file (*.IN).

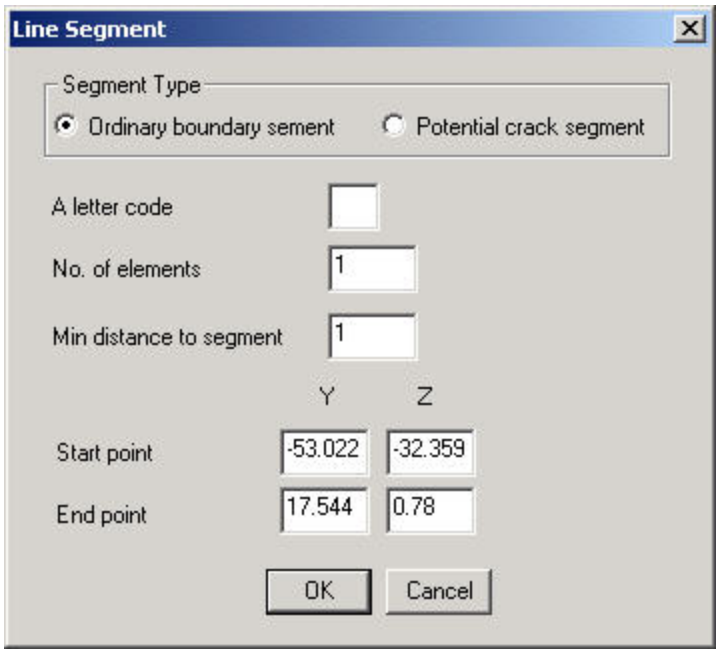

Figure A-11. Line segment dialog box.

[Geometry] - > [Circle]

Turn on the drawing mode for 'Circular' segment. Press <Left Mouse Button> and drag from center point to the point on circumference to create a 'Circular' segment. It can be edited by placing cursor over the segment and right click to open the cursor menu and select [Edit]. Figure A-12 shows 'Circular Segment Dialog Box'.

The 'Circular' segment cannot be saved in a segment file (*._SG) that contains only 'Line' segments. However, users can break a 'Circular' segment with [Edit]->[Break Segment] to 'Line' segments along circumferences and save them to the segment file. If the letter code for 'Circular' segment is omitted, it will be considered as a part of the boundary region and will be saved to the input file (*.IN).

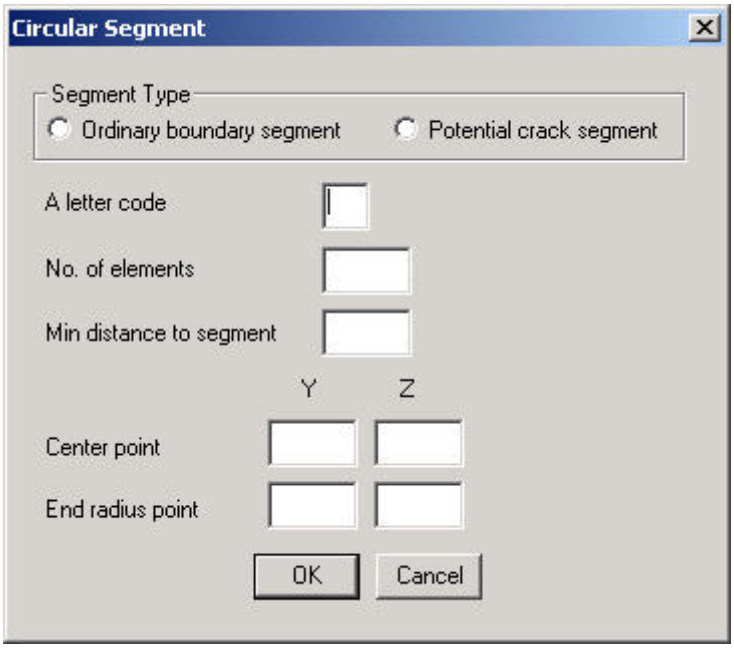

Figure A-12. Circular segment dialog box.

[Field Point]

Menu [Field Point] has of 2 submenus [Linear] and [Matrix]

[Field Point] - > [Linear]

Turn on the drawing mode for 'Linear' field point (a straight line of field points requested in a DAT file. Press <Left Mouse Button> and drag from start point to end point to create a 'Linear' field point. It can be edited by placing cursor over the field point and right click to open the cursor menu and select [Edit]. Figure A-13 shows 'Linear Field Point Dialog Box'.

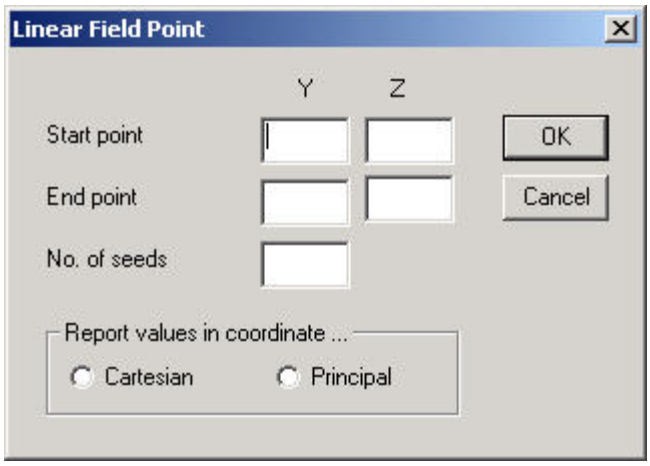

Figure A.13. Linear field point dialog box.

[Field Point] - > [Matrix]

Turn on the drawing mode for 'Matrix' field point (a matrix of field points requested in a DAT file). Press <Left Mouse Button> and drag from start point (top left corner) to end point (bottom right corner) to create a 'Matrix' field point. It can be edited by placing cursor over the field point and right click to open the cursor menu and select [Edit]. Figure A-14 shows 'Matrix Field Point Dialog Box'.

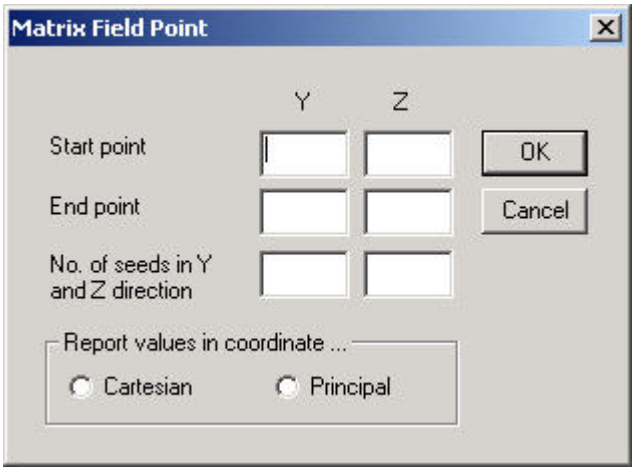

Figure A-14. Matrix field point dialog box.

[Boundary]

Menu [Boundary] has 1 submenu [Manager].

[Boundary] -> [Manager]

Open ‘Boundary Condition Dialog Box’ shown in Figure A-15 for the user to operate boundary conditions. Boundary condition code is defined by a single character. The color for boundary code can be set with a conventional RGB color method – combined red, green and blue color. The intensity of each color can be set from 0 to 255. The boundary type can be either ‘Constant’ if it does not change with time step or ‘Velocity’ if it does. Boundary condition can be set to one of these four conditions: displacement on positive side, displacement on negative side, traction and discontinuity. For every boundary element, there are two collocation points. The value on each collocation point will have the meaning according to boundary condition specified such as traction = 0 means traction free surface condition. The dialog has 6 buttons at the bottom, in which their functions will be described below.

[New] = Clear information in all text boxes so that the user can input new information

[Add] = Add the boundary condition to the boundary code list

[Delete] = Delete the boundary condition from the boundary code list

[Save Edit] = Save the edited data

[OK] = Save the edited data and leave the dialog box

[Cancel] = Cancel action made to the dialog box

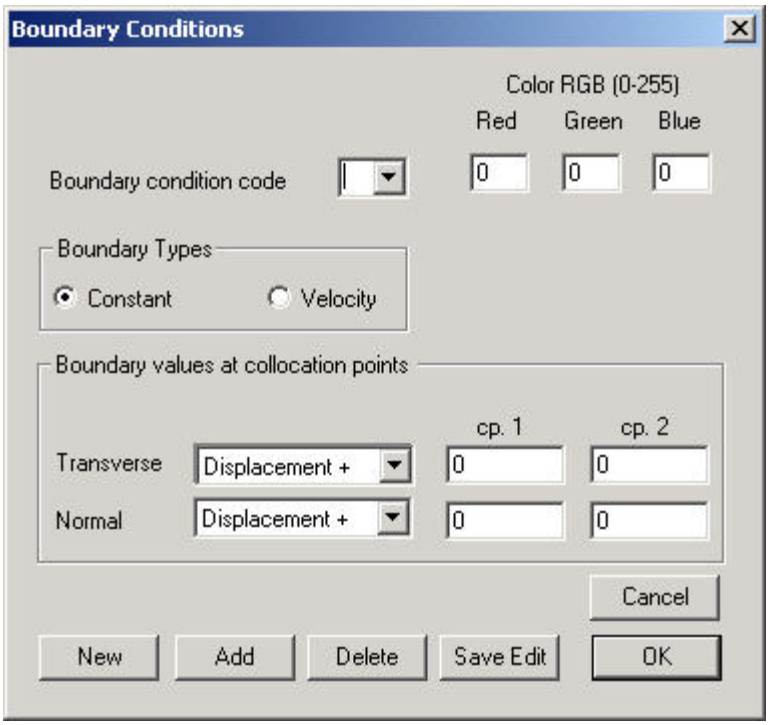

Figure A-15. Boundary condition dialog box.

[Material]

Menu [Material] has 2 submenus [Base Material] and [Cemented Material].

[Material] -> [General Parameters]

Open ‘General Parameter Dialog Box’ shown in Figure A-16 for the user to input and/or edit general parameters for background elastic material and associated stress fields.

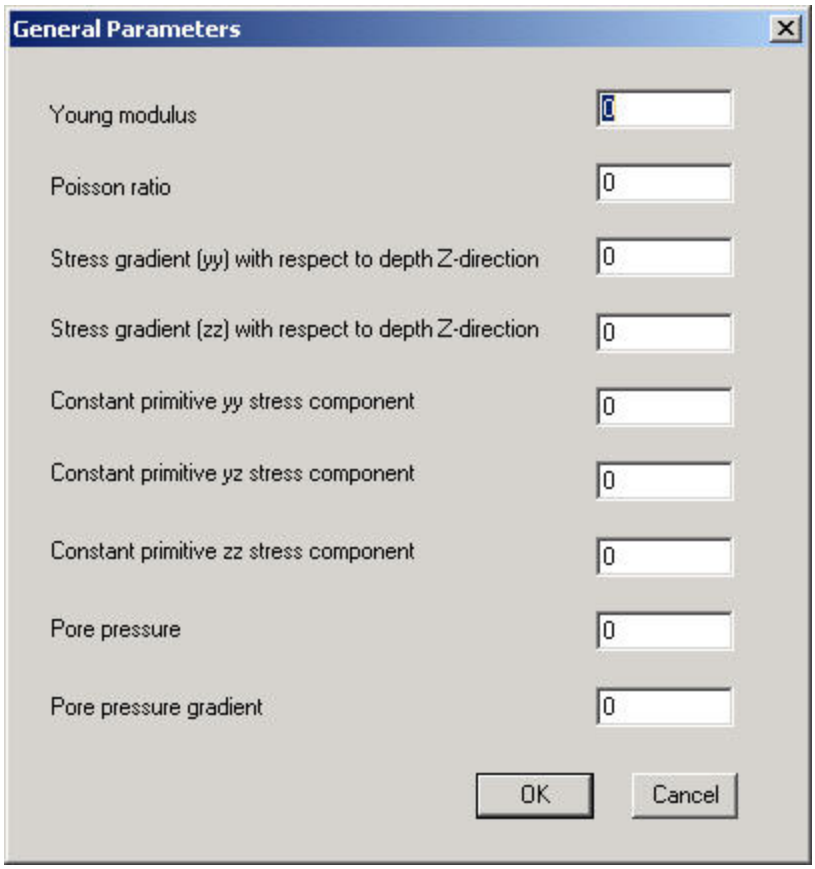

Figure A-16. General parameter dialog box.

[Material] -> [Cemented Material]

Opens ‘Cemented Material Dialog Box’ shown in Figure A-17 for the user to operate material constitutive codes used in the model. The material constitutive code is defined by a single character. The color for each material code can be set by a conventional RGB color method. The dialog box has 6 buttons [New], [Add], [Edit] [Save Edit], [OK] and [Cancel] at the bottom in which their functionalities are similar to those in ‘Boundary Condition Dialog Box’.

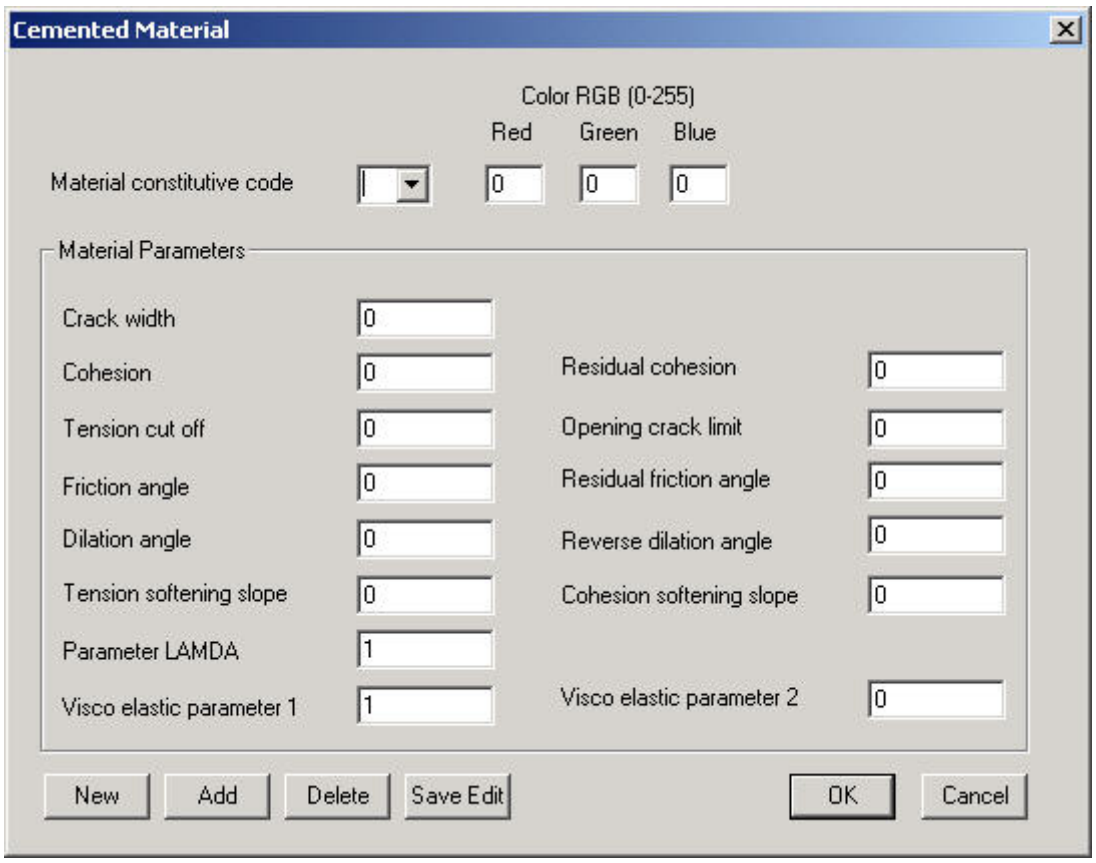

Figure A-17. Cemented material dialog box.

[Load Step]

Menu [Load Step] has 2 submenus [Create] and [Include Segment File].

[Load Step] -> [Create]

Open ‘Load Step Dialog Box’ shown in Figure A-18 for user to operate load steps. The dialog box has 6 buttons [New], [Add], [Edit], [Save Edit], [OK] and [Cancel] at the bottom in which their functionalities are similar to those in ‘Boundary Condition Dialog Box’.

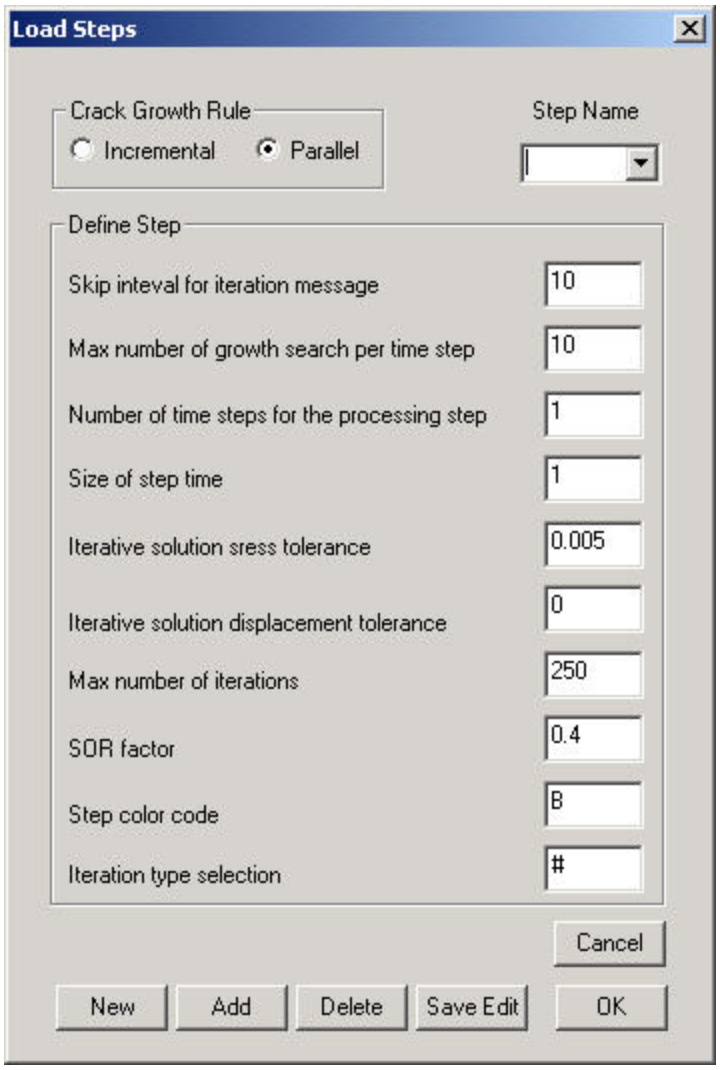

Figure A-18. Load step dialog box.

[Load Step] -> [Include Segment File]

Open ‘Include Segment File Dialog Box’ shown in Figure A-19 for the user to enter the segment file name (*._SG) to be included in the DAT file. The PRE processor requires all segments used in the problem be defined in a segment file. The PRE processor will attach this segment file name to the DAT file. Even though DIGS allow segments to be defined within the DAT file, the PRE processor will not recognize that format.

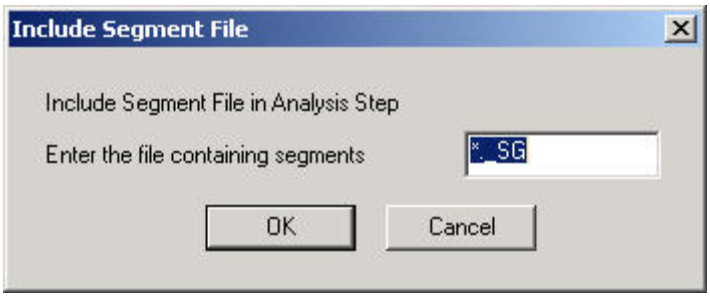

Figure A-19. Include segment file dialog box.

[Display]

Menu [Display] has 6 submenus [Display Result], [Setting], [Probe], [Previous Load Step], [Next Load Step] and [Request Output Variables].

[Display] - > [Display Result]

Submenu [Display Result] has 2 small submenus [DD Element Only] and [DD Element with Filed Point].

[Display] - > [Display Result] -> [DD Element Only]

Display the result of displacement discontinuity (DD) element only. Users can view the geometry, deformation and crack propagation.

[Display] - > [Display Result] -> [DD Element with Field Point]

Display the result of displacement discontinuity (DD) element and field points. Users can view geometry, deformation, crack propagation and field points.

[Display] - > [Setting]

Submenu [Setting] has 3 small submenus [Amplification], [Color] and [Probe Options].

[Display] - > [Setting] ->[Amplification]

Open ‘Amplification Dialog Box’ shown in Figure A-20. User can set the scale to amplify the deformation and opening crack for visualized purpose.

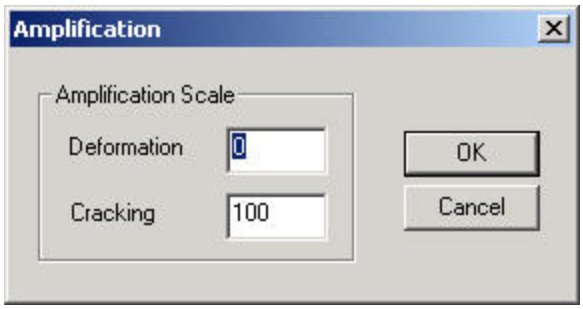

Figure A-20. Amplification dialog box.

[Display] - > [Setting] ->[Color]

Open ‘Color for DD Element Dialog Box’ shown in Figure A-21. User can set a color for each group of DD element based on its letter code (boundary condition code for ordinary boundary element and material constitutive code for potential crack element).

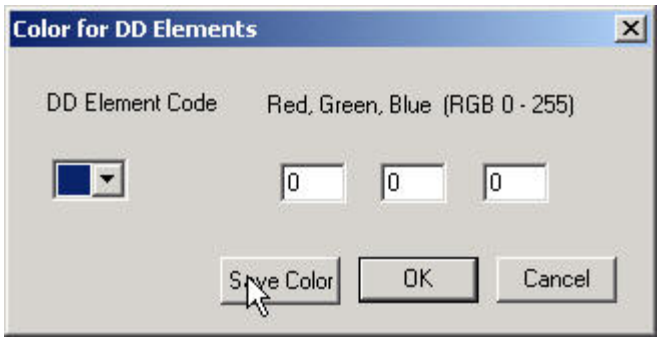

Figure A-21. Color for DD element dialog box.

[Display] - > [Setting] ->[Probe Options]

Open ‘Probe Option Dialog Box’ shown in Figure A-22. User can select one of these 3 probing options: (1) Probe DD element, (2) Probe field point in principal direction and (3) Probe field point in Cartesian coordinate. For each option, user can select the desired output variables to be monitored by marking those variables.

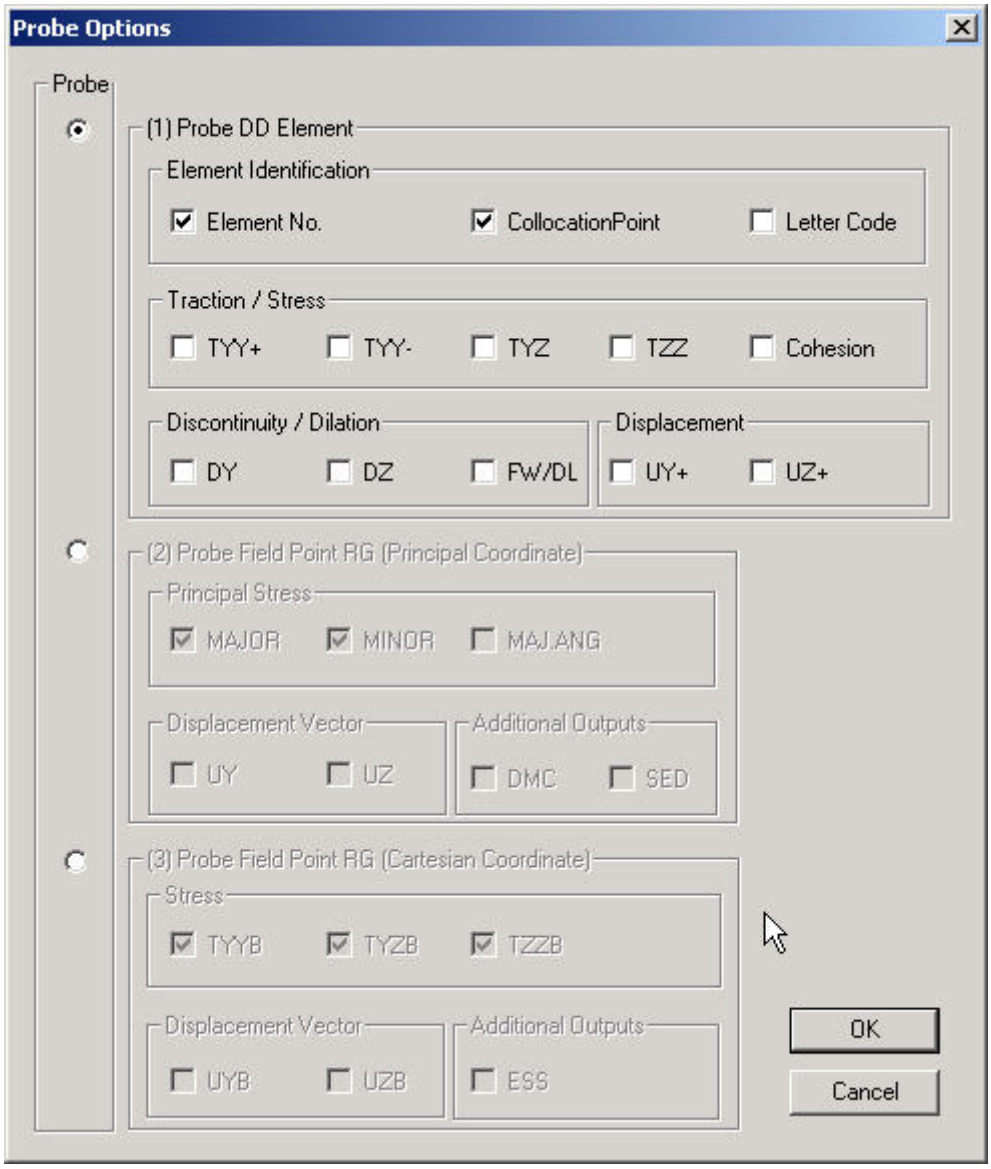

Figure A-22. Probe option dialog box

[Display] - > [Probe]

Turn on/off 'Probe' mode. When 'Probe' mode is turned on, the user can probe the output variables according to the probing option by placing cursor close to the collocation of the DD element or close to the location of field point.

[Display] - > [Previous Load Step] 

Go back to the previous load step and view the result.

[Display] - > [Next Load Step] 

Forward to next the load step and view the result.

[Display] - > [Request Output Variables]

Open ‘Request Output File Dialog Box’ shown in Figure A-23. The dialog box asks the user to enter the request output file (*.REQ) and the report output file (*.RPT).

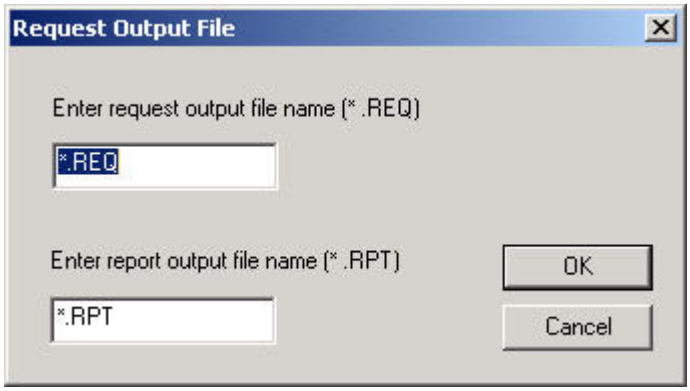

Figure A-23. Request output file dialog box.

[Help]

Menu [Help] has one submenu [About DDM]

[Help] - > [About DDM] 

Pop up ‘About DDM Dialog Box’ describing the PRE/POST program DDM.

LIST OF REFERENCES

Asphalt Institute. *Research and Development of The Asphalt Institute's Thickness Design Manual (MS-1) 9 ed*. Research Report 82-2, 1982.

Bazant, Z. P. Mechanics of Distributed Cracking. *Applied Mechanics Review*, Vol. 39, No. 5, May 1986, pp. 675-705.

Birgisson, B., C. Soranakom, J. A. L. Napier, and R. Roque. Simulation of the Cracking Behavior of Asphalt Mixtures Using Random Assemblies of Displacement Discontinuity Boundary Elements. *15th ASCE Engineering Mechanics Conference,* Columbia University, New York, 2002a.

Birgisson, B., C. Soranakom, J. A. L. Napier, and R. Roque. Modeling of Microstructure and Fracture Behavior of Asphalt Mixtures Using a Boundary Element Approach. *ASCE Journal of Civil Engineering Materials*, New York, 2002b.

Bonnaure, F., A. Gravois, and J. Udron. A New Method for Predicting the Fatigue Life of Bituminous Mixes. *Proceedings, Association of Asphalt Paving Technologists*, Vol.49, 1980, pp. 99-524.

Buttlar, W. G. and R. Roque. Development and Evaluation of the Strategic Highway Research Program Measurement and Analysis System for Indirect Tensile Testing at Low Temperatures. In *Transportation Research Record, No. 1454*, TRB, National Research Council, Washington, DC, 1994, pp. 163-171.

Chen, W. F. and D. J. Han. *Plasticity for Structural Engineering*. Springer-Verlag, New York, 1988, 250 pp.

Collop, A. and D. Cebon. A Theoretical Analysis Of Fatigue Cracking in Flexible Pavements. *Proceedings of the Institution of Mechanical Engineers*, Vol. 209, 1995, pp. 345-361.

Crawford, A. M. and J. H. Curran. Higher-Order Functional Variation Displacement Discontinuity Elements. *International Journal of Rock Mechanics and Mining Sciences*, Vol. 19, 1982, pp. 143-148.

Crouch, S. L. and A. M. Starfield. *Boundary Element Methods in Solid Mechanics*. George Allen&Unwin, London, U.K. 1983.

Elber, W. Fatigue Crack Closure Under Cyclic Tension. *Engineering Fracture Mechanics*, Vol. 2, 1970, pp. 37-45.

Ewalds, H. L. and R. J. H. Wanhill. *Fracture Mechanics-Delft*. Delftse U.M., London 1986.

Foreman, R. G., V. E. Keary, and R. M. Engle. Numeral Analysis of Crack Propagation in Cyclic-Loaded Structures. *Journal of Basic Engineering*, Vol. 9, 1967, pp. 459-464.

Francken, L. Fatigue Performance of a Bituminous Road Mix Under Realistic Test Conditions. In *Transportation Research Record, No. 712*, 1979, pp. 30-36.

Garcia, O. F. *Asphalt Mixture and Loading Effects on Surface-Cracking of Pavements*. Master's Thesis, Department of Civil & Coastal Engineering, University of Florida, 2002.

Gomez, M. and M. R.Thompson. *Mechanistic Design Concepts for Full Depth Asphalt Concrete Pavements*. Civil Engineering Studies, Transportation Engineering Series, No.41, University of Illinois at Urbana-Champaign, 1984.

Griffith, A. A. The Phenomena of Rupture and Flow in Solids. *Philosophical Transactions, Series A*, Vol. 221, 1920, pp. 163-198.

Helms, K. L. E., D. H. Allen, and L. D. Hurtado. A Model for Predicting Grain Boundary Cracking in Polycrystalline Viscoplastic Material Including Scale Effects. *International Journal of Fracture*, Vol. 95, 1999, pp. 175-194.

Jacobs, M. M. J. *Crack Growth in Asphaltic Mixes*. Ph.D. Dissertation, Delft University of Technology, Road and Railroad Research Laboratory, 1995.

Jacobs, M. M. J., P. C. Hopman, and A. A. A. Molenaar. Application of Fracture Mechanics Principles to Analyze Cracking in Asphalt Concrete. *Journal of the Association of Asphalt Paving Technologists*, Vol. 65, 1996, pp. 1-39.

Klesnil, M., and P. Lukas. Influence of Strength and Stress History on Growth and Stabilization of Fatigue Cracks. *Engineering Fracture Mechanics*, Vol. 4, 1972, pp. 77-92.

Kuijpers, J. S. and J. A. L. Napier. Effective Growth Rules for Macrofacture Simulation in Brittle Rock under Compression. *Eurock'96* (edited by G. Barla), Balkema, Rotterdam, 1996, pp. 469-479.

Lee, H. J. and Y. R. Kim. Viscoelastic Constitutive Model for Asphalt Concrete under Cyclic Loading. *Journal of Engineering Mechanics*, Vol.124, No.1, Jan.1998a, pp. 32-40.

Lee, H. J. and Y. R. Kim. Viscoelastic Continuum Damage Model of Asphalt Concrete with Healing. *Journal of Engineering Mechanics*, Vol.124, No.11, Nov.1998b, pp. 1224-1232.

Lee, H. J., J. S. Daniel, and Y. R. Kim. Laboratory Performance Evaluation of Modified Asphalt Mixtures for Inchon Airport Pavements. *The International Journal of Pavement Engineering*, Vol.1, 2000, pp. 151-169.

Malan, D. F. and J. A. L. Napier. Computer Modeling of Granular Material Microfracturing. *Tectonophysics*, Vol. 248, 1995, pp. 21-37.

Myers L. *Development and Propagation of Surface-Initiated Longitudinal Wheel Path Cracks in Flexible Highway Pavements*. Ph.D. Dissertation, University of Florida, 2000.

Myers, L., R. Roque, and B. Birgisson. Propagation Mechanicsms for Surface-Initiated Longitudinal Wheel path Cracks. *Transportation Research Record, No. 1778*, 2001, pp. 113-121

Napier, J. A. L. Modeling of Fracturing near Deep Level Gold Mine Excavations Using a Displacement Discontinuity Approach. *Proceedings of the Second International Conference on Mechanics of Jointed and Faulted Rock* (edited by H.P. Rossmanith), Balkema, Rotterdam, 1990, pp. 709-715.

Napier, J. A. L. and M. W. Hildyard. Simulation of Fracture Growth around Openings in Highly Stressed Brittle Rock. *Journal of the South African Institute of Mining and Metallurgy*, Vol. 92, 1992, pp. 159-168.

Napier, J. A. L. and A. P. Peirce, Simulation of Extensive Fracture Formation and Interaction in Brittle Materials. *Mechanics of Jointed and Faulted Rock*, (edited by H.P. Rossmanith), 1995a, pp. 63-74.

Napier, J. A. L and A. P. Peirce. Simulation of Extensive Fracture Formation and Interaction in Brittle Materials. *Proceedings of the Second International Conference on Mechanics of Jointed and Faulted Rock* (edited by H.P. Rossmanith), Balkema, Rotterdam, 1995b, pp. 63-74.

Napier, J. A. L. and D. F. Malan. A Viscoplastic Discontinuum Model of Time-Dependent Facture and Seismicity Effect in Brittle Rock. *International Journal of Rock Mechanics and Mining Sciences*, Vol. 34, 1997, pp. 1075-1089.

Napier, J. A. L., A. Daehnke, T. Dede, M. W. Hildyard, J. S. Kuijpers, D. F. Malan, E. J. Sellers, and P. A. Turner. Quantification of Stope Fracture Zone Behavior in Deep Level Gold Mines. *Journal of the South African Institute of Mining and Metallurgy*, Vol. 97, 1997, pp. 119-134.

Ostoja-Starzewki, M. Mechanics of Damage in a Random Granular Microstructure: Percolation of Inelastic Phases. *Lett Appl Engng Sci*, Vol.27, 1987, pp. 315-326.

Ostoja-Starzewski, M. and C. Wang. Linear Elasticity of Planar Delaunay Networks: Random Field Characterization of Effective Moduli. *Acta Mech*, Vol.80, 1989, pp. 61-80.

Paris, P. C. and F. Erdogan. A Critical Analysis of Crack Propagation Laws. Transactions of the ASME, *Journal of Basic Engineering*, Vol. 85, 1963, pp. 528-534.

Peirce, A. P. and J. A. L. Napier. A Spectral Multipole Method for Efficient Solution of Large-Scale Boundary Element Models in Elastostatics. Paper Submitted to *International Journal for Numerical Methods in Engineering*, 1994.

Ramsamooj, D. V. Fatigue Cracking of Asphalt Pavements. *Journal of Transportation Research Record, No. 756*, 1980, pp. 43-48.

Ramsamooj, D. V. Prediction of Fatigue Life of Asphalt Concrete Beams from Fracture Test. *Journal of Testing and Evaluation*, Vol. 19, No. 3, May 1991, pp. 231-239.

Ramsamooj, D. V. Fracture of Highway and Airport Pavements. *Journal of Engineering Fracture Mechanics*, Vol. 44, No. 4, 1993, pp. 609-626.

Roque, R., W. G. Buttlar, B. E. Ruth, M. Tia, S. W. Dickison, and B. Reid. *Evaluation of SHRP Indirect Tension Tester to Mitigate Cracking in Asphalt Pavements and Overlays*. Final Report to the Florida Department of Transportation, August, 1997, 346p.

Sangpetngam, B., B. Birgisson, and R. Roque. Development of an Efficient Hot Mix Asphalt Fracture Mechanics-Based Crack Growth Simulator. In *82nd Annual Meeting (CD-ROM), TRB, National Research Council*, Washington, D.C., 2003.

Schapery, R. A. *A Theory of Crack Growth in Visco-Elastic Media*. Report MM 2764-73-1, Mechanics and Materials Research Center, Texas A & M University, College Station, TX, 1973.

Schapery, R. A. A Theory of Crack Initiation and Growth in Visco-Elastic Media: I: Theoretical Development, II: Approximate Methods of Analysis, III: Analysis of Continuous Growth. *International Journal of Fracture*, Vol.11, No.1, pp. 141-159, Vol., No.3, pp. 369-388, and Vol.11, No.4, pp. 549-562, 1975.

Schapery, R. A. A Method for Predicting Crack Growth in Non-homogeneous Visco-Elastic Media. *International Journal of Fracture*, Sijhoff and Noorhoff International Publishers, Vol.14, No. 3, 1978, pp. 293-309.

Schapery, R. A. Corresponding Principles and a Generalized J Integral for Large Deformation and Fracture Analysis of Viscoelastic Media. *International Journal of Fracture*, Vol.25, 1984, pp. 195-223.

Sedwick, S. C. *Effect of Asphalt Mixture Properties and Characteristics on Surface-Initiated Longitudinal Wheel Path Cracking*. Master's Thesis, Department of Civil & Coastal Engineering, University of Florida, 1998.

Sellers, E. J. and J. A. L. Napier. A Comparative Investigation of Micro-Flaw Models for the Simulation of Brittle Fracture in Rock. *Computational Mechanics*, Vol.20, 1997, pp. 164-169.

Soranakom, C., B. Birgisson, J. A. L. Napier, and R. Roque. Simulation of Fracture Initiation in Hot Mix Asphalt Mixtures. In *82nd Annual Meeting (CD-ROM), TRB*, *National Research Council*, Washington, D.C., 2003.

Steen, B. V. D., A. Vervoort, and J. A. L. Napier. Numerical Modeling of Fracture Initiation and Propagation in Biaxial Tests on Rock Samples. *International Journal of Fracture*, Vol. 108, 2001, pp. 165-191.

Thompson, M. R. ILLI-PAVE Based Full-Depth Asphalt Concrete Pavement Design Procedure. *Proceedings, Sixth International Conference on Structural Design of Asphalt Pavements*, Ann Arbor, MI, 1987.

Thompson, M. R. and K. Cation. *A Proposed Full-Depth Asphalt Concrete Thickness Design Procedure*. Civil Engineering Studies, Transportation Engineering Series No. 45, University of Illinois at Urbana-Champaign, 1986.

Van der Burg, M. W. D. and E. Van der Giessen. *Delaunay-Network Modeling of Creep Failure in Regular Polycrystalline Aggregates by Grain Boundary Cavitations*. Delft University of Technology, LTM Report No. 1004, 1993.

Weertman, J. Rate of Growth of Fatigue Cracks Calculated from the Theory of Infinitesimal Dislocations Distributed on a Plane. *International Journal of Fracture Mechanics*, Vol. 2, 1966, pp. 460-467.

Winnie, D. H. and B. M. Wundt. Application of the Griffith-Irwin Theory of Crack Propagation to the Bursting Behavior of Disc, Including Analytical and Experimental Studies. *Transaction ASME*, Vol. 80, 1958, pp. 1643-1655.

Wnuk, M. P. Subcritical Growth of Fracture. *International Journal of Fracture Mechanics*, Vol.7, 1971, pp. 383-486.

Zang, Z. *Identification of Suitable Crack Growth Law For Asphalt Mixtures Using the Superpave Indirect Tensile Test (IDT)*. Ph.D. Dissertation, University of Florida, August 2000.

Zhang, Z., R. Roque, B. Birgisson, and B. Sangpetngam. Indentification and Verification of a Suitable Crack Growth Law (with Discussion). *Journal of the Association of Asphalt Paving Technologists*, Vol.70, 2001, pp. 206-241.

BIOGRAPHICAL SKETCH

Chote Soranakom was born in Nakhonrachasima, Thailand, on December 30, 1973, to Chewpore and Wongsa Soranakom. He attended Debsirin School in Bangkok and graduated in 1991.

In higher education, Chote passed the entrance examination and selected Chiang Mai University and completed his Bachelor of Science degree in civil engineering in 1995. He continued his education in Sydney, Australia, and completed his Master of Engineering degree from the University of New South Wales in 1997.

He then came to the United States and attended school at the University of Florida. His research focuses on the evaluation of the displacement discontinuity method to simulate the indirect tension strength test. Chote is currently completing an Engineering degree in civil and coastal engineering at the University of Florida with a specialization in numerical modeling.